DISSERTATION

submitted to the
Combined Faculties for the Natural Sciences and for Mathematics of the
Ruperto-Carola University of Heidelberg, Germany
for the degree of
Doctor of Natural Sciences

Identification and functional characterization of microRNAs in medulloblastoma

Presented by
M.Phil. Hsing Chen BAI
born in Taipei, Taiwan

Heidelberg 2011

Referees:
Prof. Dr. Werner Buselmaier
Prof. Dr. Peter Lichter

Oral examination date:

The investigations of the following dissertation were performed from October 2007 till June 2011 under the supervision of Prof. Dr. Peter Lichter, PD. Dr. Stefan Pfister, and Dr. Armin Pscherer in the Division of Molecular Genetics at the German Cancer Research Center (DKFZ), Heidelberg, Germany.

Declarations

I hereby declare that I have written the submitted dissertation 'Identification and functional characterization of microRNAs in medulloblastoma' myself and in this process have used no other sources or materials than those expressly indicated. I hereby declare that I have not applied to be examined at any other institution, nor have I used the dissertation in this or any other form at any other institution as an examination paper, nor submitted it to any other faculty as a dissertation.

_____ _____

(Place, Date) Hsing Chen BAI

Publications

Journal articles

1. Pfister S, Remke M, Castoldi M, **Bai AH**, Muckenthaler MU, Kulozik A, von Deimling A, Pscherer A, Lichter P, Korshunov A. Novel genomic amplification targeting the microRNA cluster at 19q13.42 in a pediatric embryonal tumor with abundant neuropil and true rosettes. Acta Neuropathol. 2009 Apr;117(4):457-64

2. **Bai AH**, Milde T, Remke M, Rolli CG, Hielscher T, Cho YJ, Kool M, Northcott PA, Jugold M, Bazhin AV, Eichmüller SB, Kulozik AE, Pscherer A, Benner A, Taylor MD, Pomeroy SL, Kemkemer R, Witt O, Korshunov A, Lichter P, Pfister SM. MicroRNA-182 promotes metastatic dissemination of non-sonic hedgehog-medulloblastoma. Acta Neuropathol. (submitted)

3. Weeraratne SD, Teider N, Amani V, Pierre-Francois J, Winter D, Kye MJ, Sengupta S, Archer T, Remke M, **BAI AH**, Wong J, Lu J, Warren P, Pfister SM, Stehen J, Pomeroy SL, Cho YJ. Pleiotropic effects of miR-183~96~182 converge to regulate cell survival, proliferation and migration in medulloblastoma. Acta Neuropathol. (submitted)

Conference abstract — oral presentation

1. **A.H. BAI**, M. Remke, P. Northcott, A. Korshunov, G. Toedt, A. Benner, M. Castoldi, W, Scheurlen, A. Pscherer, M.U. Muckenthaler, A.E. Kulozik, P. Lichter, M.D. Taylor and S. M. Pfister. Micro-RNA expression signatures discriminate molecular risk groups in medulloblastoma. 14th International Symposium on Pediatric Neuro-Oncology, Vienna, Austria, 2010. Abstract no. MED.04

Dedicated in loving memory to my mother

Acknowledgements

First and foremost, I would like to express the deepest appreciation to Prof. Dr. Peter Lichter, Head of Division Molecular Genetics for offering me the opportunity to pursude the PhD study in his division. He always shares his valuable advices and time with graduate students and created a friendly to discuss and fully supportive research environment in his division.

The accomplishment of this thesis would not have been possible without the insightful guidance from Prof. Dr. Stefan Pfister. I will always be grateful for his support, wisdom, kindness and of course, wonderful sense of humor.

Dr. Armin Pscherer provided a lot of guidance and assistance in the beginning of this course work and my new life in Germany. I will never forget his kindness and enthusiasm, and wish him has a very good career development at the new position.

Dr. Marc Remke gave his best ideas in the experimental design, indeed, his beautiful English writing skill and detailed reviewing attitude made our submitted manuscript elegant.

Furthermore it is an honor for me to have Prof. Dr. Werner Buselmaier, Prof. Dr. Harald Herrmann, and PD. Dr. Karsten Rippe participate in my thesis defense.

I am most grateful to Prof. Dr. Olaf Witt and Dr. Till Milde from Division Pediateic Oncology (G340) provided awesome animal experiments for this work.

Special gratitude goes to Prof. Dr. Andrey Korshunov who shared his profound expertise in tumor biology and neuropathology of pediatric brain tumors.

Dr. Ralf Kemkemer and Claudio Rolli from the Max Planck Institute for Intelligent Systems provided their amazing pioneer 3D microchannel technique must be acknowledged.

In my daily work I have been blessed with a friendly and cheerful group, Frauke Devens, Magdalena Schlotter, Anna Schöttler and particularly Andrea Wittmann are acknowledged for expert technical supports. Also the friendly discussion and supports from my colleagues, Jan Meier, Valentina Kovaleva, Hui Wu, Sabrina Pleier, and especially thanks to Huriye Cin, Elke Pfaff, and Marc for critical German review for the “Zusammenfassung”. Besides, all members in B060 and B062 you are always on my mind.

Last but not least, I must thank my wife, Pui Yu who did an excellent job taking care of our family, especially being acompany with my mother during her cancer therapies. And the one above all of us, the omnipresent God, for answering my prayers for giving me the strength moving forward during the 4-year wilderness PhD work.

TABLE OF CONTENTS

ABBREVIATIONS

2D	Two dimensional
3`-UTR	3`-untranslated region
3D	Three dimensional
5`-UTR	5`-untranslated region
AGO	Argonaute
APS	Ammoniumpersulfate
AU	Approximately unbiased
cDNA	complementary DNA
CLL	Chronic lymphocytic leukemia
CNS	Central nervous system
CSC	Cancer stem cells
CSF	Cerebrospinal fluid
Ct	Cycle threshold (Real-time PCR)
DASL	cDNA-mediated Annealing, Selection, Extension, and Ligation
DGCR8	DiGeorge syndrome critical region gene 8
DMEM	Dulbecco´s Modified Eagle Medium
DNA	Deoxyribonucleic acid
EGL	External granular layer
FBS	Fetal bovine serum
GCP	Granule cell progenitor
H&E	Haematoxylin & eosin
HCL	Hierarchical clustering
HKsRNAs	house keeping small RNAs
HRP	Horseradish peroxidase
IGL	Internal granule cell layer
KD	Knockdown
LC/A	Large cell / anaplastic
MBEN	Medulloblastoma with extensive nodularity
miRISC	miRNA-induced silencing complex
miRNA	microRNA
miRNP	micro-RNP
MRI	Magnetic resonance imaging
mRNA	messenage RNA
MTS	3-(4,5-dimethylthiazol-2-yl)-5-(3-carboxymethoxyphenyl)-2-(4-sulfophenyl)-2H-tetrazolium, inner salt
NCB	Normal cerebellum
PBS	Phosphate buffered saline
PCA	Principal component analysis
pCMX	pCMX-PL1 vector
PDMS	Poly(dimethylsiloxane)
PET	polyethylene terephthalate
PNET	Primitive NeuroEctodermal Tumor
pri-miRNAs	Primary miRNAs

PVDF	Polyvinyliden flouride
QRT-PCR	Quantitative real-time PCR
RIN	RNA integrity number
RMS	Rhabdomyosarcoma
RNaseIII	Ribonuclease III
RNP	Ribonucleoprotein
RT	Reverse transcription
SAM	Significance Analysis of Microarrays
SDS-PAGE	SDS-polyacrylamide gel electrophoresis
SHH	Sonic hedgehog pathway
siRNA	small interfering RNAs
SNP	Signal-nucleotide polymorphism
ssRNA	single-stranded RNA
TBE	Tris-borate-EDTA
TBS	Tris buffered saline
TBST	Tris buffered saline Tween20
TENED	Tetramethylethylenediamine
Tm	Primer melting temperature (annealing temperature)
TMA	Tissue microarray
TRBP	TAR RNA binding protein
WHO	World health organization
WNT	Wingless signaling pathway

GENE NAMES AND DEFINITION OF GENE SYMBOLS

Gene symbols written in capital letters indicate human protein (e.g. MYC).

Gene symbols written in italic capital letters indicate human gene (e.g. *MYC*).

Gene symbol	**Gene name in full**
APC	adenomatous polyposis coli
BMP	bone morphogenic protein
BRCA1	breast cancer 1, early onset
CCND1	cyclin D1
CCND2	cyclin D2
CDK6	cyclin D–kinase 6
CK1a	Caseine kinase a
CTNNB1	β-Cateine
CTTN	cortactin
EGR1	early growth response 1
EZR (VIL2)	ezrin
FOXO3	forkhead box O3
GLI1	GLI family zinc finger 1
GLI2	GLI family zinc finger 2
GLI3	GLI family zinc finger 3
KRAS	v-Ki-ras2 Kirsten rat sarcoma viral oncogene homolog
MYC (C-MYC)	myelocytomatosis viral oncogene homolog (avian)
MYCN	myelocytomatosis viral related oncogene, neuroblastoma derived (avian)
NOTCH1	notch 1
NOTCH2	notch 2
p21	cyclin-dependent kinase inhibitor 1A (p21, Cip1)
p27 (SSSCA1)	Sjogren syndrome/scleroderma autoantigen 1
p53 (TP53)	tumor protein p53
PTCH1	Patched 1
PTEN	phosphatase and tensin homolog
SFRP1	secreted frizzled-related protein 1
SMO	smoothened, frizzled family receptor
SUFU	supperressor-of-fused
Tieg-1 (KLF10)	Kruppel-like factor 10

SUMMARY

MicroRNAs (miRNAs) have been one of the most contemplated topics in molecular biology studies in the last decade. These short, non-coding RNA molecules (21-25 nucleotides) were showed to play an important role in carcinogenesis with specific expression profiles in distinct cancer types. However, the contribution of deregulated miRNAs to medulloblastoma formation remains poorly understood.

Medulloblastoma comprises the most frequent malignant brain tumor in childhood. Despite considerable therapeutic progress in the past decades, medulloblastoma still results in a comparably poor overall survival rate of 60-70%. Among clinical variables, particularly metastatic dissemination at diagnosis, which is present in about 30% of cases, is associated with dismal prognosis.

Distinct molecular subgroups with characteristic genomic aberrations and specific gene expression signatures were consistently reported by several groups and shown to be associated with largely different prognosis.

This study demonstrates that genome-wide miRNA expression profiling largely reveals molecular subgroups that had previously also been identified by mRNA expression profiling. A robust miRNA signature with 26 miRNAs was found to readily distinguish Sonic hedgehog (SHH) subgroup medullo-blastomas from other subgroups in two independent data sets obtained on different microarray platforms.

Retina-specific miRNAs, miR-182, miR-183, and miR-96 were reported to be involved in the tumorigenesis and invasiveness of numerous cancer types, however, not yet studied in medulloblastoma. These miRNAs were the most differentially regulated miRNAs within the 26-miRNA signature, were significantly upregulated in non-SHH medulloblastoma, and were associated with tumor location and metastatic dissemination. Further investigating the functional role of these candidate miRNAs in medulloblastoma cells, this study clearly demonstrates *in vitro* and *in vivo*, that overexpression of miR-182 in the

context of non-SHH medulloblastoma functionally contributes to the metastatic dissemination of medulloblastoma.

This momentous finding regarding the functional role of retina-specific miRNAs in medulloblastoma proves novel insights in the biology of metastatic medulloblastoma. Based on this knowledge, novel targeted treatment approaches may be developed for subgroups with particularly dismal prognosis.

ZUSAMMENFASSUNG

In den letzten zehn Jahren sind MicroRNAs (miRNAs) einer der meist untersuchten Forschungsinhalte in molekularbiologischen Studien. Es wurde gezeigt, dass diese kleinen, nicht-kodierenden RNA-Moleküle (21-25 Nukleotide) in der Tumorentstehung eine wichtige Rolle spielen. Auch wurde bereits nachgewiesen, dass verschiedene Krebsarten spezifische Expressionsprofile aufweisen. Allerdings ist der Beitrag der Deregulierung von miRNAs in Medulloblastomen noch weitgehend unverstanden.

Das Medulloblastom ist der häufigste bösartige Hirntumor im Kindesalter. Trotz bedeutender therapeutischer Fortschritte in den vergangenen Jahrzehnten, ergibt sich für Medulloblastome eine vergleichsweise schlechte Überlebensrate von 60-70%. Bei jungen Patienten ist eine metastatische Ausbreitung von Tumorzellen zum Zeitpunkt der Diagnose, die derzeit in etwa 30% der Fälle zu verzeichnen ist, mit einer schlechten Prognose verbunden.

Aufgrund der großen Heterogenität dieser Tumorentität können verschiedene molekulare Subgruppen anhand der Ausprägung von genomischen Aberrationen und Genexpressionsprofilen unterschieden werden, welche sich auch bezüglich ihrer Prognose für die Patienten beträchtlich unterscheiden.

Die vorliegende Arbeit ergab, dass genomweite miRNA-Expressionsprofile große Übereinstimmung mit den molekularen Subgruppen zeigten, die ihrerseits in früheren Studien auf der Basis von mRNA-Expressionsprofilen bestimmt worden waren. Darüber hinaus war es möglich, eine robuste miRNA-Signatur mit 26 miRNA Kandidaten zu identifizieren, mit der Sonic hedgehog (SHH)-Medulloblastome von anderen Subgruppen unterschieden werden können.Dies konnte in zwei unabhängigen Kohorten auf unterschiedlichen Microarray-Plattformen nachgewiesen werden.

Die Beteiligung der Retina-spezifischen miRNAs, miR-182, miR-183 sowie miR-96 an der Tumorentstehung und Invasivität von zahlreichen Krebsarten wurde bereits beschrieben. Eine Untersuchung bezüglich einer möglichen Beteiligung an der Entstehung von Medulloblastomen stand bisher allerdings aus.

In nicht-SHH Medulloblastomen waren diese miRNAs signifikant hochreguliert und mit Tumorlokalisation und Metastasierung assoziiert, während sie in einer 26-miRNA Signatur die am meisten differentiell regulierten miRNAs darstellten. Diese miRNAs waren daher Gegenstand der vorliegenden Doktorarbeit.

Weitere Untersuchungen zur funktionellen Rolle dieser miRNA-Kandidaten wurden in Medulloblastom-Zellen durchgeführt. Mittels *in vitro* und *in vivo* Analysen konnte gezeigt werden, dass die Überexpression von miR-182 in nicht-SHH Medulloblastomen zur metastatischen Ausbreitung von Medulloblastomen beiträgt.

Diese Erkenntnisse über die funktionelle Rolle der Retina-assoziierten miRNAs in nicht-SHH Medulloblastomen liefern erste Hinweise auf eine mögliche Beteiligung dieser miRNAs an der Enstehung metastatischer Medulloblastome. Diese Erkenntnisse könnten einen Beitrag für die Entwicklung gezielter Therapiestrategien für Subgruppen mit besonders schlechter Prognose leisten.

1 INTRODUCTION

1.1 The cerebellum

1.1.1 Background

The cerebellum, comprises only 10% of human brain volume, but it contains more than half of all neurons in the human brain after maturation. Besides, it is the first brain structure undergoing differentiation, but the last part to complete maturation after birth. The cerebellum receives sensory input from the periphery to fine-tune body movements and balance, thus it is the coordination center of the human body (Wang *et al.* 2001).

Anatomically, the cerebellum is located at the bottom of the skull (Fig.1-1), the biggest part of brain, the cerebrum, is right above it and a part of the midbrain called “pons” is in anterior of it. There is a solid layer called “tentorium cerebelli” between the cerebellum and the cerebrum to avoid overlaying. The only connection of the cerebellum to other parts of the brain is through the pons.

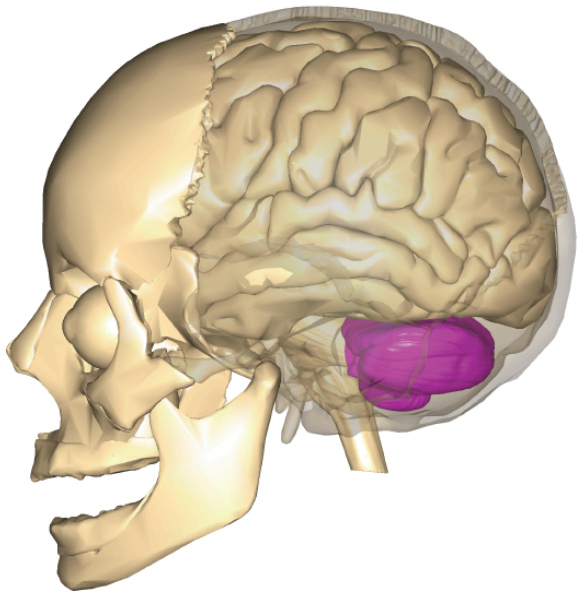

Figure 1-1. Anatomical location of cerebellum. The human skull with posterior part transparented, portion in pink indicates the cerebellum. (Image created by web tool, BodyParts3D, http://lifesciencedb.jp/bp3d/)

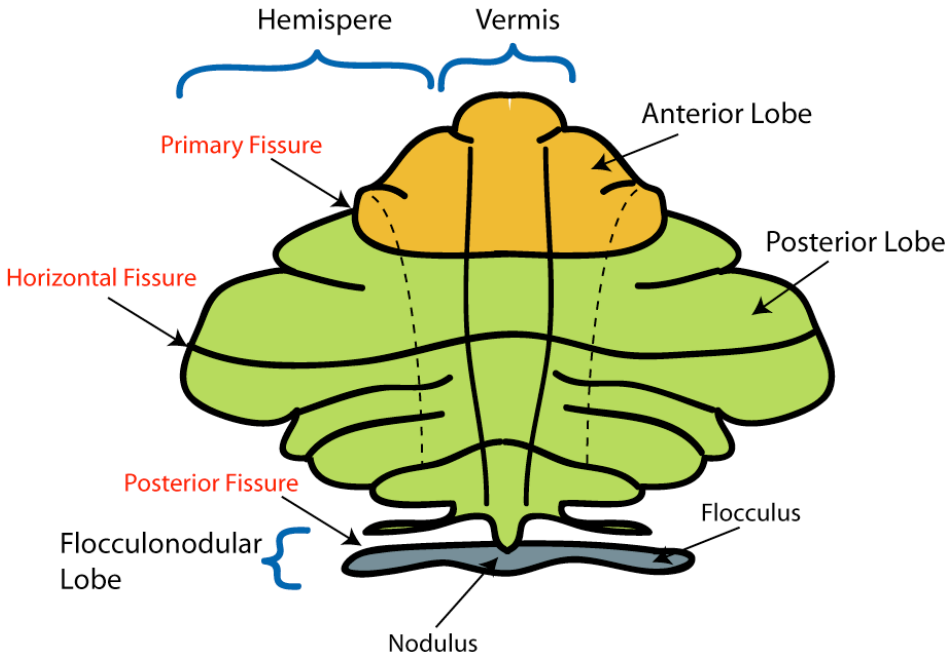

Figure 1-2. Major anatomical divisions of the cerebellum. (Image from https://brassie.ece.jhu.edu/jamwiki/en/3D_Cerebellar_Anatomy)

The cerebellum can be divided into two hemispheres and a narrow midline zone, the vermis. There is a set of large folds to divide the overall structure into 10 smaller "lobules" (Fig.1-2). The location of medulloblastoma is also indicated with these anatomic positions. Meanwhile, the fluid-filled cavity between the cerebellum and the pons is called the fourth ventricle. Together with three other connected cavities, the left and right lateral ventricles, and the third ventricle, they are known as the ventricular system. The fourth ventricle links the cerebral aqueduct and the central canal of the spinal cord, and is filled with cerebrospinal fluid (CSF) (Fig.1-3). When medulloblastoma invades into the forth ventricle, tumor cells may metastasize into the CSF thus leading to leptomeningeal spread.

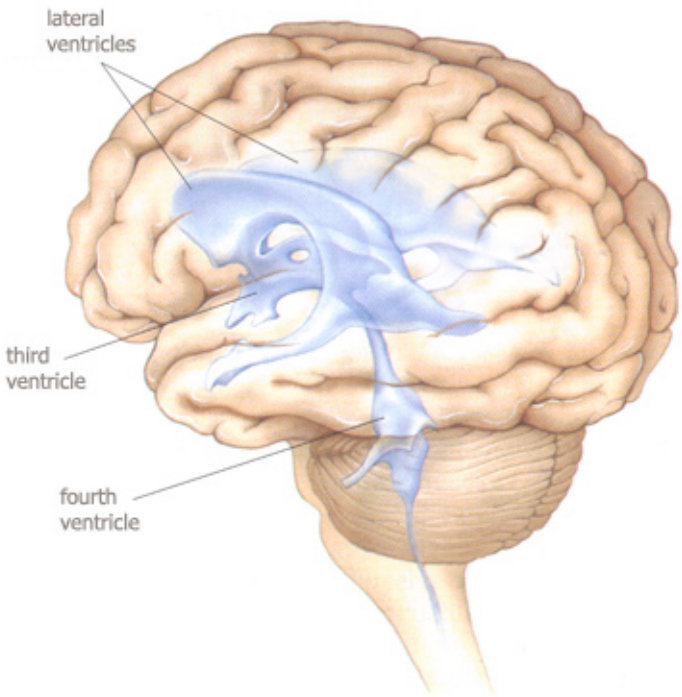

Figure 1-3. The ventricular system in human brain. (Image from (Bear 2001))

1.1.2 Cerebellar development

During embryonic development, two different germinal zones serve as sources for the neurogenesis of different cell types in cerebellum. The dorso-medial ventricular zone along the forth ventricle gives rise to Purkinje cells, which are the major output neurons of the cerebellar cortex, and also to other interneurons including Golgi, basket, and stellate cells. The second germinal zone for neurogenesis is comprised of cells within the rhombic lip called granule cell progenitors (GCPs). Several signaling pathways, such as the Sonic hedgehog (SHH) signaling pathway, promote the proliferation of GCPs and create an external granular layer (EGL) across the cerebellar anlage (Embryonic Day 12.5~15.5). After birth till the second postnatal week, GCPs exit the cell cycle and migrate inward to pass through the Purkinje cell layer and form a mature granular layer, the internal granule cell layer (IGL). Thus, the EGL entirely disappears within the first year after birth under physiologic conditions (Wang *et al.* 2001; Polkinghorn *et al.* 2007; Roussel *et al.* 2011). (Fig.1-4)

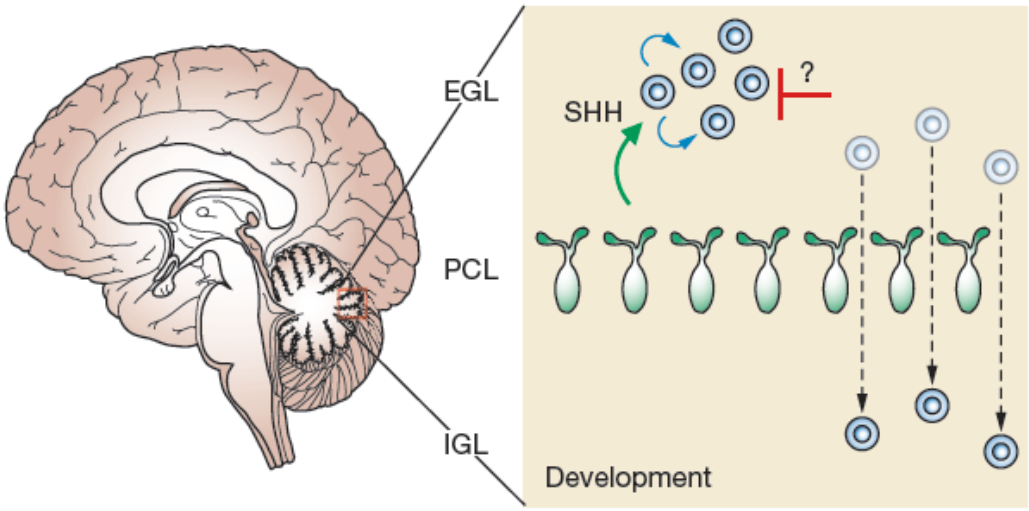

Figure 1-4. Granule cell development. During the cerebellar development, GCPs receive SHH signals from Purkinje cells, which initiat proliferation of the EGL. After birth, GCPs exit the cell cycle and start to migrate through the PCL and form the IGL. (Image from (Polkinghorn et al. 2007))

1.2 Medulloblastoma

1.2.1 Clinical background

Medulloblastoma is classified as an embryonal brain tumor of the highest malignancy grade (grade IV) according to the WHO classification. It shares the specific embryonal cellular morphology with four other embryonal brain tumors, medulloepithelioma, ependymoblastoma, atypical teratoid/rhabdoid tumor, and supratentorial PNET (Louis *et al.* 2007).

Typically medulloblastoma arise in the cerebellar midline and frequently invade the fourth ventricle. Invasion through the bottom part of the ventricle down to the brainstem is also observed (Polkinghorn *et al.* 2007) (Fig.1-5). Although advanced therapeutic strategies lead to a much better survival rate at around 60-70%, many surviving patients experience serious side effects, including cognitive impairment, psychiatric disorders, endocrine dysfunction, and skeletal growth retardation (Polkinghorn *et al.* 2007).

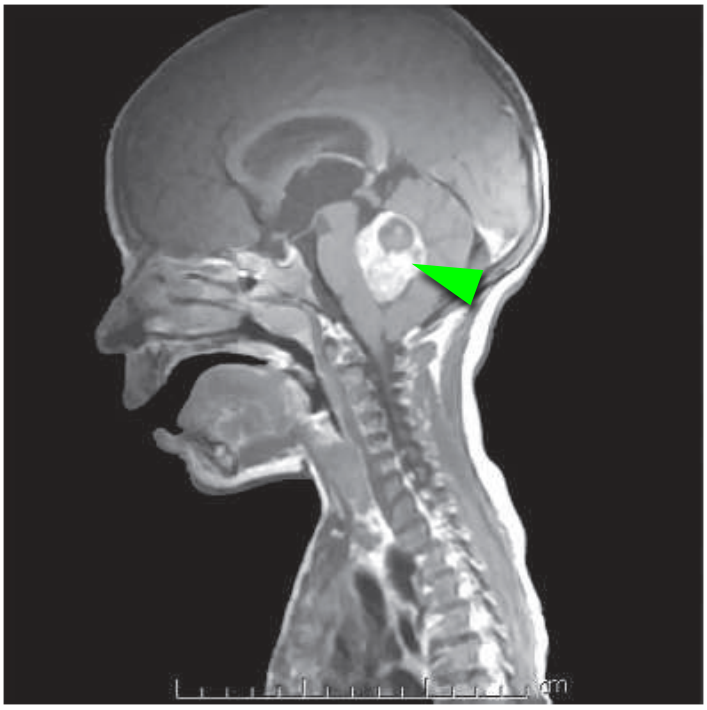

Figure 1-5. MRI scan of a 4-year-old child with medulloblastoma. The tumor mass, indicated by the green arrow, has invaded the fourth ventricle. (Image from (Polkinghorn et al. 2007))

The mean age of medulloblastoma diagnosis is between 3 and 7 years of age (Fogarty *et al.* 2005). Patient's age at diagnosis has served one of the most important prognostic factors. Patients less than 3 years of age, who comprise around 25-35% of all medulloblastoma cases, overall have a much worse prognosis and are thus considered to be high-risk patients (Polkinghorn *et al.* 2007). Patients older than 3 years are grouped into standard and high-risk groups according to metastatic stage.

More than 30% of young medulloblastoma patients exhibit metastatic dissemination via the cerebrospinal fluid (CSF) (Fouladi *et al.* 1999). The presence of tumor cells in the CSF after surgery or macroscopic metastases along the cerebrospinal cord are considered signs of risk increment. Metastatic stage is classified according to Chang's staging system into 5 stages from M0 meaning no evidence of micrometastasis or macrometastasis to M4 meaning evidence of extraneural dissemination. The detailed descriptions are listed in table1A.

Table1A. Chang's metastasis staging system (Chang *et al.* 1969)

Metastasis stage	Description
M0	No evidence of microscopic or macroscopic dissemination
M1	Microscopic tumor cell clusters found in the cerebrospinal fluid
M2	Macroscopic metastases demonstrated in the cerebellar, cerebral subarachnoid space or in the third or lateral ventricles by MRI
M3	Macroscopic metastases seedings in the spinal subarachnoid space
M4	Extraneuroaxial metastasis

Surgical removal of a tumor mass in the brain is different from removing tumors in other organs; neurosurgeons must keep the surrounding normal brain tissue untouched. Hence, the residual tumor size after surgery becomes another clinical variable to make risk assessment. In general, patients with tumor residues larger than 1.5 ml have an increased risk of tumor progression or relapse (Polkinghorn *et al.* 2007). (Table 1B)

Table1B. Prognostic risk assessment (Polkinghorn *et al.* 2007)

Standard risk	patients older than 3 years metastasic stage M0 less than 1.5 ml of residual tumor postoperatively The 5-year survival rate for this group is 67-80%
High risk	patients older than 3 years stage M1-M4 more than 1.5 ml of residual tumor postoperatively The 5-year survival rate for this group is 43-70%
High risk, infant	patients younger than 3 years regardless of M stage and large residual tumor postoperatively The 5-year survival rate for this group is 25-35%

1.2.2 Histopathology

Four histopathologic variances were described and summarized as classic, medulloblastoma with extensive nodularity (MBEN), desmoplastic, and large cell/anaplastic (LC/A) (Louis *et al.* 2007) (Fig.1-5). The classic subtype comprises about 60~68% of medulloblastoma is the most common one; it consists of small, dense, round and uniform cells. The MBEN subtype comprises the smallest portion of medulloblastoma with less than 5%, and mainly occurs in infants with good prognosis (Giangaspero *et al.* 1999). Around 25% of medulloblastomas are identified as desmoplastic subtype; these patients were reported to have a better prognosis than patients with classic, and LC/A subtype medulloblastoma (Jenkin *et al.* 2000). The LC/A subtype consists of mostly undifferentiated cells and comprises about 5% of medulloblastoma. They show a characteristic cell morphology with large, atypical nuclei and and are frequently associated with CSF dissemination and, hence, inferior outcome (Brown *et al.* 2000).

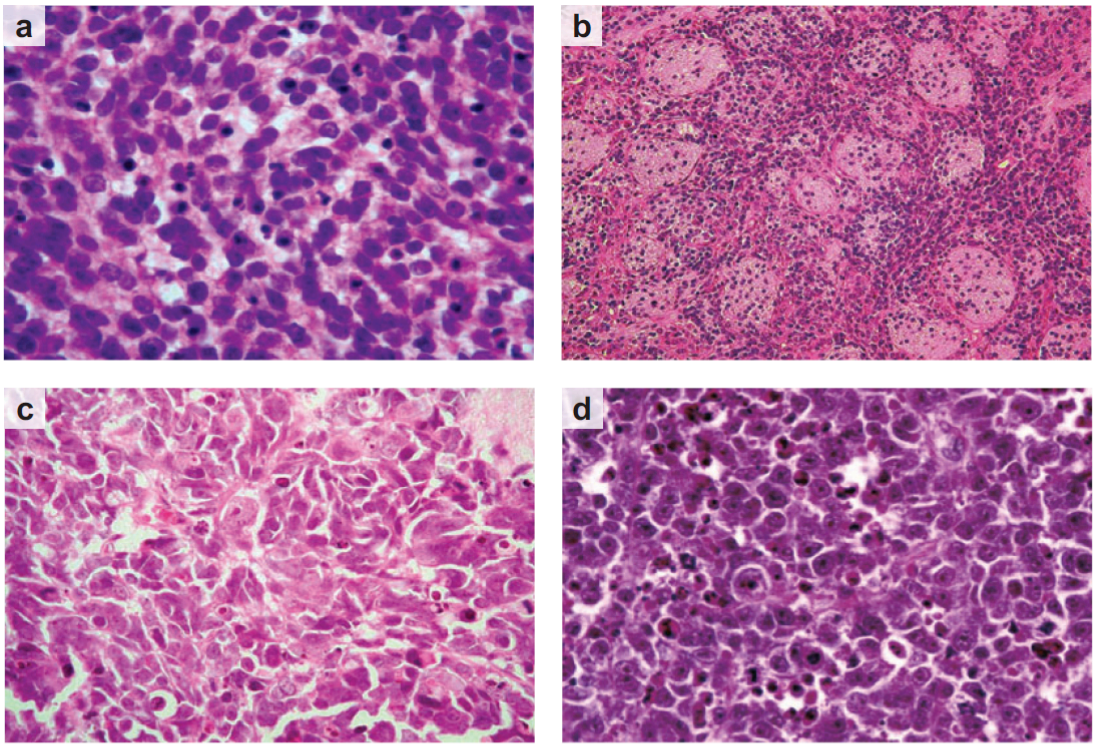

Figure 1-5. Histopathologic types of medulloblastoma. (a) Classic medulloblastomas look like a sheet of small uniform cells with a compact, dense nucleus and a high nucleus-to-cytoplasm ratio. (b) Nodular/

desmoplastic medulloblastomas show a mixed morphology with nodules of differentiated neuronal cells surrounded by low cell density desmoplastic internodular zones. (c) Anaplastic medulloblastomas are composed of pleomorphic cells with polyhedral forms and a high cell density. (d) Large-cell medulloblastomas are comprised of groups of large uniform cells with vesicular nuclei and a single nucleolus. Anaplasia is especially observed within this medulloblastoma subtype. (Image from (Gilbertson *et al.* 2008))

1.2.3 Cytogenetic aberrations in medulloblastoma

Cytogenetic aberrations have been established as important prognostic factors in medulloblastoma. Chromosome 17p deletion has been recognized as the most common chromosomal aberration in medulloblastoma for a long time. Many studies were focused on the impact of losing a copy of potential tumor suppresser genes on 17p and the prognostic role of 17p deletion in medulloblastoma (De Smaele *et al.* 2004). However, this chromosome alteration did not show a highly significant relationship with clinical outcome alone or further combined with isochromosome 17q[i(17q)], i.e. concomitant loss of 17p and gain of 17q (Cogen *et al.* 1992; Emadian *et al.* 1996; Biegel *et al.* 1997; Scheurlen *et al.* 1998; Gilbertson *et al.* 2001). Recent publication redefined the prognostic value of chromosome alteration on chromosome 17 in a large uniformly treated patient cohort (Pfister *et al.* 2009). It clearly showed gain of chromosome 17q or i(17q) to be associated with inferior prognosis.

Medulloblastoma patients with chromosome 6q gain or a trisomy of chromosome 6, and amplification of *MYC*/*MYCN* have been shown to have the worst overall survival rates (Ellison 2002; Pfister *et al.* 2009). Furthermore, *MYC*/*MYCN* amplification is strongly associated with the LC/A subtype. In contrast, patients with medulloblastomas carrying a monosomy of 6 or have balanced copy-number profiles for 6q and 17q have a more favorable clinical outcome (Ellison 2002; Pfister *et al.* 2009).

1.2.4 Molecular genetics of medulloblastoma

Medulloblastoma was first distinguished from other brain tumors in 1910 (Wright 1910). However, after 100 years' of research, the cellular origin of this tumor is still uncertain for some of the biological subgroups of medulloblastoma.

A fraction of medulloblastomas arise from the granular cell progenitors (GCP) in the external granular layer of the cerebellum. Aberrant signaling pathways and proteins regulating normal GCP development and growth cause GCPs to insist proliferation or miss appropriate control signals for stopping GCP proliferation; this finally results in the formation of medulloblastoma (Marino 2005; Knoepfler *et al.* 2006).

Recent study showed the neuronal stem cells in the the ventricular zone (VZ) germinal matrix, another primary germinal epithelia of the cerebellum which gives rise to many neuronal and glial cell types in the cerebellum, also act as an origin of medulloblastoma via different aberrant signaling pathways (Fan *et al.* 2008).

Sutter R *et al.* demonstrated that both GCP and non-GCP like neuronal stem cells, or cerebellar stem cells, could give rise to medulloblastoma in mice recently. Moreover, different embryonal signaling pathways appear to be involved in the formation of tumors from different cells of origin (Sutter *et al.* 2010). Altogether, these studies demonstrate that the origin of medulloblastoma is multiple.

1.2.4.1 Sonic hedgehog signaling pathway

The sonic hedgehog (SHH) signaling pathway is a key regulator of GCP proliferation. When SHH ligand binds to Patched 1 (PTCH1), it will release Smoothened (SMO). SMO in turn up-regulates downstream SHH targets, e.g., GLI family transpciption factors including GLI1, GLI 2, and GLI 3; meanwhile the GLI inhibitor suppressor-of-fused (SUFU) is getting inactivated. This result physiologically in an overall growth of the midbrain/hindbrain during embryonic cerebellar development (Wechsler-Reya *et al.* 1999; Blaess *et al.* 2006). (Fig.1-6)

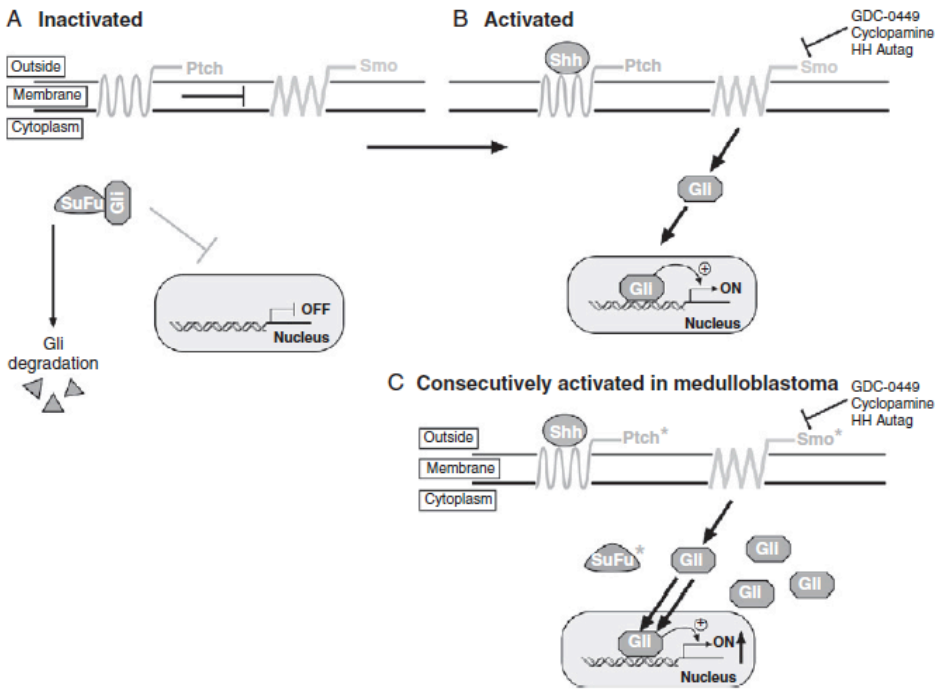

Figure 1-6. Sonic hedgehog (SHH) signaling pathway. (A) In the absence of SHH ligand, SMO is suppressed by PTCH, thus the transcripton factor GLI is inhibited by SuFu and degreaded in the cytoplasm. (B) When SHH ligand is present, SMO gets released from PATCH inhibition and activates GLI. (C) In medulloblastom, loss of PATCH and mutation of SUFU or SMO cause aberrant activity of SMO. Increased GLI accumulation thus upregulates downstream targets that affect proliferation. (* indicates the aberrant protein in medulloblastoma) (Image from (Roussel et al. 2011))

The first PTCH genetic modified mice model in the recent studies demonstrate that *PTCH1* heterozygous knockout mice have a significantly lower incidence rate of medulloblastoma after inhibition of *Gli1* suggesting that GLI has an important role in SHH-associated medulloblastoma formation (Kimura *et al.* 2005). In contrast to PTCH heterozygous mice with *Tp53* knockout, $PTCH1^{+/-}$; $Tp53^{-/-}$, showed faster medulloblastoma development and proliferation, also invasion into the brainstem matching the phenotype of SHH-driven tumors which have more serious metastatic dissemination in human (Gibson *et al.* 2010).

SHH signaling also regulates the expression of many cell cycle regulators including cyclin D1 (CCND1) and cyclin D2 (CCND2) (Kenney *et al.* 2000). During early postnatal cerebellar development, GCPs express CCND1 in the beginning and both CCND1 and CCND2 are highly expressed during the peak of neuogenesis. Knocking out both *Ccnd1* and *PTCH1* in mice has been demonstrated to lead to an inhibition of medulloblastoma formation (Pogoriler *et*

al. 2006). Another major effect of constitutive SHH signaling is the upregulation of the proto-oncogene *MYCN* (Kenney *et al.* 2000). Upregulation of *MYCN* results in an activation of D-type cyclins and repress the expression of many cyclin-dependent kinase inhibitors, which might drive GCPs to stay in the cell cycle (Knoepfler *et al.* 2006).

In medulloblastomas, about 25% exhibit SHH hyperactivation, frequently being associated with desmoplastic histology, and hemispheric tumor location (in contrast to the majority of medulloblastomas arising in the cerebellar midline) (Polkinghorn *et al.* 2007).

1.2.4.2 Wingless signaling pathway

Canonical Wingless (WNT) signaling pathway activation is initiated by the binding of Wnt ligand to its transmembrane receptor, Frizzled. This activates the Disheveled protein and destablizes a protein complex containing β-catenin (CTNNB1), GSK-3β, axin 1 and 2, the adenomatous polyposis coli (APC), and caseine kinase a (CK1a). Once CTNNB1 is released from the complex, it enters the nucleus and activates the transcription factors LEF/TCF1 thereby inducing the expression of downstream proliferative target genes such as *MYC* and *CCND1.* (Fig.1-7)

Aberrant WNT signaling is observed in 10-15% of medulloblastomas. Deregulated WNT signaling is mainly caused by mutations in *CTNNB1* (Thompson *et al.* 2006), occasionally by mutations in *APC* and *Axin* (Gilbertson *et al.* 2008), and frequently associated with monosomy of chromosome 6. Monosomy 6 is the most recognizable prognostic factor in WNT subgroup medulloblastomas, and it is associated with favorable clinical outcome (Pfister *et al.* 2009). A study by Gibson *et al*. also demonstrated that normal stem cells derived from the lower rhombic lip carrying mutant CTNNB1 on a p53 negative background give rise to tumors with classic medulloblastoma histology in mice (Gibson *et al.* 2010).

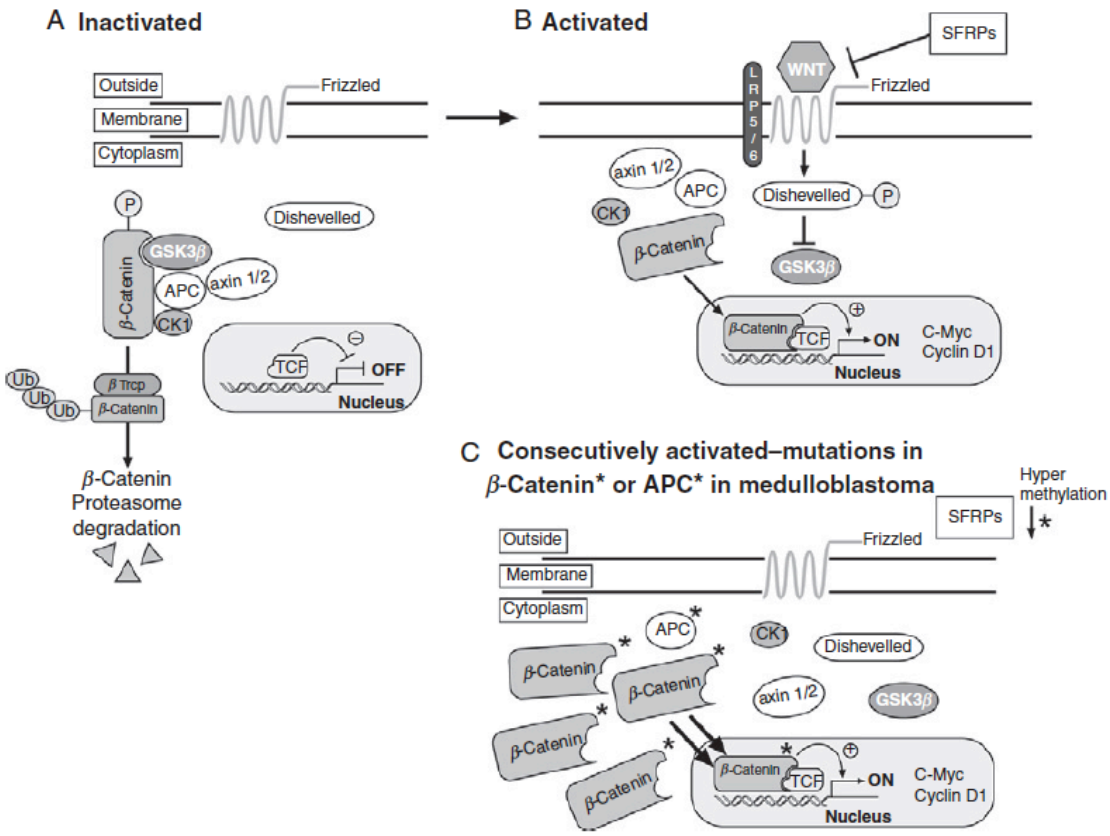

Figure 1-7. WNT signaling pathway. (A) In the absence of WNT ligand, the trans-membrane receptor frizzled is inactivated and β-catenin is kept in a complex with GSK-3β kinase, axin 1 and 2, CK1a, and APC; β-catenin is getting degraded by the proteasome. (B) When WNT ligand is present, frizzled is activated leading to an inhibition of GSK-3β kinase. β-catenin is released from the complex and activates downsteam targets such as C-Myc, and cyclinD1. (C) In medulloblastoma, mutated APC, CTNNB1, and hypermethylation of SFRP1 leads to the accumulation of β-catenin in the nucleus which leads to the constitutive activation of downstream targets. (Image from (Roussel et al. 2011))

1.2.4.3 Epigenetic mechanisms in medulloblastoma development

Epigenetic alterations also play a role in the development of medulloblastoma. Recent studies showed a lot of evidence for tumor-specific gene silencing by DNA methylation, such as silencing of the S100 gene family (Lindsey *et al.* 2007), Kruppel-like factor 4 (Nakahara *et al.* 2010), and loss of WNT inhibition owing to the epigenetic silencing of SFRPs (Pfister *et al.* 2007). Conversely, secreted frizzled-related protein 1 (SFRP1) was found to be specifically overabundant in the SHH medulloblastoma subgroup, and may be used as a

specific immunohistochemistry marker to identify the SHH subgroup (Northcott *et al.* 2010).

1.2.4.4 Molecular subgrouping of medulloblastoma

Apart from developmental pathways as discussed above, many other signaling pathways and mechanisms are involved in medulloblastoma formation. Using high-throughput molecular genetic tools, several studies showed that medulloblastoma at least consists of four distinct molecular variants. WNT and SHH subgroups were consistantly separated by all studies, whereas the remaining tumors may be seprated into 2 to 4 groups (Kool *et al.* 2008; Cho *et al.* 2010; Northcott *et al.* 2010; Remke *et al.* 2011; Remke *et al.* in press). While cinical risk stratification algorithms were prone to misclassification rates of 20-40% (Polkinghorn *et al.* 2007), taking molecular information into account will help to accurately assess the required treatment intensity for medulloblastoma patients in the near future.

1.3 MicroRNAs

1.3.1 Background

MicroRNAs (miRNAs) have been a major research focus in molecular biology for the last decade. They are endogenous, short (21-25 nucleotides), non-coding RNA molecules. Studies indicated that miRNAs control many cellular activities via regulation of almost 60% of protein-coding genes (Fabian *et al.* 2010). Furthermore, they also playing important roles in almost every cellular process and in tumorigenesis. Moreover, they have specific expression profiles in different somatic tissues and cancer types (He *et al.* 2005; Lu *et al.* 2005; Bushati *et al.* 2007).

However, the specific roles of miRNAs in medulloblastoma are rarely concerned. The only consistent finding to date was the identification of the miR-17/92 cluster as an oncogene in SHH-driven medulloblastoma (Northcott *et al.* 2009; Uziel *et al.* 2009).

Based on bioinformatic predictions, it is now believed that miRNAs control the activity of more than 60% of the mammalian protein coding genes (Friedman *et al.* 2009), however the detailed mechanism underlying the role of miRNAs as protein synthesis regulator is still unclear. From the current knowledge, most miRNAs regulate gene expression post-transcriptionally through binding to the 3`-untranslated region (3`-UTR) of their target mRNA via base-pairing, either by perfect match functionally as small interfering RNAs (siRNAs) which leads to the degrdation of target mRNA, or via partial complementary sequences leading to inhibition of target mRNA translation (Filipowicz *et al.* 2008; Fabian *et al.* 2010).

1.3.2 The biogenesis of microRNAs

The initiation of miRNA biogenesis takes place inside the nucleus. Primary miRNAs (pri-miRNAs) are either transcribed from independent miRNA genes or from the intron region of protein coding genes by using RNA polymerase II. A single pri-miRNA might be up to 1Kb or longer in size and includes 5`-caps and 3`ploy(A) tails. The pri-miRNA transcript folds into a hairpin structure with imperfect hairpin loops containing signals for dsRNA-specific nuclease cleavage. Besides, one pri-miRNA might carry one or multiple miRNAs. Such miRNAs that are located closely together within around 1Kb distance are frequently called a miRNA cluster.

The second step of miRNA processing is the cleavage of the pri-miRNA into a precursor miRNA (pre-miRNA). This step is catalyzed by the dsRNA-specific ribonuclease III (RNaseIII) endonuclease, Drosha, and its partner dsRNA binding protein, DiGeorge syndrome critical region gene 8 (DGCR8). The Drosha-DGCR8 complex cleaves the long pri-miRNA into a ~70-nucleotide hairpin-shaped pre-miRNA. The pre-miRNA is directly exported from the nucleus to the cytoplasm by Exportin-5, which is thereby essential for miRNA biogenesis (Yi *et al.* 2003; Bohnsack *et al.* 2004).

Once the pre-miRNA enters the cytoplasm, another complex including RNAaseIII endonuclease, Dicer, and the dsRNA binding protein, TAR RNA binding protein (TRBP), cleaves the pre-miRNA into a ~21-nucleotide mature miRNA duplex. One strand, usually the 5` end, is released to function as mature miRNA, whereas the other stand is degraded (Du *et al.* 2005; Bushati *et al.* 2007; Peters *et al.* 2007; Filipowicz *et al.* 2008).

Mature miRNAs are then incorporated into a ribonucleoprotein (RNP) complex called micro-RNPs (miRNPs) or miRNA-induced silencing complex (miRISC). These complexes are getting established by proteins of the Argonaute (AGO) family. AGO proteins including AGO1 to AGO4 collaborate with mature miRNAs to regulate protein synthesis via imperfect base-pair binding at the 3`-UTR of target mRNAs, whereas only AGO2 works in concert with siRNAs in the 3`-UTR of target mRNA to inhibit translation via cleavage of target mRNA (Peters *et al.* 2007; Filipowicz *et al.* 2008). (Fig.1-8)

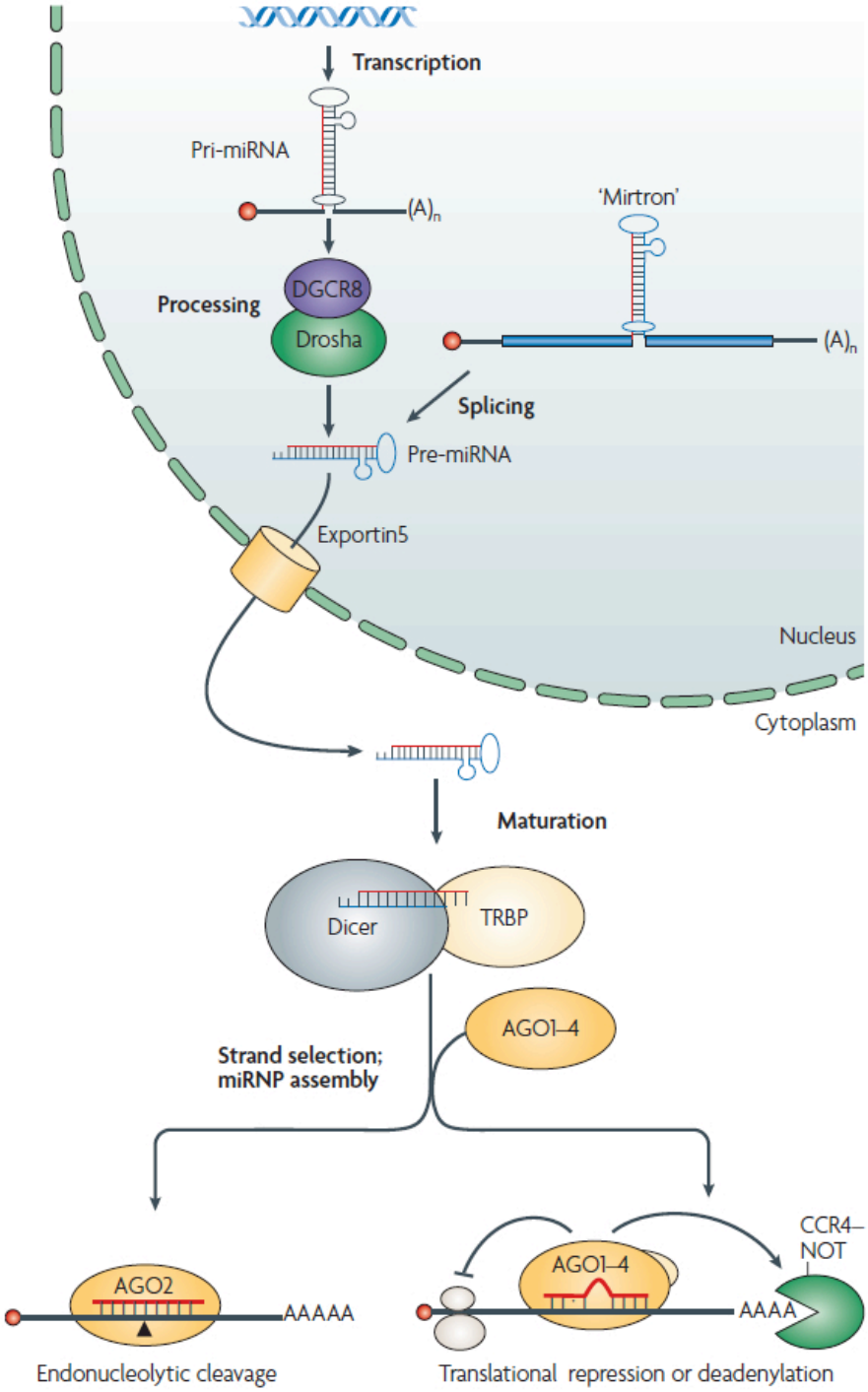

Figure 1-8. Biogenesis of miRNAs in the mammalian cell.
(image from (Filipowicz *et al.* 2008)) .

1.3.3 Mechanisms of miRNA deregulation in human cancer

It is well established, that micro-RNAs may act as either tumor suppressors or oncogenes during tumorigenesis (Deng *et al.* 2008; Medina *et al.* 2008). The basic biological function of miRNAs is the reduction of protein levels of target genes. However, recent studies also showed that some miRNAs are capable of activating mRNA translation (Vasudevan *et al.* 2007; Orom *et al.* 2008). Several studies in different cancer entities have provided evidence that miRNA dysfunction in human cancer is caused by multiple underlying mechanisms.

1.3.3.1 Transcriptional deregulation of miRNAs

The oncogene *c-MYC*, a frequently reported deregulated gene in human cancer, works closely together with the miR-17/92cluster, and the expression of many other miRNAs are also regulated by the transcription factor c-Myc (O'Donnell *et al.* 2005; Chang *et al.* 2008). When *c-Myc* is aberrantly upregulated in human cancer, it also upregulates the expression of the miR-17/92 cluster to cooperatively accelerate tumor cell proliferation and confer resistance to apoptosis (He *et al.* 2005). Thus, the miR-17/92 cluster is a prototypic cluster of “onco-miRs”.

Conversely, the tumor suppressor gene *TP53* activates the transcription of the tumor suppressor miRNA miR-34 family; they cooperate in control of cell proliferation (Corney *et al.* 2007; Hermeking 2007). Thus, transcriptional deregulation is a key step of miRNA dysfunction in human cancer.

1.3.3.2 Epigenetic regulation of miRNA genes

Epigenetic alterations including DNA methylation and histone modification have important roles in the regulation of protein-coding gene expression and chromatin remodeling in human cancer (Esteller 2008). DNA hypermethylation in the miRNA 5′-UTR is an important mechanism for the down-regulation of miRNA expression in many tumor types (Saito *et al.* 2006; Lujambio *et al.* 2007).

Recent evidence indicates that epigenetic silencing accounts for 36% of miRNA down-regulation in epithelial ovarian cancer (Zhang *et al.* 2008). Whereas hypermethylation of the miR-124a promoter region also causes the silencing of miR-124a expression and activation of the cyclin D–kinase 6 (*CDK6*), a bona fide oncogene (Lujambio *et al.* 2007).

1.3.3.3 Germline/somatic mutation of miRNAs

Germline or somatic mutations of protein-coding genes leading to the loss- or gain-of-function of tumor suppressor genes or oncogenes are widely reported in human cancer. The frequent deletion of the chromosome region13q14 in chronic lymphocytic leukemia (CLL) was the first direct evidence that miRNAs play a role in human cancer (Dohner *et al.* 2000). Sutdies focusing on the identification of germline mutation in CLL found A/C to T mutations in the pri-miRNA of miR-16-1 and miR-15a in 2 out of 75 patients. The authors demonstrated that miR-15a and miR-16-1, which are located at 13q14 were deleted in more than 50% of CLL patients, and consecutively showed reduced expression of these miRNAs (Bullrich *et al.* 2001; Calin *et al.* 2002).

Another more recent study also demonstrated DNA copy- number losses to cause downregulation of miRNA expression in approximately 15% of epithelial ovarian cancer (Zhang *et al.* 2008). Furthermore, these mutations are associated with lower expression of the mature miRNAs (Calin *et al.* 2004). Another study also identified single nucleotide polymorphisms (SNPs) distributed in the region of pri-, pre-, and mature miRNAs in human tumor tissues and cancer cell lines. However, most of these mutations did not reduce the expression of miRNAs, only one mutation found in miRNA let-7e caused a significant reduction of expression *in vivo* (Wu *et al.* 2008).

1.4 MicroRNA profiling in medulloblastoma

Modern high-throughput miRNA quantification technologies helped scientists to evaluate miRNA expression profiles in human cancer in a more reliable and faster way. Genome-wide miRNA expression studies revealed close associations between miRNA clusters and tumor subtype as well as clinical subgroups (Zhang *et al.* 2008; Ferretti *et al.* 2009).

In medulloblastoma, first miRNA profiling studies demonstrated that it is possible by miRNA signatures to discriminate histological subtype, e.g., classic from anaplastic medulloblastomas. Furthermore, miR-31 and miR-153 were shown to be downregulated in clinical high risk patients (Ferretti *et al.* 2009; Pang *et al.* 2009). Another study identified the miR-17/92 cluster to be significantly upregulated in SHH-driven medulloblastoma. The authors confirmed that these miRNAs promote proliferation and contribute to the development of medulloblastoma *in vitro* and *in vivo* (Northcott *et al.* 2009; Uziel *et al.* 2009).

In the present study as well as in a recent report by Cho *et al*. (Cho *et al.* 2010), the miR-183~96~182 cluster was found to be significantly associated with non-SHH medulloblastoma.

The miR-183~96~182 cluster was first reported to be highly expressed in adult murine retina (Xu *et al.* 2007). The authors confirmed the specific high expression levels of these miRNAs in retinal photoreceptors and the interneurons in the inner nuclear layer, but did not detect any expression in adult brain or other tissues. The cluster consists of three members, namely miR-182, miR-183, and miR-96, which are located closely together on mouse chromosome 6qA3 and the orthologous human chromosome 7q32.2, respectively. Moreover, both miRNA sequences in mouse and human are identical indicating that they are highly conserved between species. The genes within 4kb of these miRNAs are transcribed in the same direction (telomere to centromere) and have a large upstream CpG island together with multiple transcription factor binding sites, such as for OTX1 (Xu *et al.* 2007).

Recent studies reported these miRNAs to be deregulated in diverse types of human cancer including melanoma, medulloblastoma, breast cancer, pancreatic cancer, and lung cancer. However the reported mechanism of aberrant

expression, and functional impact of overabundance seems to be cell-type specific since they were largely different between different entities (Segura *et al.* 2009; Cho *et al.* 2010; Gokhale *et al.* 2010; Lowery *et al.* 2010; Yu *et al.* 2010; Zhang *et al.* 2011).

During this dissertation work, Cho *et al.* reported the distinct miRNA expression profiles in medulloblastoma subgroups (Cho *et al.* 2010). Coincidently, they also find the miR-183~96~182 is associated with non-SHH subgroups with another patient cohort in the US. However, the here presented provided more information about the detail functional role of the miR-183 family in medulloblastoma.

In summary, the miR-183~96~182 cluster might have different, even opposing functions in different cellular contexts. Thus, it was intriguing to unravel its role in medulloblastoma, in which it is very highly expressed in subsets of tumors.

1.5 Technical introduction – The 3D microchannel migration assay

The most commonly used *in vitro* functional assays to assess cell migration or invasion have been carried out on a flat surface (i.e. in two dimensions). Examples for such assays include the scratch assay (also called wound-healing assay), for which cells are seeded on plastic culture dishes or chambered glass slides, or the Boyden chamber assay, which is carried out on a polyethylene terephthalate (PET) or polycarbonate membrane with small pores on it (Fig.1-9).

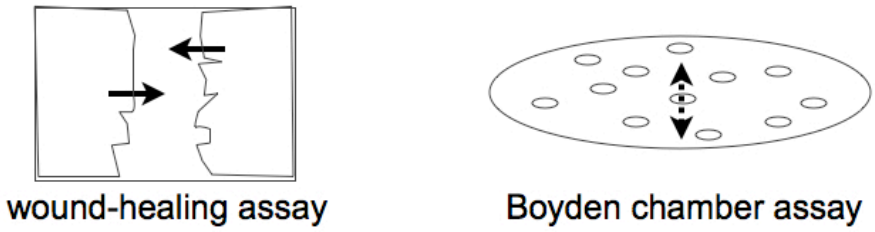

Figure 1-9. Cell migration directions in commonly used two dimensional *in vitro* migration assays. Migration of seeded cells in the wound-healing assay is observed on a plain surface, and directed towards the cells at the opposite side of the wound. In the Boyden chamber assay, the cells may vertically pass through the pores of the membrane from the upper chamber to the lower chamber. To assess invasion, the membrane may be coated with extracellular matrix proteins, e.g. the matrigel, in a way that the cells have to pass through this layer first before they can pass throuogh the pores of the membrane.

The main limitation of these two dimensional (2D) environments might be, that they do not correctly represent the situation *in vivo* (Fig.1-10). Former studies have shown that the malignant phenotype of breast cancer cells can be reversed to a non-malignant phenotype by applying beta1-integrin antibody treatment in a three dimensional (3D) culture system and *in vivo*, which could not be observed in 2D cultures (Weaver *et al.* 1997).

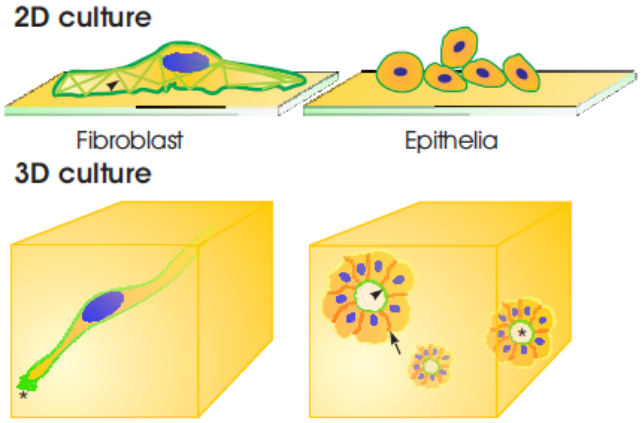

Figure 1-10. Different cell morphologies and behaviors in 2D and 3D culture. (Image from (Weaver *et al.* 1997))

To provide a better *in vitro* model to reproduce the *in vivo* 3D environment adequately, our collaborators, Dr. Ralf Kemkemer and Claudio Rolli from the Max Planck Institute for Intelligent Systems, Stuttgart, Germany, have created a micro-fabricated device with channel structures mimicking an *in vivo* 3D environment to monitor cell migration.

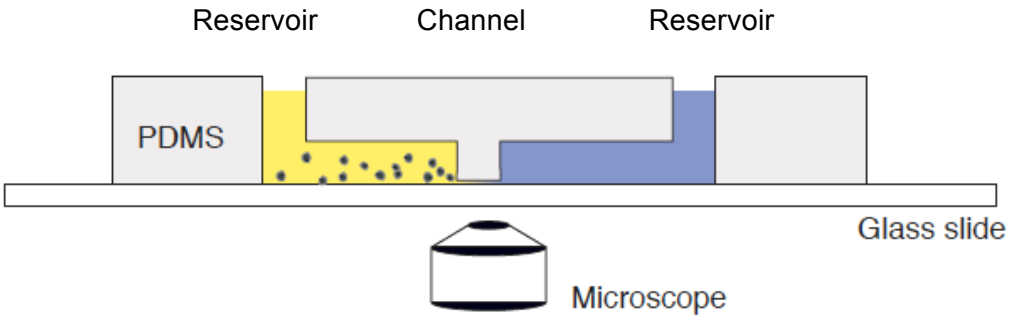

Figure 1-11. Schematic view of a 3D microchannel structure. (Image from(Rolli 2008))

The microchannel structure is made from Poly(dimethylsiloxane) (PDMS), which is a non-toxic, biologically inert, optically transparent, easy to handle and commercially available material. PDMS is very hydrophobic but its surface is treated with a thin oxidized layer, which facilitated secure mounting onto a glass surface (Rolli 2008). The schematic view in Fig. 1-11 and the microscopic view in Fig. 1-12 illustrate the two reservoirs, which are separated by the channel structures through which the cells migrate. An inverted microscope underneath

enables to observe cell migration through the microchannels in real-time. The difference between the experimental set up in this study and the original design (Rolli 2008) is that the two reservoirs in our setup contain the same culture medium and thus cells pass through the channel spontaneously without any chemoattraction.

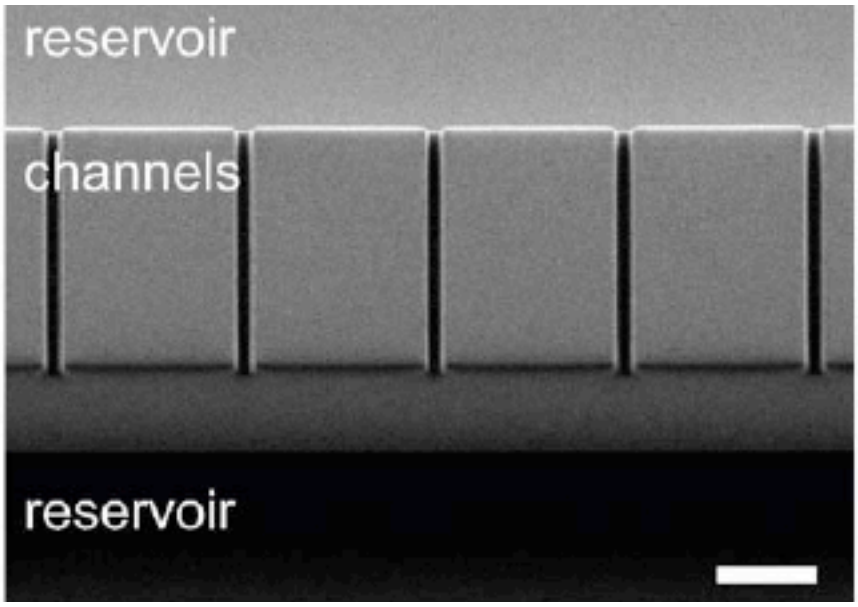

Figure 1-12. Microscopic view of microchannels. Electron microscope image of the PDMS microchannels. The structures refer to channels with the size of 7x11x150 µm (WxHxL) Scale bar, 50 µm (Image from(Rolli *et al.* 2010)).

1.6 Aim of the study

This study aimed to identify miRNA-based pathomechanisms, subgroup-specific microRNA signatures (including prognostic markers), and the functional impact of their respective target genes in medulloblastoma.

2 MATERIALS AND METHODS

2.1 Materials

2.1.1 Biochemical reagents

Substance	Supplier
2-mercaptoethanol	Sigma Aldrich, Munich, Germany
40% Acrylamide/Bis Solution (1:29)	BioRad, Munich, Germany
Agarose	Sigma Aldrich, Munich, Germany
Ammoniumpersulfate (APS)	Roth, Karlsruhe, Germany
Ampicillin	Roche Diagnostics, Mannheim, Germany
Bacto Agar	Difco Laboratories, Detroit, USA
Bacto tryptone	Difco Laboratories, Detroit, USA
Bacto yeast extract	Difco Laboratories, Detroit, USA
Bromophenole blue	AppliChem, Darmstadt, Germany
Copper-(III)-sulfate	Sigma Aldrich, Munich, Germany
Dimethylsulfoxide	Sigma Aldrich, Munich, Germany
Dithiothreitol	Sigma Aldrich, Munich, Germany
Ethanol	Merck, Darmstadt, Germany
Ethidium bromide	Sigma Aldrich, Munich, Germany
Glycerol	Roth, Karlsruhe, Germany
Glycine	Roth, Karlsruhe, Germany
Hydrochloric acid	Merck, Darmstadt, Germany
Magnesium chloride	Merck, Darmstadt, Germany
Methanol	Merck, Darmstadt, Germany
Nuclease free water	Ambion, Austin, USA
Rnase free water	Qiagen, Hilden, Germany
Skim milk powder (blotting grade)	Sigma Aldrich, Munich, Germany
SOC medium	Invitrogen, Karlsruhe, Germany
Sodium chloride	Merck, Darmstadt, Germany
Sodium acetate	Merck, Darmstadt, Germany
Sodium dodecyl sulfate	Sigma Aldrich, Munich, Germany
Tetramethylethylenediamine (TEMED)	Roth, Karlsruhe, Germany
Tris-base	Sigma Aldrich, Munich, Germany
Tween 20	Sigma Aldrich, Munich, Germany
Zeocin	Invitrogen, Karlsruhe, Germany

2.1.2 Solutions and Buffers

Solution	Composition
Laemmli-buffer (5x)	8 % SDS, 200 mM Tris, 0.08 % bromphenol blue, 40 % glycerol, 10 % 2-mercaptoethanol, pH 6.8
Phosphate buffered saline (PBS)	137 mM NaCl, 2.7 mM KCl, 9.2 mM Na2HPO4, 1.8 mM KH2PO4, pH 7.4
SDS-PAGE buffer	25 mM Tris, 200 mM glycine, 0.5% SDS, pH 8.8
Western Blot stripping solution	62.5 nM Tris-HCl, 2% SDS, 200 nm 2-mercaptoethanol, pH 6.7
Tris-borate-EDTA (TBE)	89 mM boric acid, 89 mM Tris-base, 2 mM EDTA,pH 8.0
Tris buffered saline (TBS)	150 mM NaCl, 10 mM Tris, pH 7.4
Tris buffered saline Tween20 (TBS-T)	150 mM NaCl, 10 mM Tris, 0.05% (v/v) Tween20, pH 7.4

2.1.3 Enzymes

Enzyme name	Supplier
BamH1	Roche Diagnostics, Mannheim, Germany
EcoR1	Roche Diagnostics, Mannheim, Germany
FastStart Taq DNA Polymerase	Roche Diagnostics, Mannheim, Germany
MultiScribe Reverse Transcriptase	Applied Biosystems, Foster City, USA
Proteinase K	Roche Diagnostics, Mannheim, Germany
Rnase A	Qiagen, Hilden, Germany
T4 Ligase	Fermentas, St. Leon-Roth, German
Xho1	Roche Diagnostics, Mannheim, Germany
DNase	Roche Diagnostics, Mannheim, Germany

2.1.4 Medulloblastoma cell lines

Name	Provider / Supplier
D458Med	Dr. Darell D. Bigner, Duke University North Carolina, USA
DAOY (Cat#HTB-186)	American Type Culture Collection (ATCC), Manassas, USA
Med8A	Dr. Michael D. Taylor, University of Toronto, Canada

2.1.5 Cell culture

Reagent	Supplier
24-well / 6well culture plate	SPL Life Sciences, Gyeonggi-do, Korea
6.5mm Transwell with 8um Pore Polycarbonate Membrane insert	Corning Sigma Aldrich, Munich, Germany
BD BioCoat 24-well Matrigel invasion chambers	BD Biosciences, Heidelberg, Germany
Dulbecco´s Modified Eagle Medium (DMEM)	Sigma Aldrich, Munich, Germany
Fetal bovine serum (FBS)	Gibco Invitrogen, Karlsruhe, Germany
Filtered screw cap culture flask	TPP Techno Plastic Products, Trasadingen, Switzerland
Improved MEM Zn++ Option (Richter's Modification)	Gibco Invitrogen, Karlsruhe, Germany
Lab-Tek II Chambered Coverglass (8-well)	Nunc Thermo Scientific, Langenselbold, Germany
Opti-MEM I Reduced-Serum Medium	Gibco Invitrogen, Karlsruhe, Germany
Penicillin/Streptomycin (1000 U/ml)	Gibco Invitrogen, Karlsruhe, Germany
Phosphate Buffered Saline (PBS)	Gibco Invitrogen, Karlsruhe, Germany
Trypsin/EDTA (0.05%w/v)	Invitrogen, Karlsruhe, Germany

2.1.6 Kits

Product name	Supplier
AllPrep RNA/Protein Kit	Qiagen, Hilden, Germany
BigDye Terminator Sequencing kit	Applied Biosystems, Foster City, USA
ECL Western Blot detection kit	GE Healthcare, Munich, Germany
FastStart High Fidelity PCR System	Roche Diagnostics, Mannheim, Germany
miRNeasy Mini Kit	Qiagen, Hilden, Germany
QIAamp DNA Mini Kit	Qiagen, Hilden, Germany
QIAGEN Plasmid Maxi Kit	Qiagen, Hilden, Germany
QIAprep Spin Miniprep Kit	Qiagen, Hilden, Germany
QiaQuick gel extraction kit	Qiagen, Hilden, Germany
QIAquick PCR Purification Kit	Qiagen, Hilden, Germany
RNA 6000 Nano kit	Agilent Technologies, Santa Clara, USA
TaqMan MicroRNA Reverse Transcription Kit	Applied Biosystems, Foster City, USA
TaqMan Universal PCR Master Mix	Applied Biosystems, Foster City, USA
TOPO TA Cloning Kits	Invitrogen, Karlsruhe, Germany

2.1.7 Taqman probes and anti-miR siRNA

Product name & ID	Supplier
TaqMan MicroRNA Assays 00597, has-miR-182	Applied Biosystems, Foster City, USA
TaqMan MicroRNA Assays 000484, has-miR-183	Applied Biosystems, Foster City, USA
TaqMan MicroRNA Assays 000434, has-miR-96	Applied Biosystems, Foster City, USA
TaqMan MicroRNA Assays 001093, RNU6B	Applied Biosystems, Foster City, USA
TaqMan MicroRNA Assays 001002, RNU66	Applied Biosystems, Foster City, USA
TaqMan Gene Expression Assay, HMGA2	Applied Biosystems, Foster City, USA
Ambion Anti-miR miRNA Inhibitor, AM12369, hsa-miR-182	Ambion, Applied Biosystems, Foster City, USA
Ambion Anti-miR miRNA Inhibitor, AM12830, hsa-miR-183	Ambion, Applied Biosystems, Foster City, USA
Ambion Anti-miR miRNA Inhibitor, AM10422, hsa-miR-96	Ambion, Applied Biosystems, Foster City, USA
Ambion Anti-miR miRNA Inhibitor, AM17010, Negative Control #1	Ambion, Applied Biosystems, Foster City, USA
Anti-miR hsa-let-7c miRNA Inhibitor Positive Control	Ambion, Applied Biosystems, Foster City, USA

2.1.8 Softwares

Software name & version	Supplier
Adobe Photoshop CS2	Adobe, Dublin, Rep. of Ireland
AxioVision 4.7	Carl Zeiss, Jena, Germany
AxioVision LE Release 4.8.2.	Carl Zeiss, Jena, Germany
BeadStudio ver.3	Illumina, San Diego, USA
ImageJ Version 1.44	http://rsbweb.nih.gov/ij/index.html
MultiExperiment Viewer (TM4) 4.3	http://www.tm4.org/mev/
R 2.2.2	http://www.r-project.org/
SDS 2.0	Applied Biosystems, Foster City, USA
Sequence Scanner Software v1.0	Applied Biosystems, Foster City, USA
SigmaPlot 10.0	Systat Software, San Jose, USA

2.1.9 Instruments

Instrument model	Supplier
2100 Bioanalyzer	Agilent Technologies, Santa Clara, USA
3130 Genetic Analyzer	Applied Biosystems, Foster City, USA
96-Well GeneAmp PCR System 9700	Applied Biosystems, Foster City, USA
ABI PRISM 7900 Sequence Detection System	Applied Biosystems, Foster City, USA
Axioskop 40 microscope	Carl Zeiss, Jena, Germany
Axiovert 200M Cell Observer	Carl Zeiss, Jena, Germany
BeadArray Reader	Illumina, San Diego, USA
Gel electrophoresis power supply	E-C Apparatus Corporation, Holbrook, USA
Heating block QBT	Grant Instruments, Cambridge, UK
Mikro-Disemebrator S	B.Braun Biotech International, Melsungen, Germany
Mini Protean gel electrophoresis system	BioRad, Munich, Germany
Mini Trans-Blotwet gel transfer system	BioRad, Munich, Germany
NanoDrop ND-1000 spectrometer	NanoDrop, Wilmington, USA
Symphony whole-body 1.5 T MRI scanner	Siemens, Erlangen, Germany
Universal Microplate Reader	Bio-Tek Instruments, Winooski, USA
UV Gel Documentation	BioRad, Hercules, USA
Varifuge 3.0	Heraeus Instruments, Hanau, Germany
Vi-CELL XR 2.03	Beckman Coulter, Krefeld, Germany

2.1.10 Miscellaneous

Product name	Supplier
Anti-β-actin antibody (mouse monoclonal anti-human)	Santa Cruz Biotechnology, Santa Cruz, USA
Anti-SFRP1 antibody (Rabbit polyclonal anti-human)	Abcam, Cambridge, UK
BLOCK-iT Alexa Fluor Red Fluorescent Control	Invitrogen, Karlsruhe, Germany
CellTiter 96 AQueous Non-Radioactive Cell Proliferation Assay (MTS)	Progema,Madison, USA
DNA ladders (100 bp, 1 kb)	Fermentas, St. Leon-Roth, German
Goat anti-mouse secondary antibody, HRP-coupled	Cell Signaling, Danvers, USA
Goat anti-rabbit secondary antibody, HRP-coupled	Cell Signaling, Danvers, USA
Lipofectamine 2000	Invitrogen, Karlsruhe, Germany
One Shot TOP10 Chemically Competent E. coli	Invitrogen, Karlsruhe, Germany
Polyvinyliden flouride (PVDF) membrane	Roche Diagnostics, Mannheim, Germany
Strips of 8 Thermo-Tubes & flat cap strips	Thermo Fisher Scientific, Waltham, USA
Spectra multicolor broad range ladder	Fermentas, St. Leon-Roth, German

2.2 Methods

2.2.1 Clinical materials

All medulloblastoma tissue samples were contoinuously collected by Dr. Andrey Korshunov at the Department of Neuropathology, Burdenko Institute, Moscow, Russia, between 1994 and 2007 (n=111) after informed consent to all patients. Diagnoses were confirmed by histological and immunohistochemical assessment following the criteria of the WHO classification by at least two neuropathologists including a central pathology review in Moscow (Louis *et al.* 2007). Approval to link laboratory data to clinical and pathological data was obtained from the institutional review board. Metastatic disease was detected by cranio-spinal imaging and cerebrospinal fluid cytology following the Chang classification (Chang *et al.* 1969). All patients were treated according to standardized therapy protocols of the German HIT study group (Kortmann *et al.* 2000; von Hoff *et al.* 2009).

Table 2A Clinical-pathological characteristics of the patients

Screening data set

Variable	Medulloblastoma Subtypes										Fisher's exact test
	SHH		WNT		Group C		Group D		All		
	11	(34.4%)	4	(12.5%)	3	(9.4%)	14	(43.8%)	32	(100%)	*P*
Age, years											
≤3	3	(27.3%)	0	(0.0%)	1	(33.3%)	0	(0.0%)	4	(12.5%)	
4-17	4	(36.4%)	3	(75.0%)	2	(66.7%)	10	(71.4%)	19	(53.1%)	0.03
≥18	4	(36.4%)	1	(25.0%)	0	(0.0%)	4	(28.6%)	9	(34.4%)	
Gender											
Female	1	(9.1%)	2	(50.0%)	1	(33.3%)	5	(35.7%)	9	(28.1%)	0.25
Male	10	(90.9%)	2	(50.0%)	2	(66.7%)	9	(64.3%)	23	(71.9%)	
Localisation											
Hemispheric	8	(72.7%)	1	(25.0%)	0	(0.0%)	1	(7.1%)	10	(31.2%)	<0.01
Midline	3	(27.3%)	3	(75.0%)	3	(100.0%)	13	(92.9%)	22	(68.8%)	
Histology											
Classic	4	(36.4%)	4	(100.0%)	0	(0.0%)	11	(78.6%)	19	(59.4%)	
MBEN/ desmoplastic	5	(45.5%)	0	(0.0%)	0	(0.0%)	0	(0.0%)	5	(15.6%)	<0.01
L/CA	2	(18.2%)	0	(0.0%)	3	(100.0%)	3	(21.4%)	8	(25.0%)	
Metastatic stage											
M0	7	(63.6%)	3	(75.0%)	2	(66.7%)	6	(42.9%)	18	(56.2%)	0.66
M1-3	4	(36.4%)	1	(25.0%)	1	(33.3%)	8	(57.1%)	14	(43.8%)	

Table 2A (cont'd.)

QRT-PCR validation data set

Variable	Medulloblastoma Subtypes										Fisher's exact test
	SHH		WNT		Group C		Group D		All		
	30	(38.0%)	7	(8.9%)	14	(17.7%)	28	(35.4%)	79	(100.0%)	*P*
Age, years											
≤3	8	(26.7%)	0	(0.0%)	2	(14.3%)	0	(0.0%)	10	(12.7%)	
4-17	15	(50.0%)	4	(57.1%)	11	(78.6%)	23	(82.1%)	55	(69.6%)	0.01
≥18	7	(23.3%)	3	(42.9%)	1	(7.1%)	5	(17.9%)	14	(17.7%)	
Gender											
Female	11	(36.7%)	3	(42.9%)	4	(28.6%)	9	(32.1%)	27	(44.2%)	0.91
Male	19	(63.3%)	4	(57.1%)	10	(71.4%)	19	(67.9%)	52	(65.8%)	
Localisation											
Hemispheric	8	(26.7%)	2	(28.6%)	0	(0.0%)	1	(3.6%)	11	(13.9%)	0.01
Midline	22	(73.3%)	5	(71.4%)	14	(100.0%)	27	(96.4%)	68	(86.1%)	
Histology											
Classic	24	(80.0%)	7	(100.0%)	12	(85.7%)	28	(100.0%)	71	(89.9%)	
MBEN/ desmoplastic	5	(16.7%)	0	(0.0%)	1	(7.1%)	0	(0.0%)	6	(7.6%)	0.10
L/CA	1	(3.3%)	0	(0.0%)	1	(7.1%)	0	(0.0%)	2	(2.5%)	
Metastatic stage											
M0	26	(86.7%)	6	(85.7%)	8	(57.1%)	18	(64.3%)	58	(73.4%)	0.09
M1-3	4	(13.3%)	1	(14.3%)	6	(42.9%)	10	(35.7%)	21	(26.6%)	

Independent validation data set (Northcott *et al.* 2009)

Variable	Medulloblastoma Subtypes										Fisher's exact test
	SHH		WNT		Group C		Group D		All		
	28	(31.1%)	7	(7.8%)	25	(27.8%)	30	(33.3%)	90	(100.0%)	*P*
Age, years											
≤3	13	(46.4%)	1	(14.3%)	5	(20.0%)	1	(3.3%)	20	(22.2%)	
4-17	8	(28.6%)	6	(85.7%)	20	(80.0%)	28	(93.3%)	62	(68.9%)	<0.01
≥18	7	(25.0%)	0	(0.0%)	0	(0.0%)	1	(3.3%)	8	(8.9%)	
Gender											
Female	16	(57.1%)	3	(42.9%)	7	(28.0%)	9	(30.0%)	35	(38.9%)	0.11
Male	12	(42.9%)	4	(57.1%)	18	(72.0%)	21	(70.0%)	55	(61.1%)	
Histology											
Classic	17	(60.7%)	7	(100.0%)	20	(80.0%)	24	(80.0%)	68	(75.6%)	
MBEN/ desmoplastic	10	(35.7%)	0	(0.0%)	3	(12.0%)	3	(10.0%)	16	(17.8%)	0.13
L/CA	1	(3.6%)	0	(0.0%)	2	(8.0%)	3	(10.0%)	6	(6.7%)	

Abbreviations: MBEN, medulloblastoma with extensive nodularity; L/CA, large cell / anaplastic; SHH, sonic hedgehog pathway.

Our collaborators from Toronto (group of Dr. Michael Taylor) provided their published miRNA dataset (Northcott *et al.* 2009) as a validation data set for this study. In the Northcott study, 90 medulloblastoma samples were analyzed on a different miRNA microarray platform (Northcott *et al.* 2009)(Table 2A).

2.2.2 MicroRNA preserved total RNA preparation

All tissue samples were snap frozen immediately upon surgical resection. Frozen tissues were homogenized with a Micro-Disemebrator (B.Braun Biotech International, Melsungen, Germany) into fine powder under low temperature. Homogenized frozen tissue was digested with 700 µl Qiazol solution and miRNA preserved total RNA was extracted by using the miRNeasy kit (Qiagen, Hilden, Germany) following the manufacturer's instruction. All RNA samples were eluted in 30 µl RNase free water.

RNA concentrations were determined by NanoDrop ND-1000 spectrometer (NanoDrop, Wilmington, USA) measurement. RNA quality was assessed by use of the RNA 6000 Nano kit (Agilent Technologies, Santa Clara, USA). Only samples with a RIN (RNA integrity number) higher than 8.0 wereused for further experiments (Schroeder, Mueller*, et al.* 2006) (Appendix 8.1).

2.2.3 MicroRNA microarray and bioinformatics analysis

The genome-wide microRNA expression prolife of the screening set was revealed by hybridization to the Illumina microRNA DASL microarray V2 containing 1146 Human miRNAs(Illumina, San Diego, USA). Raw data were normalized by quantile normalization by using the Illumina software BeadStudio (ver.3). Normalized values were log2 transformed. Unsupervised hierarchical clustering (HCL) was performed using Ward's linkage and dissimilarity based on Euclidian distance. Cluster reliability was assessed using a bootstrap-based approach (Suzuki *et al.* 2006), which gives approximately unbiased (AU) probabilities. Principal component analysis (PCA) was applied as additional unsupervised approach. Significance Analysis of Microarrays (SAM) was performed with the TMEV software (ver. 4.3) (http://www.tm4.org/mev/) testing each miRNA separately for difference in expression between SHH and non-SHH tumors. MiRNAs with a false discovery rate (FDR) equals to 0 were selected identifying miRNA signatures best disrciminating between two predefined subgroups.

2.2.4 Quantitative real-time PCR and statistic analysis

TaqMan MicroRNA Assays (Applied Biosystems, Foster City, USA) were used to verify the expression levels of candidate miRNAs (hsa-miR-182, ABI assay ID 00597; hsa-miR-183, ABI assay ID 000484; hsa-miR-96, ABI assay ID 000434). Fifty ng of good quality (RIN>8.0) total RNA was use for the stem-loop reverse transcription (RT) of the mature miRNA. Stem-loop cDNA was then synthesised with the looped RT primer specifically binding to the distinct miRNA. Finally, quantitative real-time PCR (QRT-PCR) was performed in triplicates using florescence labelled TaqMan probes on an ABI 7900HT PCR system. Expression levels of miRNAs were normalized to two house keeping small RNAs (HKsRNAs) RNU6B (ABI assay ID 001093) and RNU66 (ABI assay ID 001002) and the relative expression ratio further compared with a pooled normal cerebellum (NCB) total RNA (Clontech Laboratories, Inc.) comprised of a pool of 24 donors.

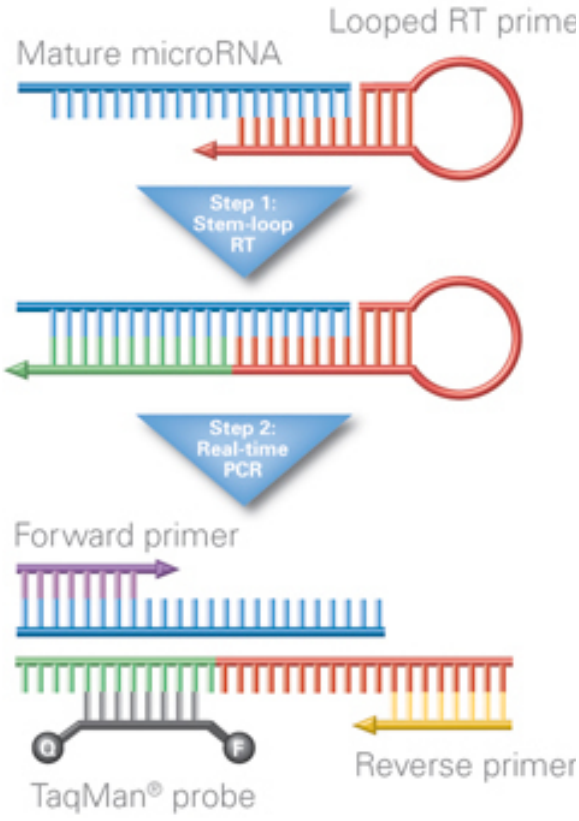

Figure 2-1. MicroRNA TaqMan QRT-PCR chemistry.
(Image from Applied Biosystems website,
http://www.appliedbiosystems.com/absite/us/en/home.html)

The raw read value from the real-time PCR machine is Ct (cycle threshold), which is defined as the number of cycles required for the fluorescence signal to cross the threshold (after background subtraction): The higher the quantity, the lower the observed Ct value. The relative amount of the candidate miRNA is calculated by the equation ($2^{-\Delta\Delta Ct}$), where,

$\Delta\Delta Ct$ = (Ct tissue – Ct house keeping) – (Ct NCB-Ct house keeping)

While 2^{-0} = 1 (value of NCB minus itself), thus we have a comparative basal value of NCB of 1 and counted values larger than 1 as upregultaion, whereas lower than 1 was defined as downregulation.. After log2-transformation, up- or downregulation of the candidate miRNAs is defined as positive (>0) or negative (<0) log2-ratio, respectively.

2.2.5 Statistic analysis

Correlation between miRNA expression and QRT-PCR values was assessed with Spearman's correlation coefficient (Spearman's rho) including confidence intervals based on Fisher's z-transformation. The distribution of candidate miRNA expression was tested for differences in tumor location, stage, location, and biological core subgroups with the two-sided Mann-Whitney test. Fisher's exact test was used to compare clinical-pathological characteristics between tumor variants. *In vitro* experiments with scratch assays and 3D microchannel migration assays were analyzed comparing the ratio of final and initial measurements with the control group. For growth rate experiments, the ratio between growth rate at each time point and growth rate at day 1 was compared with the control group. Non-parametric relative effects between groups were tested using Dunnett contrasts (many-to-one comparison) with p-values being adjusted for multiple testing (Hasler *et al.* 2008).

P-values below 0.05 were considered statistically significant. Statistical analyses were performed with the R/Bioconductor software environment, version 2.13/2.8 using the add-on R package pvclust (R Development Core Team 2011) and nparcomp (Munzel *et al.* 2001).

2.2.6 Cell culture

The QRT-PCR results showed high, moderate, and low expression of miRNA candidates in medulloblastoma cell lines DAOY (Cat#HTB-186, ATCC), D458Med (kindly provided by Dr. Darell D. Bigner, Duke University North Carolina, USA) and Med8A (kindly provided by Dr. Michael D. Taylor, University of Toronto, Canada) respectively. As a result, these cell lines were chosen for further *in vitro* functional studies. (Fig. 2-2).

D458Med is cultured in Improved MEM Zn++ option medium (Invitrogen, Karlsruhe, Germany) supplemented with 20% fetal bovine serum (FBS), whereas DAOY and Med8A are cultured in Dulbecco´s Modified Eagle Medium (DMEM) (Sigma Aldrich, Munich, Germany) supplemented with 10% FBS. All cultures were maintained at 5% CO_2 and cells were split at a ratio of 1:5 approximately every week.

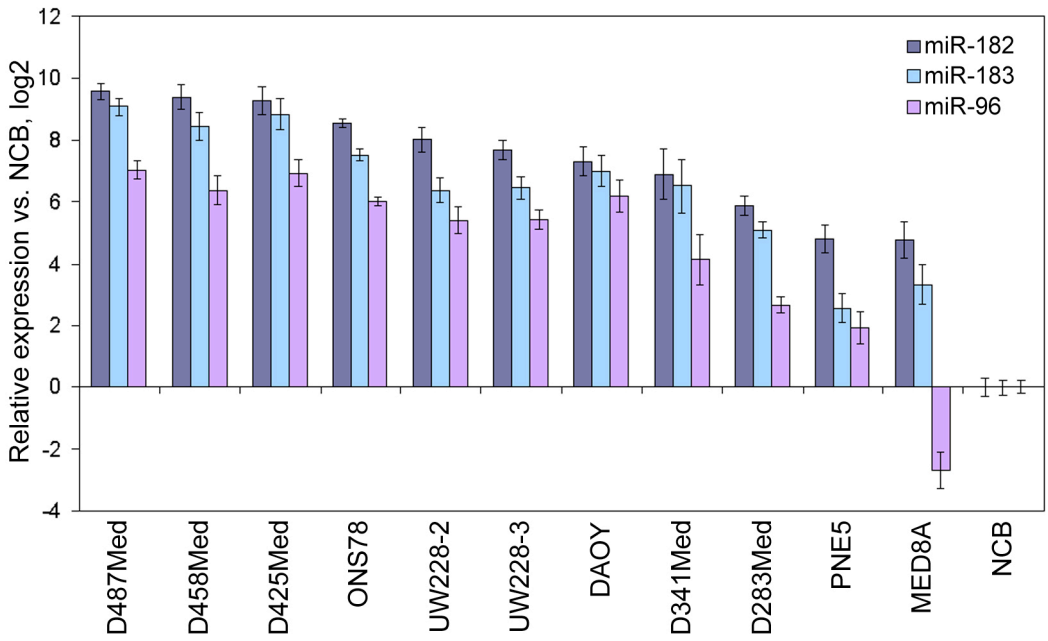

Figure 2-2. Expression levels of the three miRNA candidates in medulloblastoma cell lines. The three selected cell lines, D458Med, DAOY, and Med8A showed high, intermediate and low expression of candidate miRNAs, respectively. The expression level of miR-96 in Med8A cells was very close to NCB, both had Cts >40.

2.2.7 Overexpression vector construction

PCR fragments containing the whole pri-miRNA sequence of the candidate miRNAs were amplified with specific primers (Table 2B). All 5`-ends of the primers were added with designated restriction sites. ThepCMX-PL1 vector (pCMX) used for miRNA overexpressionwas a generous gift from Dr. Roland Schüle (Women's Hospital and Center for Clinical Research, Medical School Freiburg, Germany) (Pscherer *et al.* 2006).

Table 2B PCR primer sequences

Primer code	Primer sequence (5`~3`)	Tm	Product size
miR182-F1	CAGAATTCGCCTGGACCATCCTAACTGT	59.0	296bp
miR182-R1	CTGCTCGAGCTCTGCCACTACCCAGCAGT	59.0	
miR183-F1	CAGGATCCCTTGTGAAGAGGTGGGATGG	60.5	325bp
miR183-R1	CTGCTCGAGTTCCGACGTCTAGGAGCACT	60.0	
miR96-F1	CAGAATTCGCCTTGAGTGCTCCTAGACG	60.0	360bp
miR96-R1	CTGCTCGAGGTGAGGAGGCCTTGAGGAG	59.9	

Restriction Enzyme sequences at 5` ends: CAGAATTC (EcoR1); CTGCTCGAG (Xho1); CAGGATCC (BamH1).

Genomic DNA used as PCR template was isolated form cultured cell pellets using the QIAamp DNA Mini Kit (Qiagen, Hilden, Germany) after RNase A (Qiagen, Hilden, Germany) and proteinase K (Roche Diagnostics, Mannheim, Germany) digest overnight.

Both the vector and PCR products were digested with restriction enzymes overnight (EcoR1, 10U; Xho1, 10U; BamH1, 20U). Digested products were separated by agarose gel (Sigma Aldrich, Munich, Germany) to confirm the complete digestion. Separated products were cut out from the agarose gel and cleaned up using the QiaQuick gel extraction kit (Qiagen, Hilden, Germany) and the ligation carried out with 1U T4 ligase (Fermentas, St. Leon-Roth, German) and a mixture of vector and PCR product in a ratio of 1:10 in a final volume of 15 µl by incubation overnight at 8°C.

The completed ligation product was mixed with One Shot TOP10 chemically competent cells (Invitrogen, Karlsruhe, Germany), incubated on ice for 30 minutes, then heat shocked in a 42°C water bath for 30 seconds. SOC medium (Invitrogen, Karlsruhe, Germany) was added to competent cells and incubate at 37°C with 250 rpm shaking. Competent cells were evenly spread on a pre-warmed agar plate with 100mg/ml ampicillin (Roche Diagnostics, Mannheim, Germany) and incubated overnight for the competent cells to grow.

Colonies were inoculated in LB-broth with 100 mg/ml ampicillin at 37°C with 250rpm shaking. Plasmid DNA was isolated from the inoculated product next day using the QIAprep Spin Miniprep Kit (Qiagen, Hilden, Germany). The sequences of the vector containing plasmid DNA were verified by BigDye Terminator Sequencing (Applied Biosystems, Foster City, USA) on a 3130 Genetic Analyzer (Applied Biosystems, Foster City, USA). Vectors with the correct sequence of the insert fragment were used for the transfection experiments.

2.2.8 Stable overexpression and transient knockdown of miRNA candidates

Selected cell lines were harvested and adjusted to a cell density of $8x10^4$ cell/ml using the Vi-CELL XR 2.03 cell counter (Beckman Coulter, Krefeld, Germany). Then 500 µl (adherent cells, DAOY / Med8A) or 750 µl (suspension cells, D458Med) of cell suspension were seeded in a 6-well plate containing culture medium without antibiotics one day before transfection. The next day, 1 µg of plasmid DNA (candidate miRNA containing pCMX or empty pCMX vector only) and 1.5 µl Lipofectamine 2000 (Invitrogen, Karlsruhe, Germany) were diluted with 50 µl Opti-MEMI Reduced-Serum Medium (Gibco Invitrogen, Karlsruhe, Germany), respectively. The two solutions were incubated at room temperature for 10 minutes and then mixed together and incubated at room temperature again for 20 minutes to generate nucleic acid-Lipofectamine complexes. The complexes were added directly to cultured cells in the 6-well plate and incubated at 37°C and 5% CO_2 for 24 hours.

After a 24-hour-incubation, the culture medium was changed to selective drug medium containing 25 mM (DAOY) or 30 mM (D458Med and Med8A) zeocin (Invitrogen, Karlsruhe, Germany) for stable clone selection. While control cells with mock-transfection (transfection done with lipofectamin only, without any plasmid DNA) died rapidly, zeocin resistant cells in the transfection samplesgrew normally in the selective drug medium.

Five to eight single colonies were picked and first grew in 24-well plates and progressively expanded to 75 cm^2 flasks whenever 90% confluence was reached. Expression levels of candidate miRNAs were checked by QRT-PCR, and the two colonies with the highest overexpression of the respective candidate miRNA without influencing the expression of other cluster members were selected for further *in vitro* functional studies. (Fig. 2-3)

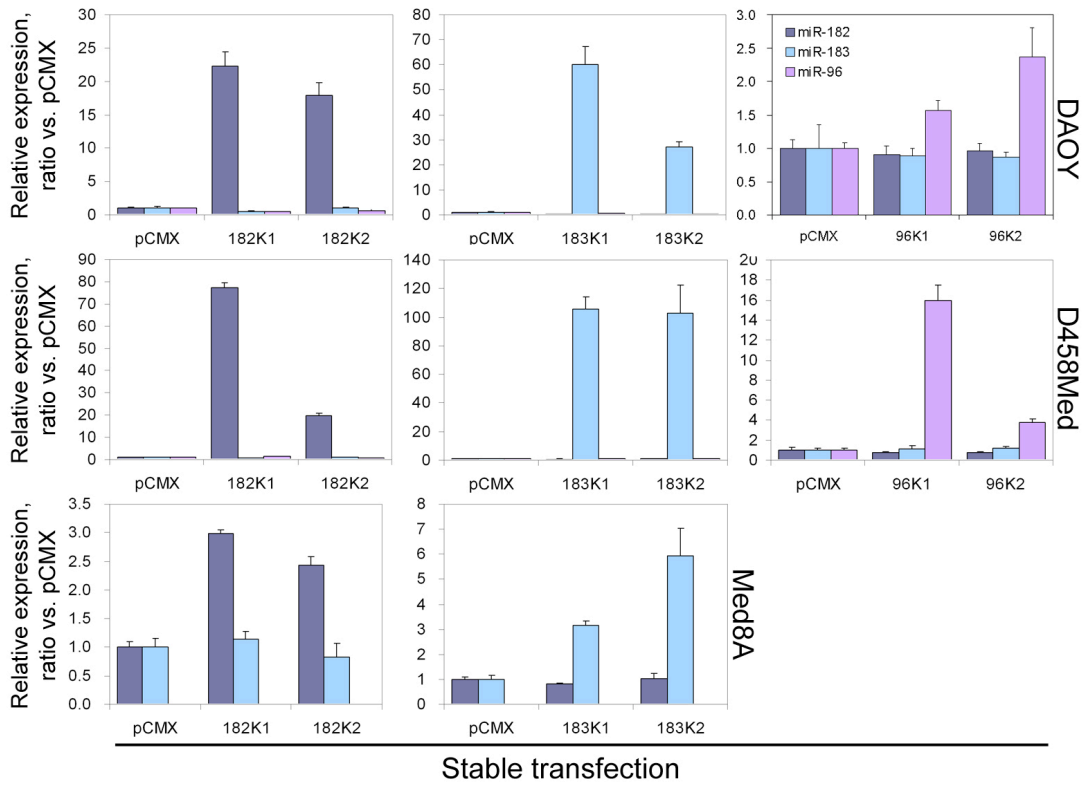

Figure 2-3. QRT-PCR confirming overexpression of candidate miRNAs in stably transfected medulloblastoma cell lines without influencing the expression levels of other cluster members. Baseline miR-96 expression was too low to be detected in Med8A, and there was no successfully transfected Med8A clone for miR-96 retrieved after several trials.

The same cell culture conditions as for the overexpression were used for the transient knockdown (KD) of miRNAs. Nucleic acid-Lipofectamine complexes were prepared with Ambion Anti-miR miRNA Inhibitors (hsa-miR-182, AM12369; hsa-miR-183, AM12830; hsa-miR-96, AM10422) (Applied Biosystems, Foster City, USA) and Lipofectamin 2000. These small and chemically modified single-stranded RNA (ssRNA) molecules, also called small interfering RNAs (siRNAs) are designed to specifically bind to and inhibit the biogenesis of endogenous miRNAs. The final concentration of anti-miRs was adjusted to 50nM in 500µl culture medium in 6-well culture plates. In parallel, the transfection efficiency was monitored by transfection with 25nM of BLOCK-iT Alexa Fluor Red Fluorescent Control (Invitrogen, Karlsruhe, Germany), under a fluorescence microscope with an emission light at 565nm, excited by 555nm light source after 6 to 24 hours incubation.

Related *in vitro* functional assays were made after 24 hours of knockdown. Expression levels of candidate miRNAs were also checked by QRT-PCR after KD treatment. Expression levels of targeted miRNAs were reduced by at least 30% without off target effects on other miRNAs within the mir-183 cluster (Fig. 2-4).

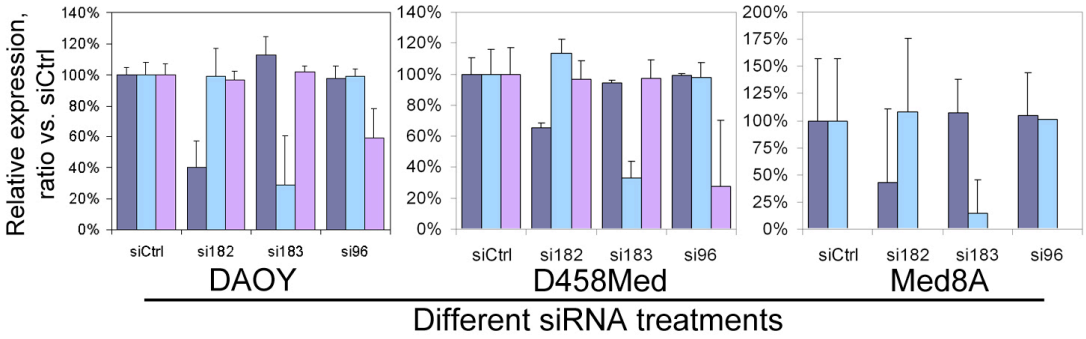

Figure 2-4. QRT-PCR showing expression levels of candidate miRNA upon anti-miRs treatment for 24 hours. As for the overexpression experiments, the expression of miR-96 was too low to be detected.

2.2.9 Scratch assay

Only cell lines growing in a monolayer may be investigated by this functional assay. DAOY and Med8A cells selected for this study were seeded at 90% confluence on chambered cover glass (Nunc Thermo Scientific, Langenselbold, Germany). After the cells had adhered firmly on the glass, the medium was changed to serum free medium. After serum starvation overnight (>16 hours), an artificial scratched wound was introduced with a P10 pipette tip in the middle of the chamber.

Time-lapse pictures at every hour were captured with a phase-contrast live-cell imaging system with humidified chamber at 37°C (Zeiss Cell Observer; Carl Zeiss, Jena, Germany).

Picture at time points 0h and 12h were used to determine the wound healing speed (migration speed towards each other) of the tested cell line. Three different positions along the wound were captured and the widths of the wound were measured by using the Zeiss AxioVision image analysis software. Differences of the wound width between time point 0h and 12h of each experimental condition were calculated. For each experimental condition, we calculated the ratio between the tested cell line against the control cell line (cell line transfected with empty vector or treated with scrambled siRNA control).

2.2.10 Boyden chamber assay

Two different assay platforms were used in this study. The migration ability of medulloblastoma cells was measured in transwells with 8µm-pore polycarbonate membrane insert (Corning Sigma Aldrich, Munich, Germany). The invasion ability was determined by using BD BioCoat Matrigel invasion chambers (BD Biosciences, Heidelberg, Germany). After serum starvation for 24h cells were harvested and resuspended in serum free medium. Cell density was determined by using a Vi-CELL XR 2.03 cell counter (Beckman Coulter, Krefeld, Germany). $1x10^5$ cell or $5x10^5$ cells were seeded in the upper reservoir of the migration or invasion chambers, respectively. Normal culture medium with FBS was added in the lower reservoir as a chemoattractant. After 16 to 24 hours of incubation, migrated cells were attached to the bottom of the transwell membrane. A cotton swab was used to wipe off the un-migrated cells still remaining on the upper surface of the transwell membrane. Migrated cells on the bottom of the transwell membrane were fixed with methanol, stained with heamatoxlin, washed in water and dehydrated with 70% and 100% ethanol, respectively. After air drying overnight, the transwell membrane was removed from the plastic insert and mounted on a glass slide for cell counting.

Cell counting was made on an Axioskop 40 microscope (Carl Zeiss, Jena, Germany) using the 65X objective (Fig. 2-5). Total cell number and total number of microscopic field observed were recorded. Relative cell count (number of cell per microscopic field) of each experimental condition was compared with the respective control.

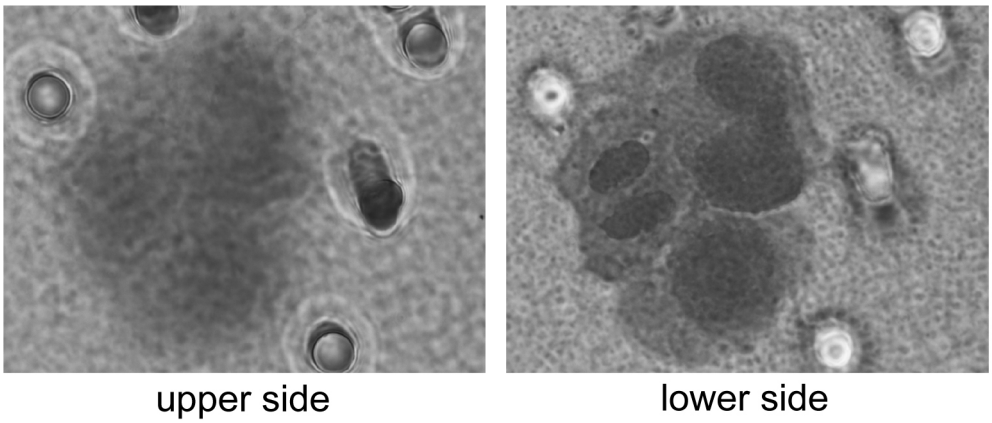

Figure 2-5. Microscopic view of the polycarbonate membrane from the migration assay insert (65X). Left picture: upper side of the membrane showing 8µm pores in a smooth circular shape. Right picture: the edges of the pores on this side are showing an irregular shape with migrated cells in the middle of the image.

2.2.11 3D microchannel assay

Poly(dimethylsiloxane) (PDMS) based microchannel chips were kindly provided by Dr. Ralf Kemkemer (Max Planck Institute for Intelligent Systems, Stuttgart, Germany). Channel structures with the dimensions of 5x11x300 µm, 7x11x300 µm, and 10x11x100 µm (WxHxL) were bio-functionalized prior to use by incubation with a 50µg/ml fibronectin solution. Chips were fixed on a Teflon holder and $2x10^5$ cells were seeded on the chip in close proximity to the channels. After cells were attached on the chip, the chamber was filled with culture medium and live-cell imaging was started.

Phase-contrast time-lapse pictures of multiple positions were captured every 10 minutes with an automated inverted microscope (Zeiss Cell Observer; Carl Zeiss, Jena, Germany) equipped with a heated and air-humidified chamber. Images were recorded and processed with the Zeiss AxioVision image analysis software and ImageJ (http://rsbweb.nih.gov/ij/).

Cell behavior was analyzed and categorized into three activities: penetration, invasion, and permeation. While “penetration” refers to cells that penetrate the channels with their cytoplasm to a depth of at least 20 µm, but did not completely enter into the channel, cells that completely entered the channel structure and stopped there or turned around back to the starting point or still moving within the channel were called “invasion”. Whenever cells migrated completely to the other side of the channel, this was counted as “permeation” (Rolli *et al.* 2010).

After assessing cell activities in each individual channel overnight, the invasiveness of the cells is defined as the percentage of invasive activity (invasion and permeation) of all cells that were trying to enter the channels. The relative invasiveness change was set as the ratio of invasiveness of tested cell lines against the respective control cell line (empty vector transfected or scrambled siRNA treated) to facilitate the comparison with all other experiments in the study.

2.2.12 Meduloblastoma experiments *in vivo*

$5x10^5$ DAOY cells with stable overexpression of miR-182 or control vector, respectively, were injected into the left cerebellar hemisphere of CB17/SCID mice (Charles River Laboratories) using a stereotact. After injection all mice were monitored by magnetic resonance imaging (MRI) every two months. All MRI examinations were performed using a custom-developed transmit/receive small animal coil in a conventional whole-body 1.5 T MRI scanner (Symphony, Siemens, Erlangen). Lesions including brain tumors were localized on T2w turbospinsecho images (TE: 109 ms; TR: 4000; FoV: 40x30 mm; matrix: 128; voxel size: 0,3x0,3x1 mm^3). Mice were sacrificed once a tumor was discovered, and tissue was collected for Haematoxylin & eosin staining and analysed by a experienced neuropathologist.

3 RESULTS

One hundred and eleven medulloblastoma tissues were included in this study aiming to discriminate medulloblastoma subgroups based on their miRNA signatures. Significant miRNA candidates were then selected for functional studies, thus to clarify the role of candidate miRNAs in medulloblastoma development, maintenance, and dissemination.

3.1 MicroRNA profiling and candidate microRNA identification

Investigation of genome-wide miRNA expression profiles in 32 primary medulloblastomas was done on Illumina microRNA DASL arrays. Raw data were normalized by quantile normalization and log2-transformed. Micro-RNA signatures were integrated with molecular subgroup information of the medulloblastoma tissue samples, which were obtained in a previous study (Remke *et al.* 2011).

The Unsupervised hierarchical clustering (HCL) identified three subgroups in the screening set based on miRNA profiles: (i) SHH-driven medulloblastomas were all grouped into an individual cluster, (ii) group C and group D medulloblastoma tumors comprised the second cluster, and (iii) the third cluster was consisting of all WNT medulloblastomas and three samples from each of the other groups (Ward's linkage, euclidian distances) (Fig.3-1).

Principal component analysis (PCA), an alternative method for unsupervised classification into subgroups substantiated the findings from the HCL analysis and resulted in a very similar separation of the screening cohort (Fig.3-2).

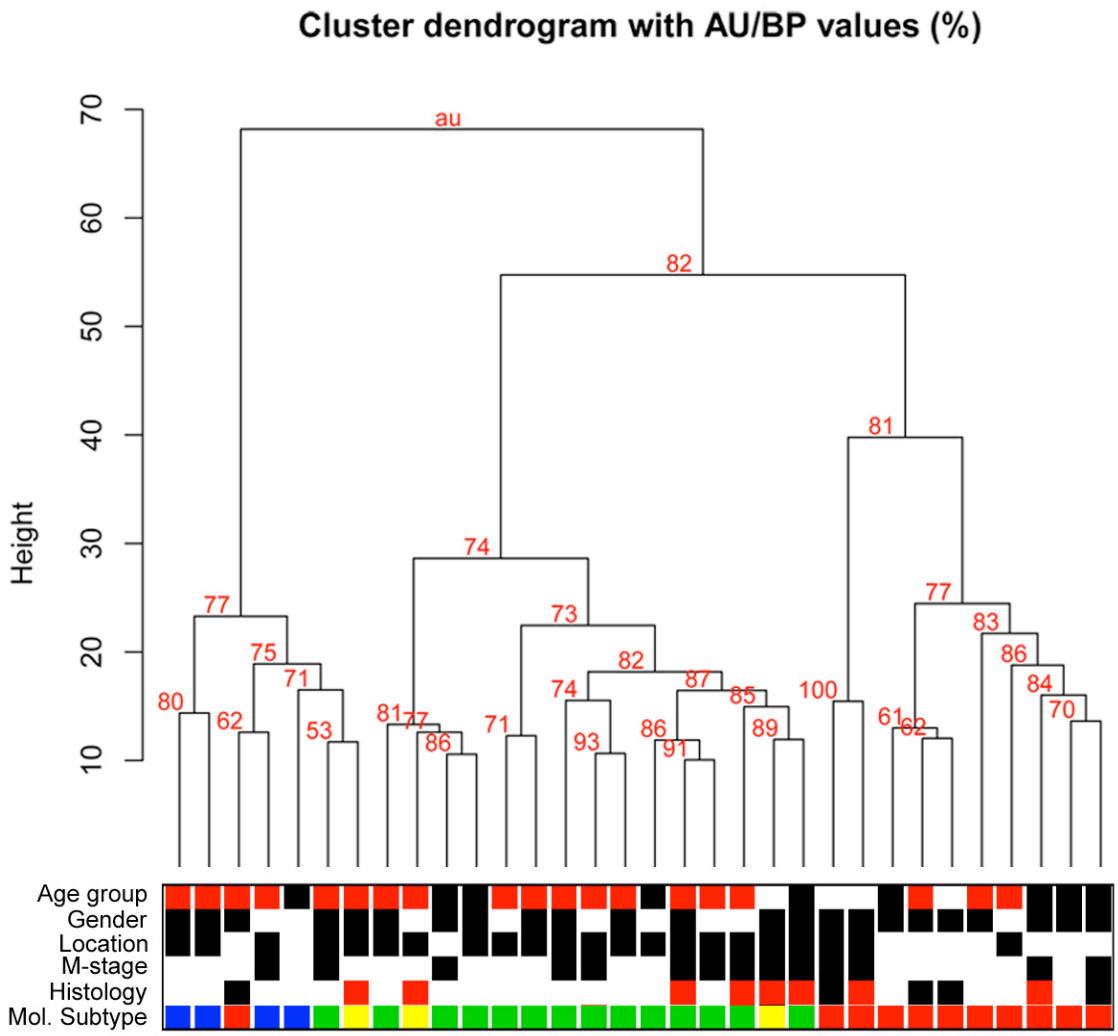

Figure 3-1. Unsupervised hierarchical clustering (HCL) of the screening set (n=32). HCL clearly separated the screening cohort into three clusters with high reliability. Clinico-pathological characteristics are summarized under the heatmap. Age groups include infants (≤ 3 years, white), children (4-17, red), and adults (≥ 18 years, black). Gender includes females (white) and males (black). Location includes hemispheric (white) and midline (black). Metastatic stage (M stage) includes M0 (white) and M1-3 (black). Histology includes classic (white), large cell /anaplastic (red), and MBEN/desmoplastic (black). Molecular subgroups (Mol. Subtype) include SHH (red), WNT (blue), group C (yellow), and group D (green). This color scheme applies to all figures in this dissertation.

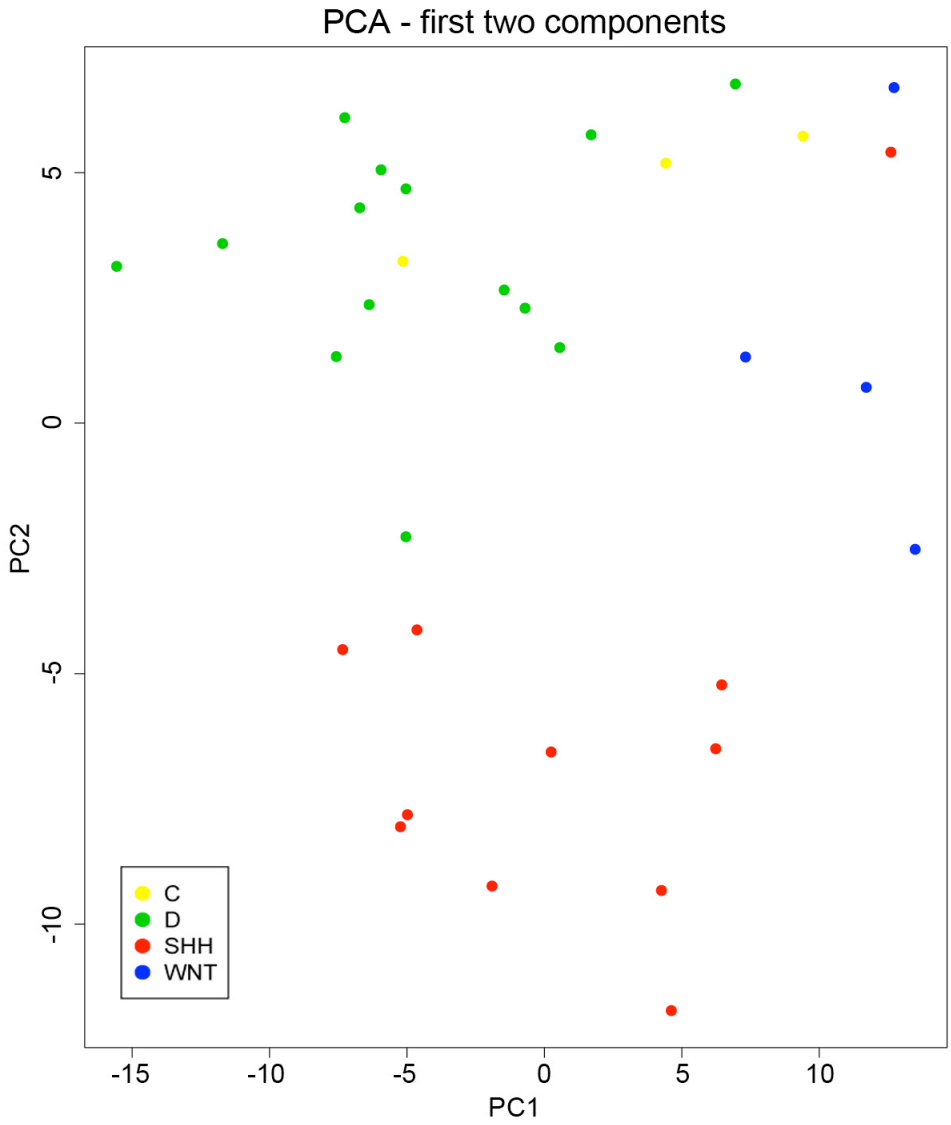

Figure 3-2. Two-dimensional principal component analysis (PCA). Confirming group separation of screening set obtained by unsupervised HCL shown in Figure 3-1.

When trying to delineate the fundamental expression differences between SHH- and non-SHH medulloblastomas by Significance Analysis of Microarrays (SAM), a robust 26-miRNA signature (Table 3A) was obtained (Fig.3-3). SHH medulloblastomas remain in an individual cluster. The remaining tumors were observed to fall into two additional clusters, one of them mainly consisting of group D tumors and the second one being mainly comprised of WNT, group C and group D tumors.

Table 3A. The 26-miRNA signature from SAM analysis

	miRNA	Fold change	
1	hsa-miR-96	0.1604	Downregulation in SHH-MB
2	hsa-miR-183	0.2448	
3	hsa-miR-455	0.2840	
4	hsa-miR-182	0.3054	
5	hsa-miR-138	0.3944	
6	hsa-miR-204	0.4328	
7	hsa-miR-490	0.4808	
8	hsa-miR-582	0.5004	
9	hsa-miR-135b	0.5985	
10	hsa-miR-181c	0.6085	
11	hsa-miR-491	0.6958	
12	hsa-miR-338	0.6990	
13	hsa-miR-331	0.8725	
14	hsa-miR-143	1.3859	Upregulation in SHH-MB
15	hsa-miR-511	1.8112	
16	hsa-miR-146a	1.9267	
17	hsa-miR-20b	1.9398	
18	hsa-miR-363	2.0014	
19	hsa-miR-92b	2.0410	
20	hsa-miR-28	2.0642	
21	hsa-miR-214	2.0664	
22	hsa-miR-199a	2.2310	
23	hsa-miR-221	2.3306	
24	hsa-miR-200b	2.5287	
25	hsa-miR-155	2.5746	
26	hsa-miR-10a	6.7915	

MB : medulloblastoma

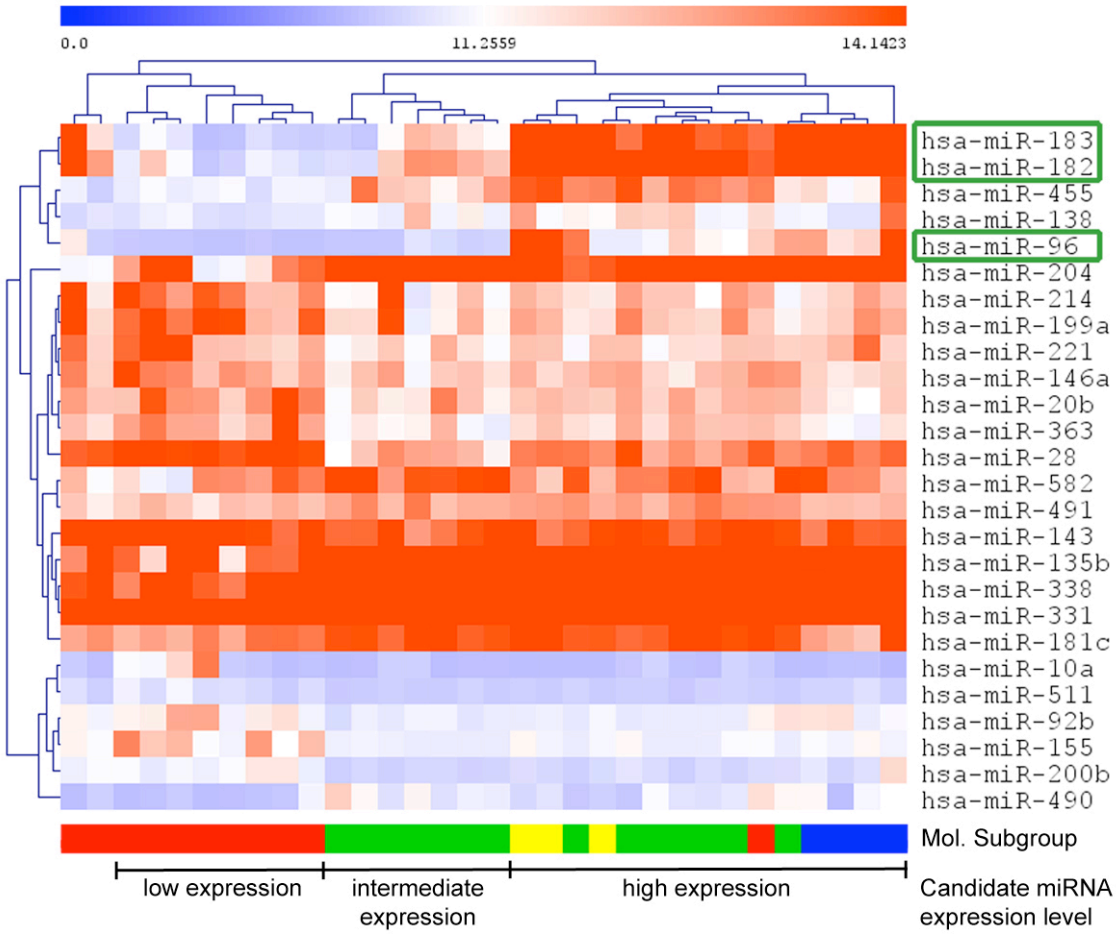

Figure 3-3. Supervised HCL using the 26-miRNA-signature in the screening cohort. Primary medulloblastoma samples were clustered into three groups SHH medulloblastomas, a cluster that only contained group D medulloblastomas, and a third cluster containing all group C and WNT medulloblastomas as well as some additional group D tumors. Dark green boxes indicate the three candidate miRNAs, which show high, intermediate and low expression in the three clusters, respectively.

Applying the same miRNA signature to our validation dataset, which was obtained in a completely non-overlapping cohort in a different lab on a different microarray platform (Nortchott, 2009), SHH medulloblastomas could again be readily separated from non-SHH medulloblastomas. The remaining samples were separated into two clusters again, one of them mainly consisting of group D medulloblastomas, and the other one including WNT and group C tumors in the majority. (Fig.3-4).

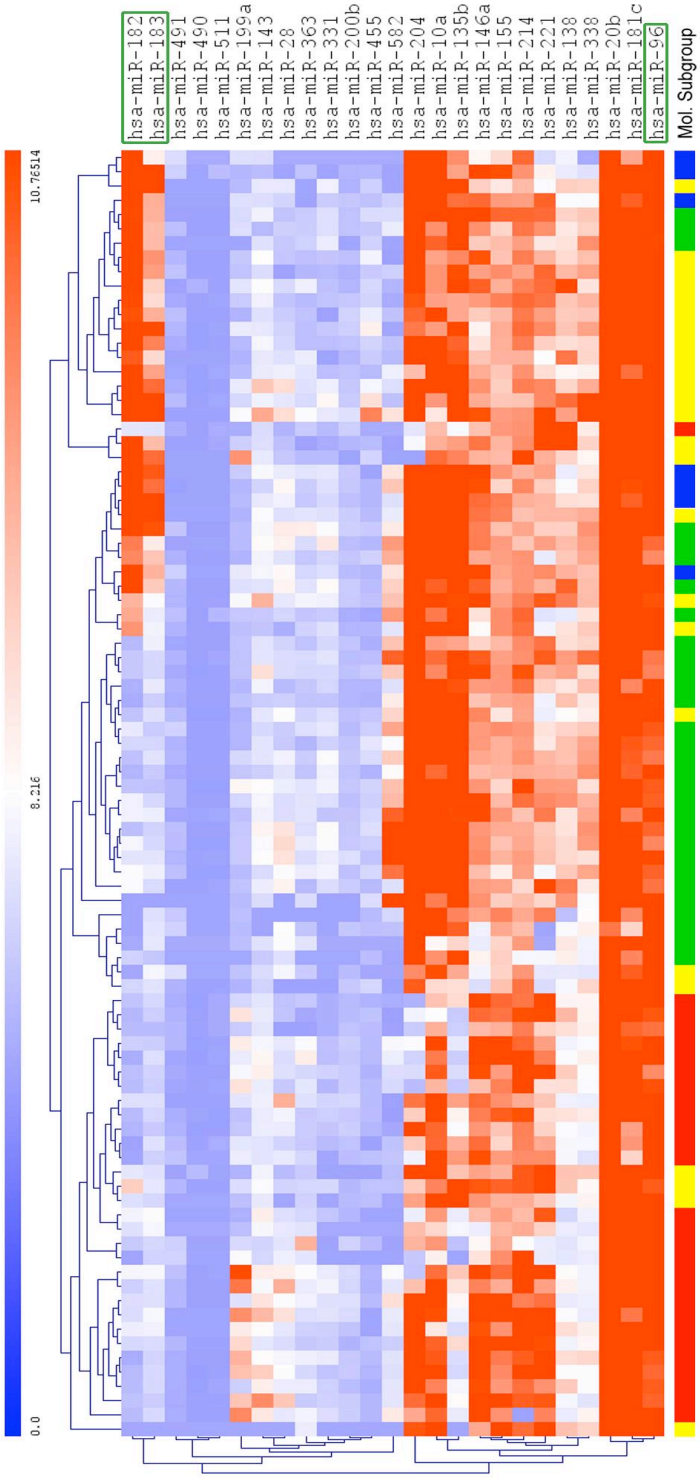

Figure 3-4. Supervised HCL of the validation set (n=90) using the miRNA signature obtained in the screening cohort. In the validation cohort, only 25/26 signature miRNAs were included since miR-92b expression was not determined in the validation dataset. All SHH medulloblastoma tumors, with only one outlier, grouped into the cluster on the left hand side. The cluster in the middle is mainly comprised of group D medulloblastomas, whereas group C and WNT medulloblastomas were mainly found in the third cluster. Dark green boxes indicate three candidate miRNAs, the retina-specific miRNAs.

From the 26-miRNA signature, retina specific miRNAs, hsa-miR-182 (miR-182), hsa-miR-183 (miR-183), and hsa-miR-96 (miR-96), were the most differentially regulated miRNAs (Table 3A). Based on this, we focused our further investigations of this miRNA cluster. In the validation dataset, however, the same strong association with disease subgroups was only observed for miR-182 and miR-183, but not for miR-96 (Fig.3-5).

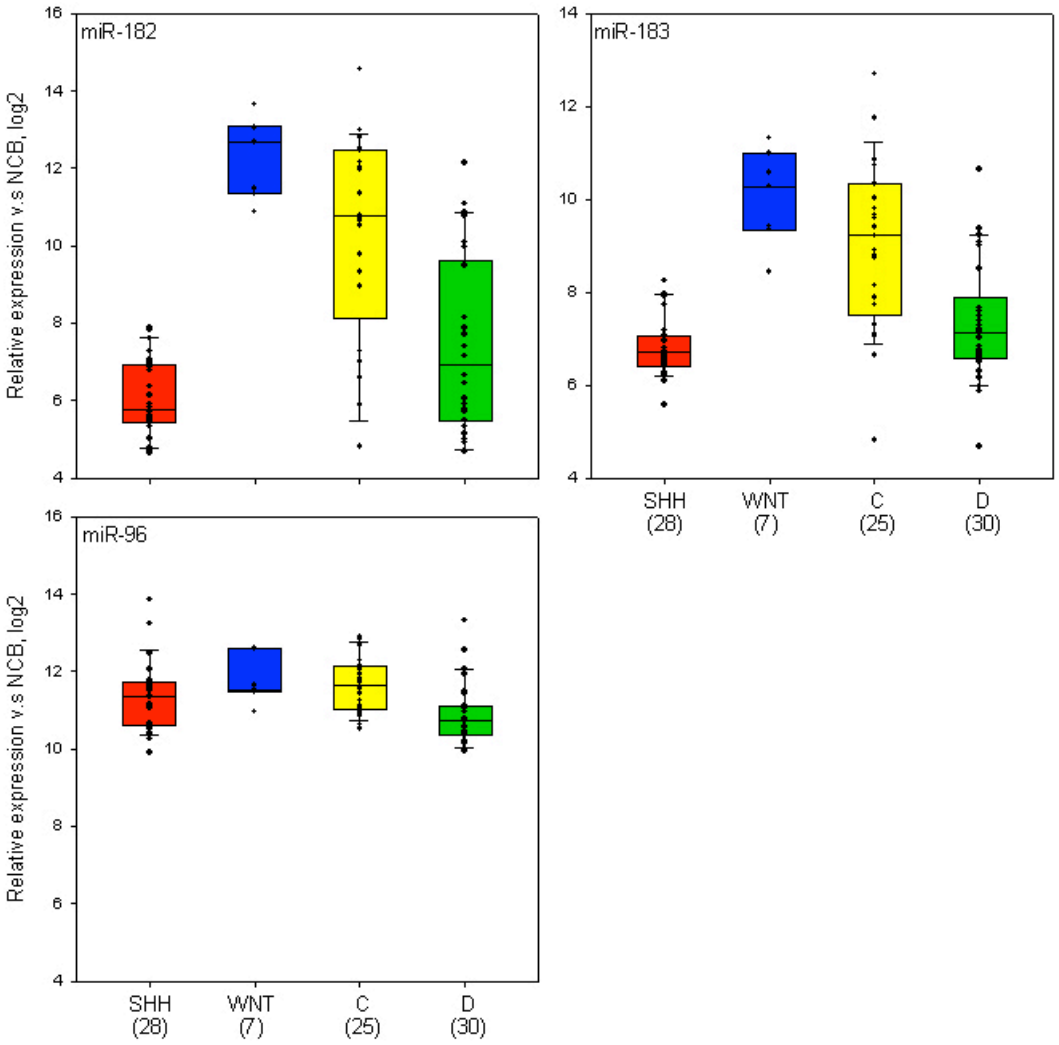

Figure 3-5. Expression levels of candidate miRNAs in the validation cohort. Both miR-182 and miR-183 showed low expression in SHH medulloblastoma, intermediate expression in group D medullo-blastoma, and high expression in WNT and group C medulloblastoma, which confirmed the findings in our screening dataset. However, the expression patterns of miR-96 were not concurrent with the screening dataset.

3.2 Technical validation of microarray data

Taqman based QRT-PCR was used to further investigate the expression levels of candidate miRNAs, miR-182, miR-183, and mir-96, in a cohort of 111 medulloblastoma samples consisting of the 32 samples (previously analyzed on the microarray) as well as 79 non-overlapping cases. Comparing the expression levels obtained by microRNA microarrays with the results from the QRT-PCR, results were highly reproducible (Spearman's rho>0.9, p<0.0001) (Fig.3-6).

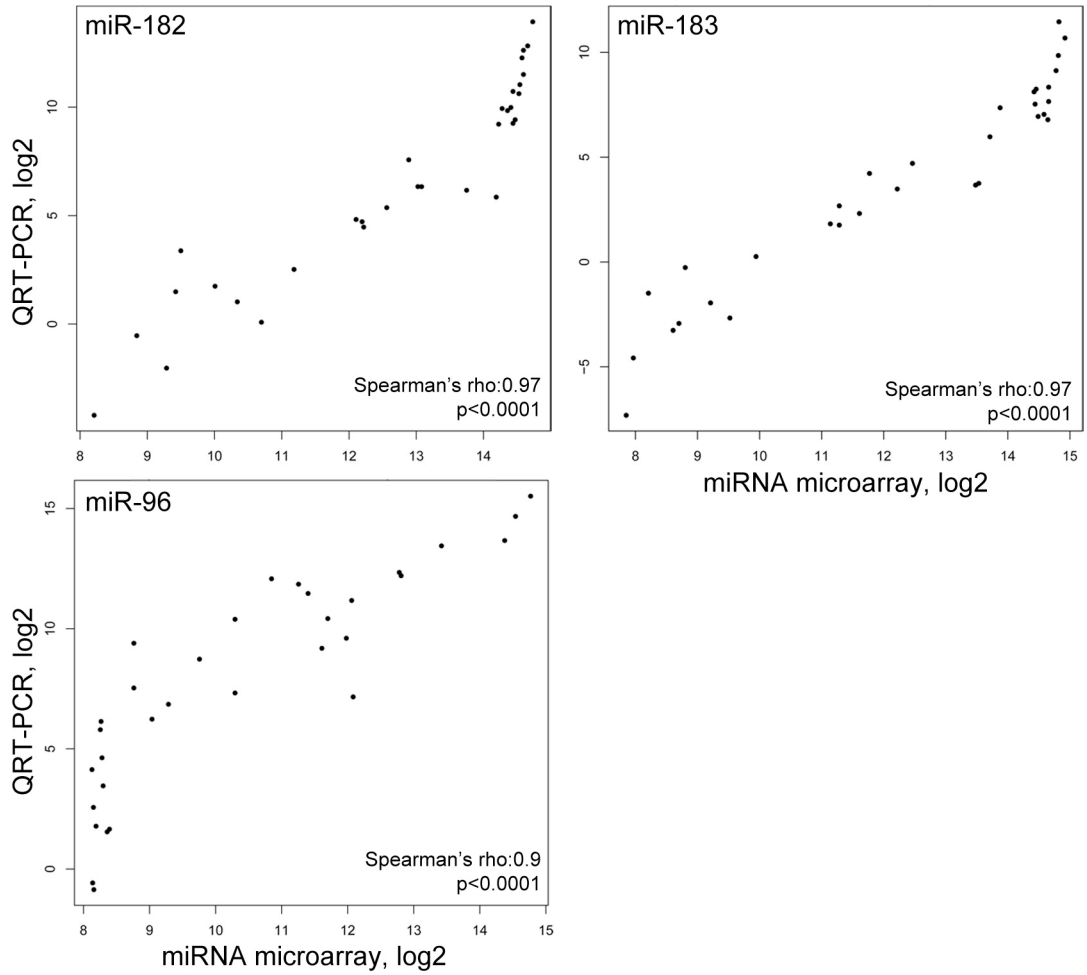

Figure 3-6. Correlation of QRT-PCR results with microRNA microarray results Showing a good technical reproducibility of the microarray data (p<0.0001)

QRT-PCR results from the QRT-PCR validation data set (n=79) confirmed our findings obtained in the screening cohort, namely the same characteristic expression patterns among medulloblastoma subgroups (p<0.0001) (Fig.3-7).

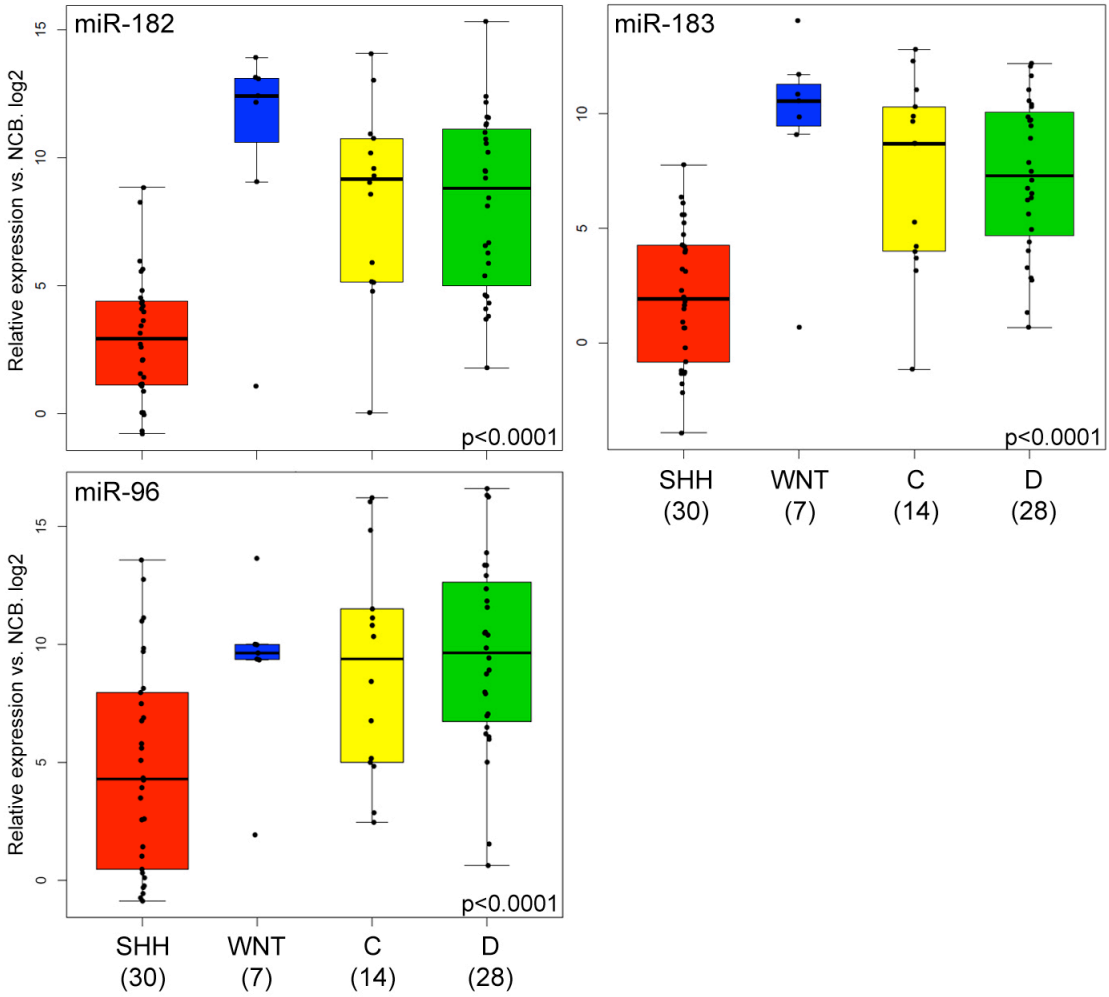

Figure 3-7. QRT-PCR detecting expression levels of candidate miRNAs in the validation set (n=79). SHH medulloblastoma have expression levels similar to normal cerebellum (NCB), whereas non-SHH medulloblastomas have a significantly higher expression of miR-182 and miR-183. (*p-value<0.0001). Subgroup-specific expression patterns were not as striking for miR-96.

Integrating QRT-PCR results with clinico-pathological parameters, the expression of candidate miRNAs was signaficantly associated with tumor location and metastatic stage (Fig.3-8). Midline medulloblastomas showed a significantly higher expression of all candidate miRNAs in comparison with hemispheric tumors. Comparing expression levels with metastatic stage, miR-182 and miR-96 were found to be significantly higher expressed in metastatic medulloblastoma (Fig.3-8). No significant correlation was found between candidate miRNA expression patterns and patient age, gender, overall survival time, progression-free survival time, or histopathological type (data not shown).

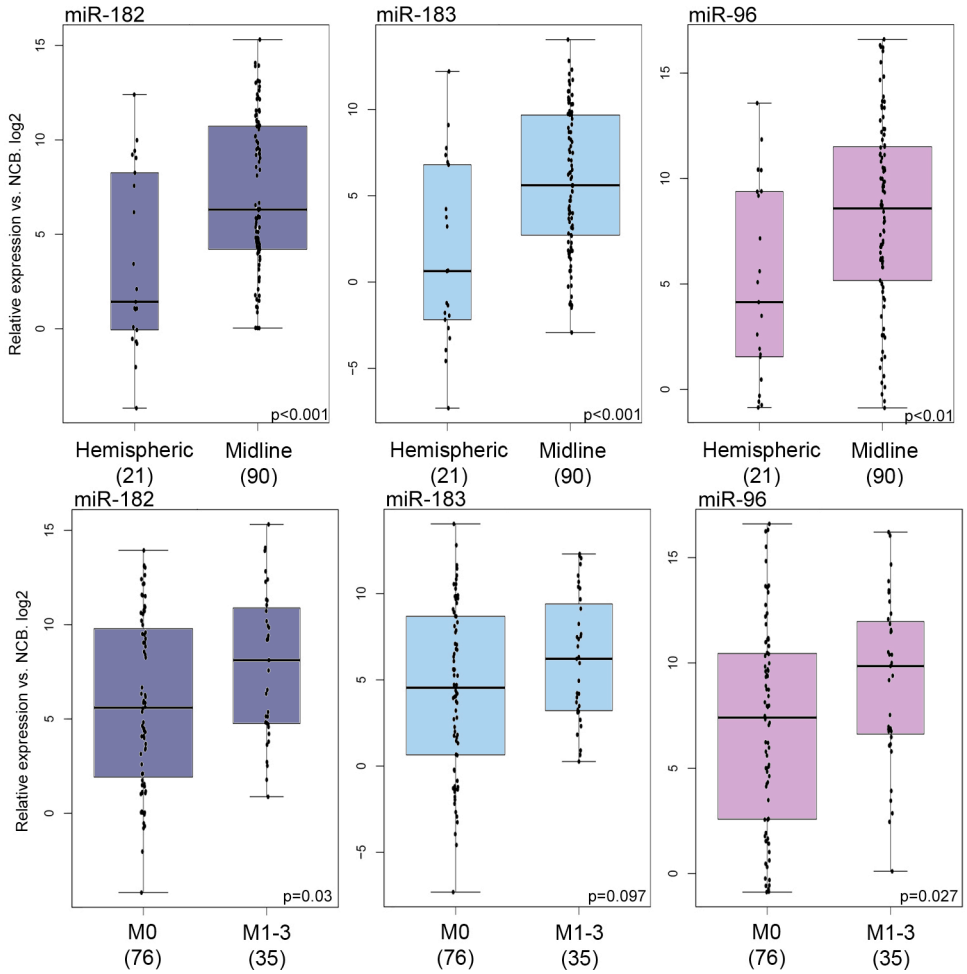

Figure 3-8. Expression of candidate miRNAs is associated with tumor location and metastatic stage. All candidate miRNAs are higher expressed in midline medulloblastoma,whereas miR-182 and miR-96 are significantly associated with metastatic stage.

3.3 *In vitro* functional studies

A robust miRNA signature discriminated SHH medulloblastoma from the other subgroups in both the screening data set and the validation data set with the miR-183~96~182 cluster being the most differentially expressed cluster between these two groups. After confirming this expression pattern in a larger test set, we especially focused on miR-182, because it showed clear association with important clinical determinants, mostly metastatic dissemination. However, all three members of this cluster were further subjected to *in vitro* functional studies to assess the importance and specific role of each candidate miRNA in medulloblastoma

To investigate the functional roles of these retina specific miRNAs, we generated stably transfected medulloblastoma cell lines showing constitutive overexpression of each candidate miRNA. Transient knockdown of individual miRNAs complemented our functional investigations.

Unfortunately, the stable transfection of miR-96 was not successful in the medulloblastoma cell line Med8A despite several trials. We failed to retrieve any single colony from the zeocin containing selective medium after transfection. As a result, only 2 Med8A stable cell lines with miR-182 or miR-183 overexpression are presented. Two other medulloblastoma cell lines, DAOY and D458 Med, were successfully transfected with all three miRNAs.

3.3.1 Proliferation assay (MTS)

We used a non-radioactive colorimetric cell proliferation assay (MTS) to assess the metabolic activities of medulloblastoma cells after stable transfection or transient knockdown of candidate miRNAs.

Optical density (OD) at day 1 was used as baseline value; thus, all following data points are relative to day 1. MTS results obtained in the three medullo-blastoma cell lines showed that neither stable overexpression nor transient knockdown of any of the candidate miRNAs had a significant impact on the metabolic activity and thus proliferation of medulloblastoma cells (Fig.3-9).

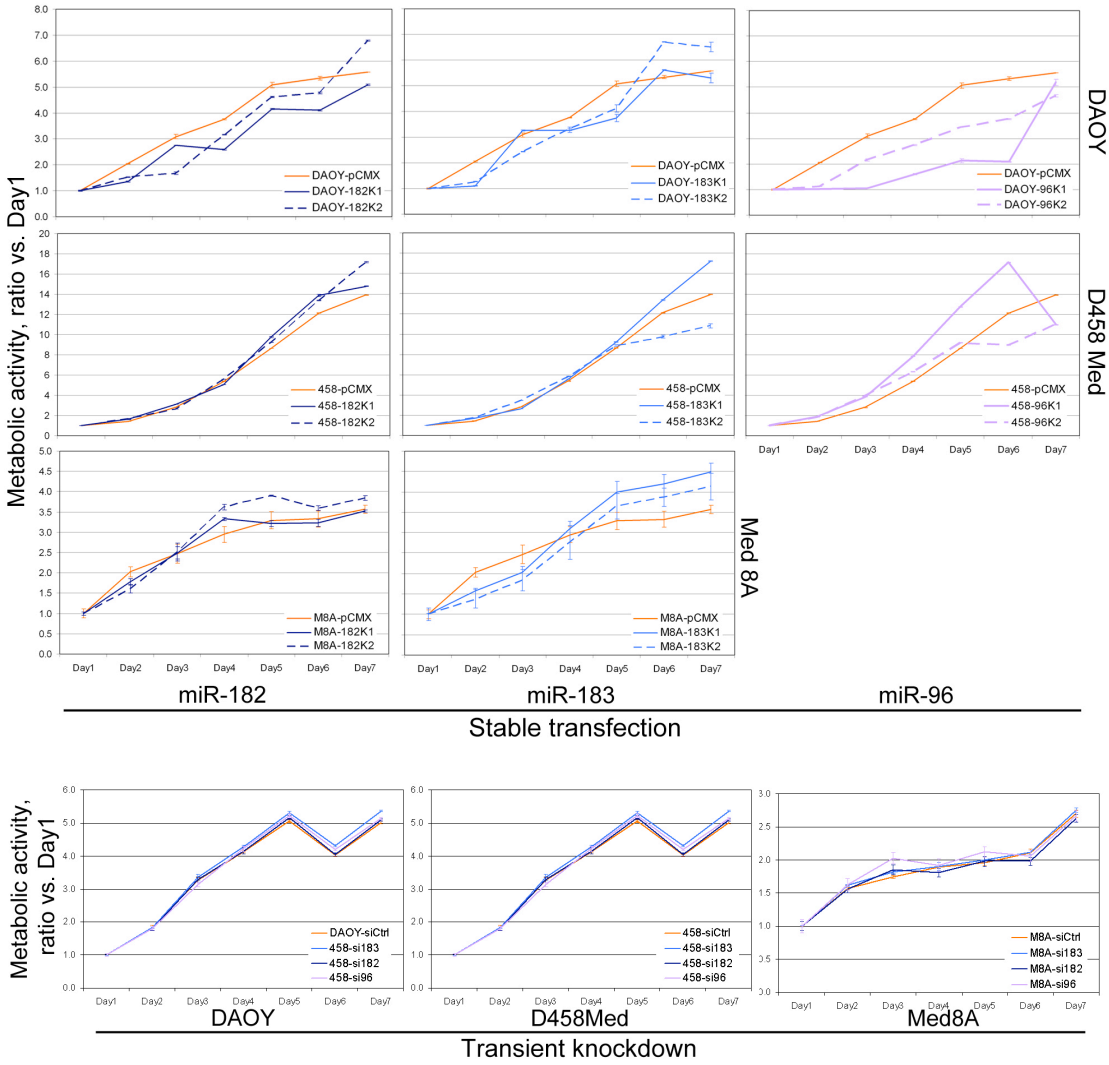

Figure 3-9. Proliferation assay (MTS) indicating that neither over-expression nor knockdown of any of the three candidate miRNAs had a significant impact on the metabolic activity of medulloblastoma cells. Metabolic activities of stably transfected cell lines were compared to the respective empty vector (pCMX) controls over 7 days (overexpression of miR-182 in dark blue, miR-183 in light blue, and miR-96 in purple). Bottom panels illustrate the growth rate of three medulloblastoma cell lines after transient knockdown of candidate miRNAs.

3.3.2 Scratch assay

Whereas proliferation was not affected by stable overexpression or transient knockdown of retinal miRNAs in all selected medulloblastoma cell lines, another interest of this study is the role of the candidate miRNAs in medulloblastoma cell migration. Therefore, different *in vitro* migration assays were applied.

The scratch assay is a time- and cost-effective *in vitro* functional assay to test the migratory speed of a cell line. The main limitation of this assay is that it is restricted to cells growing in a monolayer.

Two of the three medulloblastoma cell lines included in our study, DAOY and Med8A, grow in a monolayer and were subjected to scratch assays upon stable overexpression and transient knockdown of candidate miRNAs. After 12 hours incubation, two different DAOY clones with stable miR-182 overexpression (DAOY-182K1, DAOY-182K2) showed an at least 4-fold increase in migration speed when compared to DAOY transfected with empty vector (DAOY-pCMX)(Fig.3-10).

Overexpression of miR-183 in DAOY (DAOY-183K1, DAOY-183K2), in contrast, did not lead to obvious differences in the migration speed (Fig.3-10) neihter did miR-96 overexpression. (Fig.3-11)

Transient knockdown of either miR-182 or miR-183 in DAOY cells revealed a strong reduction in migration speed by around 80% relative to the scrambled negative control (siControl). Knocking down miR-96 also excerted a moderate effect on DAOY cell migration (Fig. 3-12).

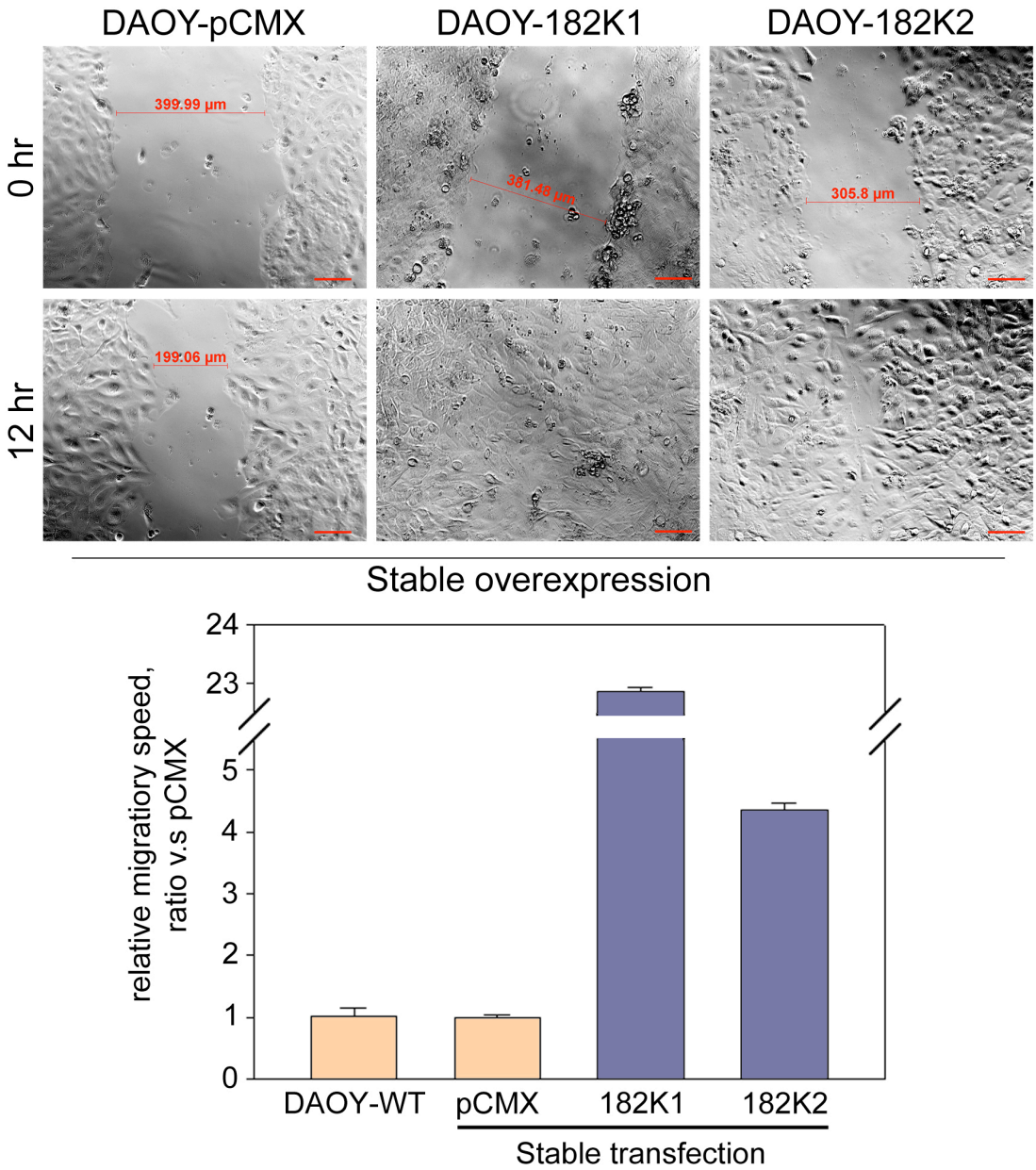

Figure 3-10. Phase contrast images show the time-lapse captures of the scratch assay at 0h and 12h. More than 4 fold increment of migration speed was observed in the two miRNA-182 over-expressing DAOY clones (182K1, 182K2) compared to empty vector transfected DAOY cells (pCMX). Both DAOY single colonies with miR-182 overexpression could heal the whole scratch within 12 hours. Scale bar: 100 µm. Error bars indicate the mean±SD of three independent experiments.

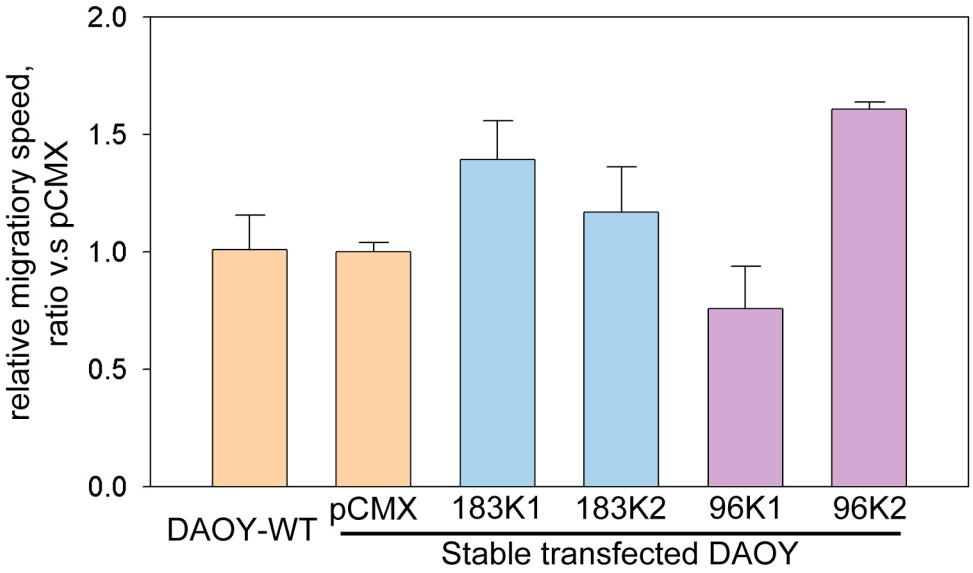

Figure 3-11. Overexpression of either miR-183 or miR-96 did not significantly increase the migration speed of DAOY. Error bars indicate the mean±SD of three independent experiments.

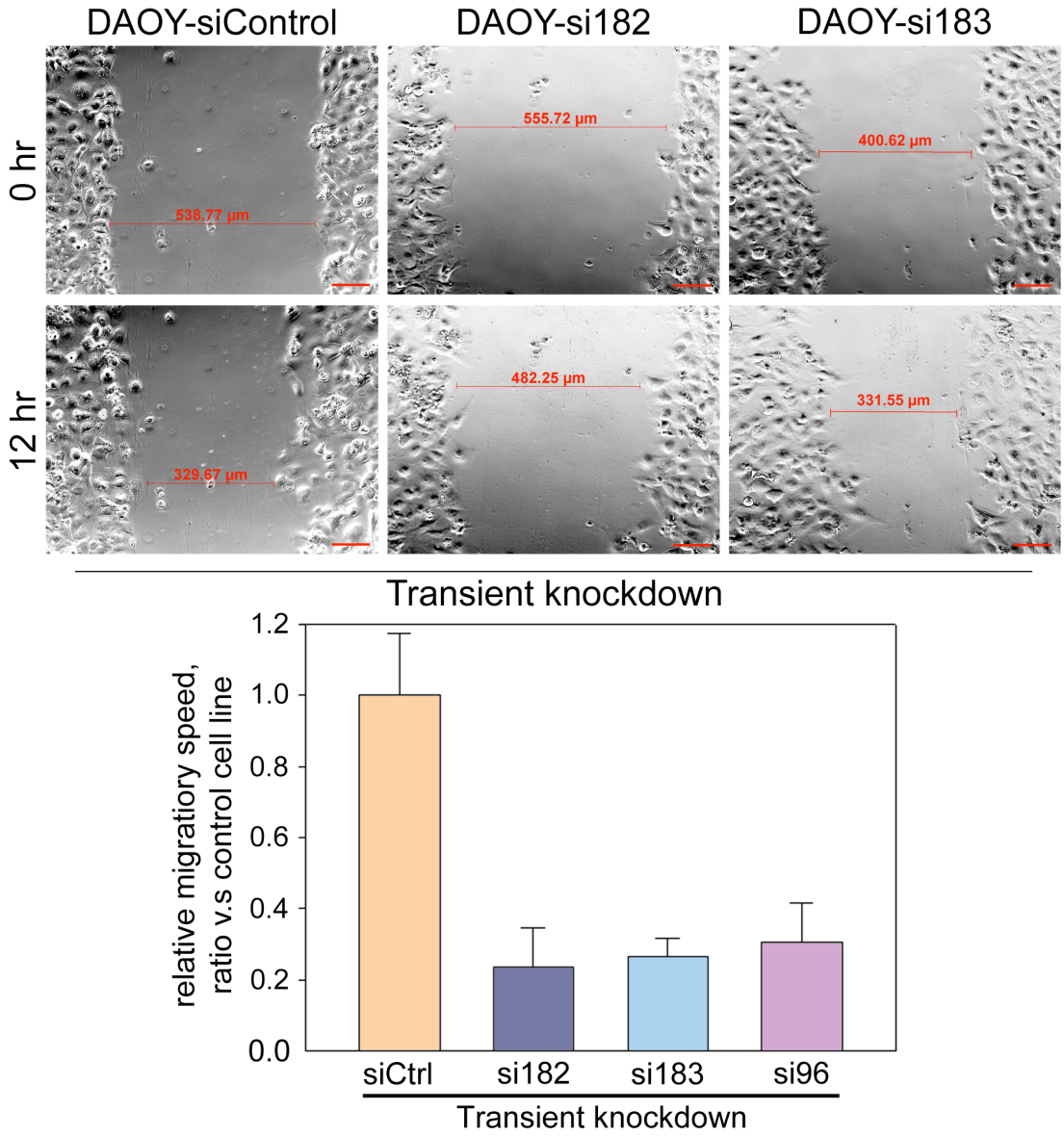

Figure 3-12. Scratch assay showed similar reduction of migration of DAOY after transient knockdown of the candidate miRNAs. The images above show the time-lapse pictures of scratch assay of DAOY cell 24 hours after transient siRNA treatment. Scale bar: 100 µm. The bar chart underneath shows the dramatically reduced migration speed after siRNA treatment of DAOY cell. All error bars indicate the mean±SD of three independent experiments.

Another medulloblastoma cell line, Med8A, which has the lowest expression levels of the three candidate miRNAs among all tested cell lines (Fig. 2-2) was also subjected to scratch assays upon miRNA overexpression. Overexpression of miR-182 in Med8A cells had a moderate effect of increased migration in Med8A cells, whereas Med8A cells overexpressing miR-183 showed no change in their migration phenotype As expected based on the low baseline expression of retinal miRNAs in this cell line, no change in the migration phenotype was observed after transient knockdown of all candidate miRNAs in Med8A cells (Fig.3-13).

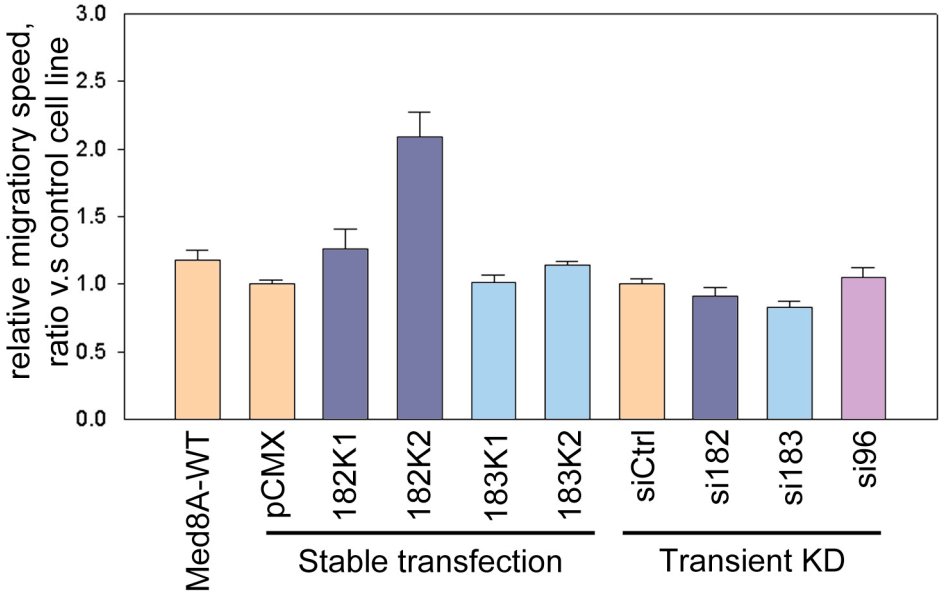

Figure 3-13. Scratch assay showing moderately increased migration of Med8A cells after miR-182 overexpression, whereas no phenotypic changes were observed upon overexpression of miR-183, and miR-96. Error bars indicate the mean±SD of three independent experiments.

3.3.3 Boyden chamber assays

The upper and lower reservoirs of a Boyden chamber are separated by a pored membrane insert. For the migration assay, inserts with a plain polycarbonate membrane with 8 µm sized pores were used, whereas for the invasion assay, the membranes were coated with matrigel. Cells were seeded in the upper reservoir in serum free medium, whereas the lower reservoir was filled with complete growth medium. The number of cells in the lower reservoir after a defined incubation period indicates the migration or invasion ability of the tested cell line.

Overall, the results of the Boyden chamber assays nicely confirmed observations from the scratch assays. DAOY cells with miR-182 overexpression showed an at least 2-fold increment of migration compared to empty vector in both the migration and invasion assays. Overexpression of miR-183 and miR-96 also by Boyden chamber assay did not lead to a significant increment in cell migration and invasion. Again consistent with our previous results, we observed a significant reduction of cell migration upon siRNA knockdown of miR-182 In DAOY cells further substantiating the important function of miR-182 in medulloblastoma cell migration (Fig. 3-14)

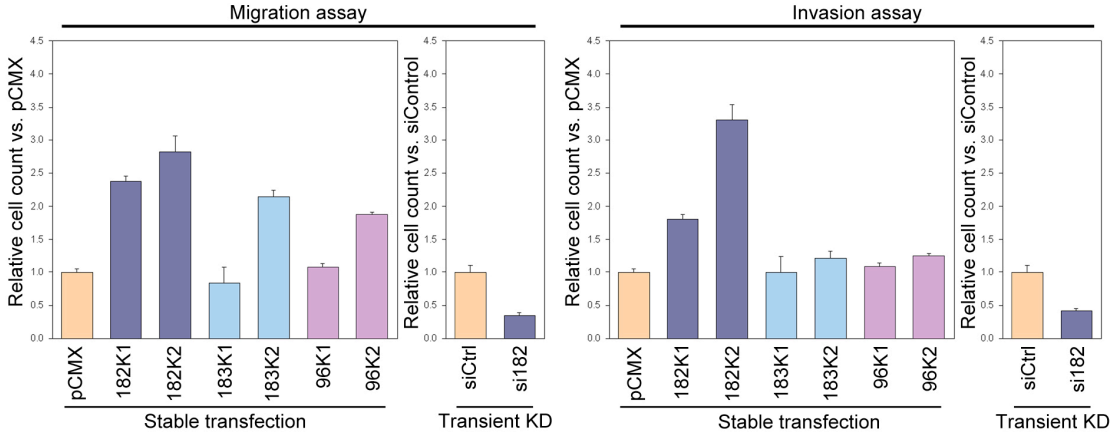

Figure 3-14. Boyden chamber assays confirmed that miR-182 expression is significantly associated with the migratory phenotype of DAOY cells. Overexpression of miR-183 and miR-96 did not change the invasion ability or migratory phenotype of DAOY cells. Transient knockdown (KD) of miR-182 significantly reduced DAOY cell migration. Error bars indicate the mean±SD of three independent experiments.

Consistent with the scratch assay results, one of two miR-182 overexpressing Med8A clones (182K2) showed a higher cell migration and invasion in the Boyden chamber assays, whereas no difference was observed for the second miR-182 overexpressing clones, and for miR-96 or miR-183 overexpression (Table 3B)

Table 3B. Boyden chamber assay results – Med8A stable transfected cells

	Migration assay				Invasion assay			
		Index	Field observed	Cell count		Index	Field observed	Cell count
Test 1	pCMX	0.00	94	0	pCMX	0.03	79	2
	182K1	0.05	87	4	182K1	0.07	84	6
	182K2	0.10	87	9	182K2	0.23	80	18
	183K1	0.00	94	0	183K1	0.02	88	2
	183K1	0.00	92	0	183K2	0.00	86	0
Test 2	pCMX	0.00	97	0	pCMX	0.00	81	0
	182K1	0.00	82	0	182K1	0.04	82	3
	182K2	0.03	80	2	182K2	0.09	77	7
	183K1	0.00	92	0	183K1	0.00	82	0
	183K2	0.00	89	0	183K2	0.00	89	0
Test 3	pCMX	0.01	92	1	pCMX	0.03	79	2
	182K1	0.01	92	1	182K1	0.07	84	6
	182K2	0.00	96	0	182K2	0.15	80	12
	183K1	0.00	88	0	183K1	0.02	88	2
	183K2	0.02	85	2	183K2	0.00	86	0

Field observed: number of microscopic view (63X objective) observed.
Index = Cell count / Fields observed

The third medulloblastoma cell line, which was subjected to Boyden chamber assays upon knockdown and overexpression of retinal miRNAs, was D458Med, a cell line that is growing half in suspension and half adherent. Boyden chamber assays showed a significant increase of migration and invasion upon miR-182 overexpression in D458Med cells (182K1, 182K2 in fig. 3-15) and conversely the opposit effect upon transient knockdown of miR-182 (Fig. 3-15)

Consistent with the results obtained for the two other cell lines, no significant differences in migration and invasion was observed upon overexpression or knockdown of miR-183 or miR-96 in D458Med.

As a result of all *in vitro* migration experiments, we further focused on the role of miR-182 in medulloblastoma cell migration.

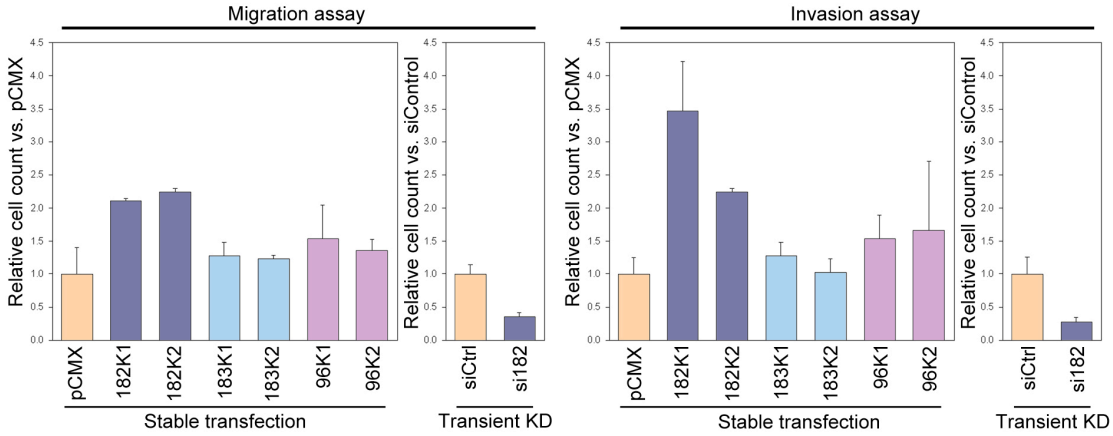

Figure 3-15. Boyden chamber assays showed miR-182 expression to be significantly associated with the migratory phenotype of D458Med cells.

3.3.4 Microchannel assay

Microchannel experiments were carried out in close collaboration with our collaborators Dr. Ralf Kemkemer and Claudio Rolli from the Max Planck Institute for Intelligent Systems, Stuttgart, Germany. This micro-fabricated device with channel structures mimicking a 3-dimensional *in vivo* environment was first described by Rolli *et al.* (Rolli 2008; Rolli *et al.* 2010). This method enabled us to monitor cell migration through accurately defined structures in real-time.

The interaction between cells and the channels were categorized into three activities: penetration, invasion, and permeation (Rolli *et al.* 2010). The invasiveness of tested cell is defined as the percentage of invasive activity (invasion and permeation) in all activities observed. Time-lapse pictures in Fig. 3-16 were captured from video S1, showing an example of a DAOY cell permeating a 5 μm wide channel (The three different cell behaviors are demonstrated in video S1~S4).

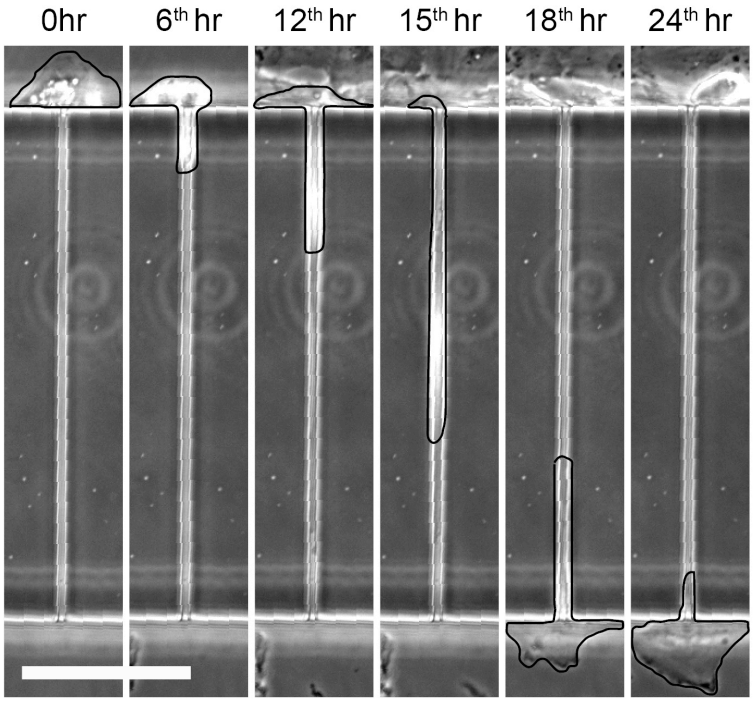

Figure 3-16. Images from a time-lapse video of a DAOY cell permeating a 5x11x300 μm (WxHxL) channel. The outline of cells was manually marked with black lines for better visualization. Scale bar, 100 μm

For microchannel experiment, the specially designed microchannel chip contains 4 different sized channels thus we can observe cell behaviors in them in parallel within one experiment. According to previous experiences from the collaborator, maintenance of the channel structure of the smallest channel, 3x11x100 µm, is very difficult. Besides, cells usually cannot get into the channel of this small size. As a result, we focused on the three bigger channels with 5 µm, 7 µm, and 10 µm width respectively.

We chose to investigate DOAY cells, which had shown the strongest phenotypic differences in established migration assays. In the first experiment, we compared DAOY cells with empty vector, one miR-182 overexpresing clone, transient knockdown of miR-182 and untreated mock control. We observed a gradually decreased invasiveness from the widest channels to the smalles ones. However, 7x11x300 µm and 10x11x100 µm channels showed similar invasiveness between miR-182 overexpression and empty vector control or miR-182 knockdown against mock control. In contrast to this, strong differences in migration propensity were observed in the smallest sized channels (5x11x300 µm) upon overexpression and knockdown of miR-182, respectively. (Fig. 3-17)

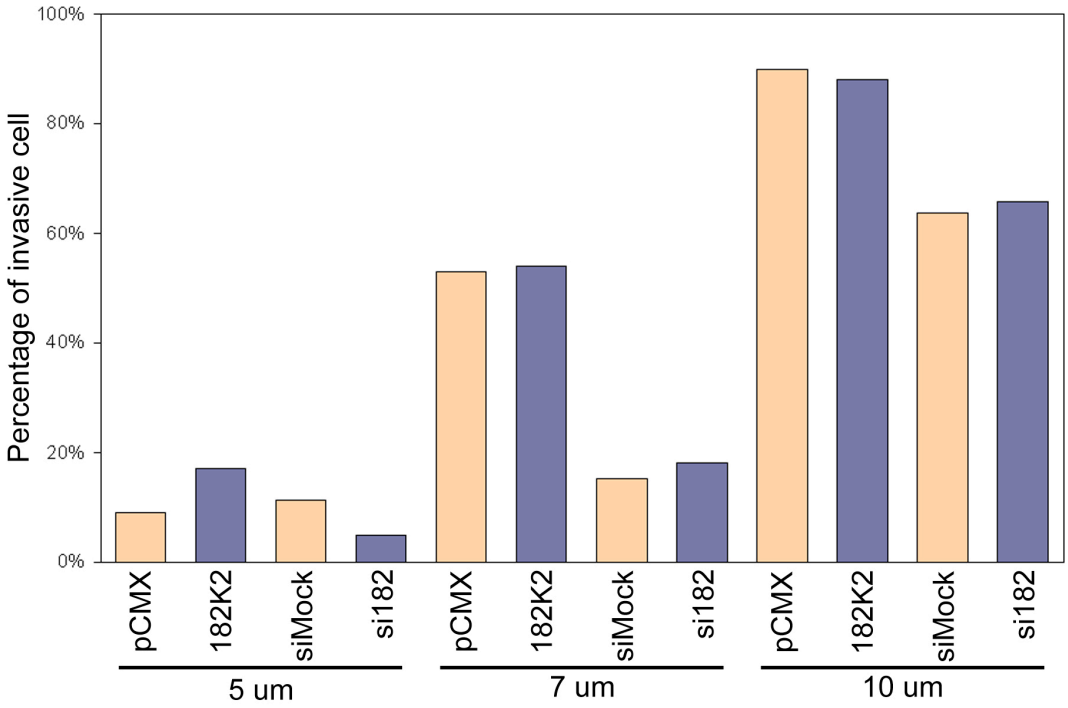

Figure 3-17. The first experiment with microchannels showed that 5 µm wide channels are the most selective condition to detect differences in the invasiveness of DAOY.

After this encouraging finding, we carried out two more replication experiments testing all different conditions of DAOY cells in 5 µm micro-channels. In three individually processed tests, stable overexpression of miRNA-182 increased the average invasiveness to 2.6-fold (182K1) and 2.9-fold (182K2) compared to empty vector transfected DAOY cells (pCMX). Inversely, DAOY with transient KD of miR-182 showed a significantly reduced invasiveness of 0.6-fold against the negative control. (Fig. 3-17; Video S1-S4)

Another adhesive medulloblastoma cell line, Med8A, was also subjected to microchannel assays. Consistent with our findings in DAOY, as well as in the scratch assay, Med8A cells transfected with empty vector (pCMX) showed virtually no migration and were not capable of invading the 5µm channels. After miR-182 overexpression, Med8A cells became moderately invasive, and a considerable proportion of cells were able to invade the microchannels (Fig. 3-18; Video S5/S6)

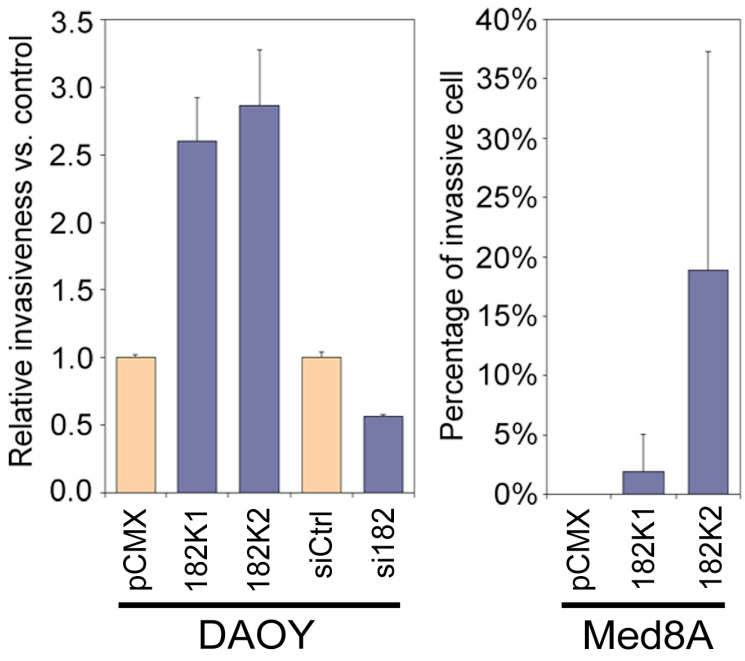

Figure 3-18. 3D microchannel assay showing that the relative invasiveness was doubled in both single DAOY colonies with miR-182 overexpression, and was decreased by about 50% after siRNA treatment compared to empty vector transfected control (pCMX) and scrambled negative siRNA control (siCtrl). No invasive cells were observed in Med8A with empty vector (pCMX), but observed in both single colonies with miR-182 overexpression (182K1, 182K2). Basal migration was 0% for Med8A-pCMX, such that it was not possible to provide a fold change here rather than an absolute frequency. Error bars indicate the mean±SD of three independent experiments.

3.4 Overexpressing miR-182 *in vivo*

To further assess the pro-migratory properties of miR-182 *in vivo*, we performed orthotopic xenograft experiments with our colleborator Prof. Dr. Olaf Witt and Dr. Till Milde from the Division of Clinical Cooperation Unit Pediatric Oncology, DKFZ. DAOY cells with empty vector transfected were compared versus overexpression of miR-182. MRI revealed tumor formation at 4.6 months (mean, range: 3-7) after implantation. Once a tumor was discovered, mice were sacrificed and the xenogragt was taken out for analysis. Haematoxylin & eosin staining of xenograft sections demonstrated tumor formation by all clones irrespective of the transfected construct. The pathologist found that DAOY-182K1 and DAOY-182K2 had extensively infiltrated into the surrounding normal cerebellum tissues, giving rise to countless small colonies widely distributed throughout the brain (green arrowheads in Fig.3-18 a, b, d, e), whereas the control clone DAOY-pCMX formed tumors with a clear boundary (Fig.3-18 c, f). Notably, both xenografts derived from DAOY-182K1, and DAOY-182K2 showed a morphology with larger cells, reminiscent of large cell / anaplastic (LC/A) type medulloblastoma (Fig.3-18 g, h, i). Furthermore, miR-182 overexpressing tumors frequently demonstrated leptomeningeal dissemination (Fig.3-18 j - o). Overexpression of miR-182 did not affect the latency of the xenograft formation, which was in line with our *in vitro* results on cell proliferation.

Figure 3-18. (on the next page) Haematoxylin & eosin staining of DAOY xenograft sections. (**a**), (**b**) Both DAOY-182K1 and DAOY-182K2 invaded into adjacent normal cerebellum, forming small colonies, indicated by green arrows. (**c**) DAOY-pCMX formed a xenograft in solid tumor with clear boundary, indicated by yellow arrows. (**d**), (**e**) Magnified view of the Infiltrating colonies of DOAY-182K1 and DAOY-182K3 into the normal cerebellum. (**f**) Magnified view of the boundary between normal cerebellum and DAOY-pCMX xenograft. (**g**), (**h**), (**i**) Both DAOY-182-K1 and DAOY-182K2 showed larger cellular size than DAOY-pCMX, morphologically resembling LC/A medulloblastoma, which is associated with a highly malignant and invasive clinical phenotype. (**j**) – (**o**) A higher incidence of leptomeningeal spread was seen in tumors overexpressing miR182 compared to controls (black boxes: position of the 400x image in the 100x image).

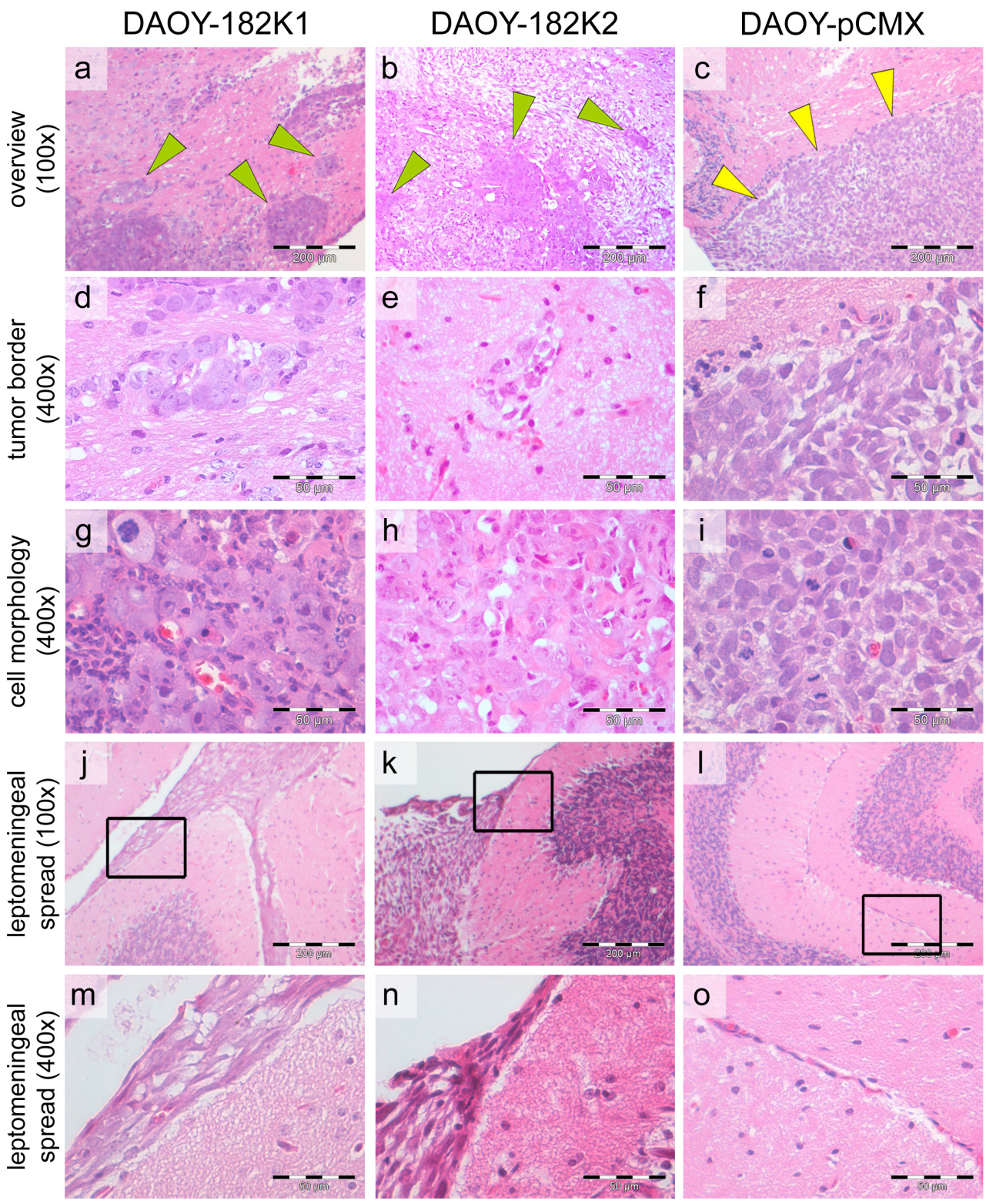
DAOY-182K1
DAOY-182K2
DAOY-pCMX
overview (100x)
tumor border (400x)
cell morphology (400x)
leptomeningeal spread (100x)
leptomeningeal spread (400x)
a
b
c
d
e
f
g
h
i
j
k
l
m
n
o
200 µm
50 µm

3.5 Video clip legends.

Video 1 (Video1_DAOY-182K2.avi)
DAOY cells stably transfected with miR-182 were seeded closely to the channels. A representative permeation activity is shown in the third channel on the right hand side. Duration 24 h; scale bar, 100 µm.

Video 2 (Video2_DAOY-pCMX.avi)
DAOY cells stably transfected with empty vector (pCMX). All four channels on the right hand side showed the typical penetrative behavior. Cells continuously tried to enter the channels throughout the experimental period, while nuclei were not able to enter the channels. Duration 24 h; scale bar, 100 µm.

Video 3 (Video3_DAOY-si182.avi)
DAOY cells with miR-182 knockdown after 24h. Less invasive activity was observed and the cells were only trying to enter the channels for short periods of time. Duration 24 h; scale bar, 100 µm.

Video 4 (Video4_DAOY-siCtrl.avi)
DAOY cells with scrambled siRNA treatment. A DAOY cell invaded into the channel and migrated until the middle of the channel. Then the cell returned to the starting point. This special invasion behavior could be observed in the second channel on the right hand side. Duration 24 h; scale bar, 100 µm.

Video 5 (Video5_Med8A-182K2.avi)
Med8A cells stably transfected with miR-182. Most of the cells remained in the same position, and generally did not enter the channel. The fourth channel on the left hand side showed a example for a single invasion. Duration 24 h; scale bar, 100 µm.

Video 6 (Video6_Med8A-pCMX.avi)
Med8A cells stably transfected with empty vector. All cells included in the field of view remained in a similar position. No invasive behaviors were observed at all. Duration 23:20 h; scale bar, 100 µm..

4 DISCUSSION

The present study provided clear evidence for subgroup-specific miRNA expression profiles in medulloblastoma. In line with the association of high miR-182 expression with metastatic disease in patients, miR-182 was shown to play an important role in medulloblastoma cell migration *in vitro* and *in vivo*. These findings collectively might help to develop novel targeted treatment options for disseminated medulloblastoma.

4.1 Non-SHH medulloblastoma display a distinct microRNA expression pattern

Several recent studies have demonstrated that medulloblastoma is not a single disease, but consists of biologically distinct subgroups (Kool *et al.* 2008; Cho *et al.* 2010; Northcott *et al.* 2010; Remke *et al.* 2011) and is likely derived from different cells of origin (Gibson *et al.* 2010; Sutter *et al.* 2010). In this study, 111 medulloblastoma samples with detailed clinico-pathological information were investigated for characteristic miRNA expression patterns. Both by unsupervised hierarchical clustering (HCL) (Fig.3-1) and Principal component analysis (PCA) analysis (Fig.3-2), SHH-driven mebulloblastomas showed the clearest separation from other medulloblastoma subtypes based on genome-wide miRNA expression patterns.

Whereas previous transcriptome-based studies identified four major subgroups of medulloblastoma (Northcott *et al.* 2010; Remke *et al.* 2011), miRNA expression profiles in the present study revealed three major clusters by unsupervised HCL or PCA. This might be owing to the small sample size and especially under-representation of group C medulloblastoma samples in our screening cohort (9% in screening cohort; 26% in Northcott *et al.* study). Besides, our screening data set contains of a larger proportion of adult patients than the Northcott *et al.* study (34.4% vs. 13%), thus the subgrouping would fit to the recently published study indicating that adult medulloblastoma mainly consist of three major subgroups, SHH, WNT and group D (Remke *et al.* 2011). A larger and more representative cohort of childhood medulloblastomas may thus be required to finally answer this question.

4.2 Novel miRNA candidates found aberrantly upregulated in Non-SHH medulloblastoma

A robust 26-miRNA signature identified by SAM analysis was readily able to separate SHH medulloblastomas from non-SHH medulloblastomas (Fig.3-3). The reliability of this signature was confirmed in an independent validation data set with a larger sample size obtained on a different microRNA microarray platform.

Pang *et al.* summarized frequently deregulated miRNAs in medulloblastoma from three earlier major studies, which all focused on a very prominent onco-miR cluster, namely the miR-17/92 cluster, which is frequently activated in SHH medulloblastoma, as well as on the single miRNAs miR-128-1/2, miR-19a, miR-106b, and miR-191 (Northcott *et al.* 2009; Pang *et al.* 2009). However, our study was the first to identify a miRNA cluster that might be functionally involved in the dissemination of non-SHH medulloblastomas based on the association with metastatic disease in primary medulloblastoma samples.

The miRNA signature in this study was comprised of many novel miRNA candidates, which have not been previously implicated in medulloblastoma or other cancer types, such as miR-455 (hsa-miR-455), miR-182 (hsa-miR-182), miR-183 (hsa-miR-183), and miR-96 (hsa-mir-96), which were all found to be overabundant in non-SHH medulloblastoma (Table 3A).

Three candidate miRNAs (miR-182, miR-183, and miR-96) were chosen from the four most differentially regulated miRNA candidates in the miRNA signature based on the fact that they comprise a common miRNA cluster on chromosome 7q. Under physiological conditions, these miRNAs show a highly specific expression pattern restricted to human and murine sensory organs (Xu *et al.* 2007). It was previously established that they play an important role in retinal development and stem-cell maintenance in mice (Loscher *et al.* 2007; Loscher *et al.* 2008; Viswanathan *et al.* 2009).

4.3 Mir-183 miRNA cluster is significantly associated with metastatic stage of medulloblastoma

In the present study, the expression patterns of candidate miRNAs were confirmed with QRT-PCR in both the screening cohort and a non-overlapping validation cohort. Non-SHH medulloblastoma showed a higher expression of all three retinal miRNAs, whereas the expression in SHH medulloblastomas was similar as the expression detected in a pooled normal cerebellum RNA sample.

An earlier study demonstrated miR-182 and miR-183 were overexpressed in WNT subgroup medulloblastoma (Gokhale *et al.* 2010). This study, however, clearly showed that aberrant expression of the three retina-specific miRNAs is not limited to this subgroup. This finding was independently confirmed in a third dataset recently published by Cho *et al.* (Cho *et al.* 2010).

Abundance of all members of the miR-183~96~182 cluster was shown to be significantly higher in medulloblastomas located in the cerebellar midline, whereas miR-182 and miR-96 also showed a significantly higher expression in metastatic medulloblastoma. Notably, the significant association with tumor location is in line with previously reports showing that SHH medulloblastoma is frequently found in the cerebellar hemispheres rather than in the cerebellar midline (Polkinghorn *et al.* 2007) and is associated with a lower incidence of metastatic dissemination (Northcott *et al.* 2009). Metastatic stage at diagnosis is an important clinical factor to predict patient outcome in medulloblastoma. However, the expression of retina-specific miRNAs was not significantly associated either with overall or progression-free survival in our dataset. This might be explained by the fact, that WNT subgroup medulloblastomas, which have the best outcome of all medulloblastoma subtypes (Northcott *et al.* 2009; Pfister *et al.* 2009), were also contained in the “non-SHH” cluster derived from miRNA profiles.

4.4 Mir-183 and miR-96 have milder effect on the metastatic phenotype of medulloblastoma cells *in vitro*

The first miR-183~96~182 cluster member along the transcription direction within the orthologous region chromosome 7q32.2 is miR-183. It was reported to act as an oncomir and to promote tumor cell migration via downregulation the tumor suppressor genes *EGR1* and *PTEN* (Sarver *et al.* 2009). The authors found that miR-183 is overexpressed in multiple cancer cell lines including synovial sarcoma, rhabdomyosarcoma (RMS), and colon cancer. Indeed, they showed that the transcription factor *EGR1*, which is downregulated in subsets of these tumors, *is a* downstream target of miR-183,. Applying anti-miR-183 treatment, expression of *EGR1* was rescued, and another tumor suppressor gene, *PTEN,* was also reactivated. Functionally, anti-miR-183 treatment could block the migration phenotype of these cells (Sarver *et al.* 2010).

Conversely, other studies reported overexpression of miR-183 to inhibit the migratory phenotype of lung and breast cancer cells (Wang *et al.* 2008; Lowery *et al.* 2010). As a common finding, both studies showed that miR-183 is a potential metastasis inhibitor via regulation of VIL2 and Ezrin, key components of metastatic dissemination (Hunter 2004).

Similar contradictory findings have also been reported for miR-96. Yu *et al.* demonstrated that miR-96 acts as a tumor suppressor gene in pancreatic cancer through silencing of the *KRAS* oncogene. In addition, overexpression of miR-96 inhibited proliferation, migration, and invasion of pancreatic cancer cells *in vitro* and also affected tumor cell growth *in vivo* (Yu *et al.* 2010).

Shortly thereafter, another group showed that miR-96 was working as an onco-miR in breast cancer by silencing the tumor suppressor gene *FOXO3a*. and its downstream targets p21 and p27, both well-known cyclin D1 inhibitors. This would ultimately result in the induction of proliferation of breast cancer cells in the proposed model (Lin *et al.* 2010).

In the present study, the overexpression of miR-183 and miR-96, did not significantly elevate the migratory ability of DAOY and D458Med cell lines. This was at first surprising, because these three miRNAs candidates were reported to be transcripted in a single polycistronic transcript (Xu *et al.* 2007). Furthermore,

the same study demonstrated that two members could synergize to reach a better inhibition of predicted target genes. However, it might still be the case, that each member of the cluster has a distinct biological role in fine-tuning the expression levels of different sets of target genes post-transcriptionally and thereby excerting distinct cellular functions (Doench *et al.* 2003; Zeng *et al.* 2003).

4.5 MiR-182 has the strongest impact on the migration phenotype of medulloblastoma cells *in vitro* and *in vivo*

MicroRNA miR-182 has also been implicated in the inhibition of proliferation and invasion of human lung cancer cells in a recent study (Zhang *et al.* 2011). The authors further identified the cortactin gene (*CTTN*) as a miR-182 target. Overexpression of miR-182 decreased the expression levels of *CTTN* in lung cancer cells thereby suppressing proliferation and invasion *in vitro* and *in vivo*. The *CTTN* gene is frequently upregulated in breast cancer and associated with decreased survival owing to the high incidence of lymph node and distal metastases. Taken together with previous results from Wang *et al.,* miR-182 and miR-183 might co-operate as tumor suppressor genes in lung cancer

Contradicting these findings in a different cellular context, there is also strong evidence now showing the role of miR-182 a tumor promoter in breast cancer. Maskwa *et al*. provided solid evidence that one of the frequently deregulated genes in breast cancer, *BRCA1*, is silenced in sporadic breast cancer by hyperactivation of miR-182 (Moskwa P 2011). The tumor promoting role of miR-182 was further substantiated in melanoma cells, where it exerts at least a part of its effect via suppression of *FOXO3* (forkhead box O3) (Segura *et al.* 2009). Furthermore, a later study successfully rescued the dissemination of melanoma cells in mice by applying an anti-miR-182 treatment (Huynh *et al.* 2011).

Three different *in vitro* migration assays were used in this study. Both the classic (scratch assay and Boyden chamber assay) and a novel methodology (3D microchannel assay) showed concurrent findings. MiR-182 showed the most obvious impact on the scratched wound healing speed and the ability to migrate through a small pored membrane in the Boyden chamber assay across all three medulloblastoma cell lines tested. Consistent with this, opposite results were observed after anti-miR siRNA treatment. Although DAOY and D458Med have relatively high endogenous miR-182 expression levels, elevation of miR-182 expression levels was able to increase the migration propensity even more.

Conversely, the knockdown of miR-182 in Med8A cells, which have a very low miR-182 baseline expression, had no influence on the migration ability of these cells. For the overexpression study of miR-182 in Med8A only one of two stably overexpressing clones showed a clearly increased migration, whereas the second clone only showed a trend. This might be explained by of the fact that Med8A cells with their low baseline miR-182 expressionmight be less dependent on miR-182 than medulloblastoma cells with a high baseline expression of this miRNA.

Nevertheless, DAOY with miR-182 stably overexpressed also showed a very strong migratory and invasion phenotype *in vivo*, which also lead to a more pronounced leptomeningeal spread of the xenograft *in vivo*, thus frimly confirming the important role of miR-182 in the metastatic dissemination of non-SHH medulloblastoma.

Further strengthening this distinct function of miR-182, our collaborators from Boston recently found an increased migration propensity in another medulloblastoma cell line, UW426, and confirmed our findings in DAOY. Cho *et al*. corroborated that miR-182 has the strongest effect on the migration phenotype and the mildest effect on apotosis and cell viability (data co-submitted with our manuscript).

In conclusion, our study shows the first convincing evidence that overexpression of miR-182 elevates the pro-migratory phenotype of medulloblastoma cells *in vitro* and *in vivo*. Thereby we provide strong indication, that overexpression of miR-182 in non-SHH medulloblastoma contributes to leptomeningeal metastatic dissemination. Thus, targeted inhibition of miR-182 could serve as a molecular therapeutic strategy for the treatment of patients with metastatic medulloblastoma as pre-clinically demonstrated for melanoma.

5 REFERENCES

Bear, M. F., Connors, B.W. & Paradiso, M.A. (2001). Neuroscience. Maryland, Lippincott Williams & Wilkins.

Biegel, J. A., A. J. Janss, C. Raffel, L. Sutton, L. B. Rorke, J. M. Harper and P. C. Phillips (1997). "Prognostic significance of chromosome 17p deletions in childhood primitive neuroectodermal tumors (medulloblastomas) of the central nervous system." *Clinical cancer research : an official journal of the American Association for Cancer Research* **3**(3): 473-478.

Blaess, S., J. D. Corrales and A. L. Joyner (2006). "Sonic hedgehog regulates Gli activator and repressor functions with spatial and temporal precision in the mid/hindbrain region." *Development* **133**(9): 1799-1809.

Bohnsack, M. T., K. Czaplinski and D. Gorlich (2004). "Exportin 5 is a RanGTP-dependent dsRNA-binding protein that mediates nuclear export of pre-miRNAs." *RNA* **10**(2): 185-191.

Brown, H. G., J. L. Kepner, E. J. Perlman, H. S. Friedman, D. R. Strother, P. K. Duffner, L. E. Kun, P. T. Goldthwaite and P. C. Burger (2000). ""Large cell/anaplastic" medulloblastomas: a Pediatric Oncology Group Study." *Journal of neuropathology and experimental neurology* **59**(10): 857-865.

Bullrich, F., H. Fujii, G. Calin, H. Mabuchi, M. Negrini, Y. Pekarsky, L. Rassenti, H. Alder, J. C. Reed, M. J. Keating, T. J. Kipps and C. M. Croce (2001). "Characterization of the 13q14 tumor suppressor locus in CLL: identification of ALT1, an alternative splice variant of the LEU2 gene." *Cancer research* **61**(18): 6640-6648.

Bushati, N. and S. M. Cohen (2007). "microRNA functions." *Annual review of cell and developmental biology* **23**: 175-205.

Calin, G. A. and C. M. Croce (2006). "MicroRNA signatures in human cancers." *Nature reviews. Cancer* **6**(11): 857-866.

Calin, G. A., C. D. Dumitru, M. Shimizu, R. Bichi, S. Zupo, E. Noch, H. Aldler, S. Rattan, M. Keating, K. Rai, L. Rassenti, T. Kipps, M. Negrini, F. Bullrich and C. M. Croce (2002). "Frequent deletions and down-regulation of micro- RNA genes miR15 and miR16 at 13q14 in chronic lymphocytic leukemia." *Proceedings of the National Academy of Sciences of the United States of America* **99**(24): 15524-15529.

Calin, G. A., C. G. Liu, C. Sevignani, M. Ferracin, N. Felli, C. D. Dumitru, M. Shimizu, A. Cimmino, S. Zupo, M. Dono, M. L. Dell'Aquila, H. Alder, L. Rassenti, T. J. Kipps, F. Bullrich, M. Negrini and C. M. Croce (2004). "MicroRNA profiling reveals distinct signatures in B cell chronic lymphocytic leukemias." *Proceedings of the National Academy of Sciences of the United States of America* **101**(32): 11755-11760.

Chang, C. H., E. M. Housepian and C. Herbert, Jr. (1969). "An operative staging system and a megavoltage radiotherapeutic technic for cerebellar medulloblastomas." *Radiology* **93**(6): 1351-1359.

Chang, T. C., D. Yu, Y. S. Lee, E. A. Wentzel, D. E. Arking, K. M. West, C. V. Dang, A. Thomas-Tikhonenko and J. T. Mendell (2008). "Widespread microRNA repression by Myc contributes to tumorigenesis." *Nature genetics* **40**(1): 43-50.

Cho, Y. J., A. Tsherniak, P. Tamayo, S. Santagata, A. Ligon, H. Greulich, R. Berhoukim, V. Amani, L. Goumnerova, C. G. Eberhart, C. C. Lau, J. M. Olson, R. J. Gilbertson, A. Gajjar, O. Delattre, M. Kool, K. Ligon, M. Meyerson, J. P. Mesirov and S. L. Pomeroy (2010). "Integrative Genomic Analysis of Medulloblastoma Identifies a Molecular Subgroup That Drives Poor Clinical Outcome." *J Clin Oncol*.

Cogen, P. H., L. Daneshvar, A. K. Metzger, G. Duyk, M. S. Edwards and V. C. Sheffield (1992). "Involvement of multiple chromosome 17p loci in medulloblastoma tumorigenesis." *American journal of human genetics* **50**(3): 584-589.

Corney, D. C., A. Flesken-Nikitin, A. K. Godwin, W. Wang and A. Y. Nikitin (2007). "MicroRNA-34b and MicroRNA-34c are targets of p53 and cooperate in control of cell proliferation and adhesion-independent growth." *Cancer research* **67**(18): 8433-8438.

De Smaele, E., L. Di Marcotullio, E. Ferretti, I. Screpanti, E. Alesse and A. Gulino (2004). "Chromosome 17p deletion in human medulloblastoma: a missing checkpoint in the Hedgehog pathway." *Cell cycle* **3**(10): 1263-1266.

Deng, S., G. A. Calin, C. M. Croce, G. Coukos and L. Zhang (2008). "Mechanisms of microRNA deregulation in human cancer." *Cell cycle* **7**(17): 2643-2646.

Doench, J. G., C. P. Petersen and P. A. Sharp (2003). "siRNAs can function as miRNAs." *Genes & development* **17**(4): 438-442.

Dohner, H., S. Stilgenbauer, A. Benner, E. Leupolt, A. Krober, L. Bullinger, K. Dohner, M. Bentz and P. Lichter (2000). "Genomic aberrations and survival in chronic lymphocytic leukemia." *The New England journal of medicine* **343**(26): 1910-1916.

Du, T. and P. D. Zamore (2005). "microPrimer: the biogenesis and function of microRNA." *Development* **132**(21): 4645-4652.

Ellison, D. (2002). "Classifying the medulloblastoma: insights from morphology and molecular genetics." *Neuropathology and applied neurobiology* **28**(4): 257-282.

Emadian, S. M., J. D. McDonald, S. C. Gerken and D. Fults (1996). "Correlation of chromosome 17p loss with clinical outcome in medulloblastoma." *Clinical cancer research : an official journal of the American Association for Cancer Research* **2**(9): 1559-1564.

Esteller, M. (2008). "Epigenetics in cancer." *The New England journal of medicine* **358**(11): 1148-1159.

Fabian, M. R., N. Sonenberg and W. Filipowicz (2010). "Regulation of mRNA translation and stability by microRNAs." *Annual review of biochemistry* **79**: 351-379.

Fan, X. and C. G. Eberhart (2008). "Medulloblastoma stem cells." *Journal of clinical oncology : official journal of the American Society of Clinical Oncology* **26**(17): 2821-2827.

Ferretti, E., E. De Smaele, A. Po, L. Di Marcotullio, E. Tosi, M. S. Espinola, C. Di Rocco, R. Riccardi, F. Giangaspero, A. Farcomeni, I. Nofroni, P. Laneve, U. Gioia, E. Caffarelli, I. Bozzoni, I. Screpanti and A. Gulino (2009). "MicroRNA profiling in human medulloblastoma." *International journal of cancer. Journal international du cancer* **124**(3): 568-577.

Filipowicz, W., S. N. Bhattacharyya and N. Sonenberg (2008). "Mechanisms of post-transcriptional regulation by microRNAs: are the answers in sight?" *Nature reviews. Genetics* **9**(2): 102-114.

Fogarty, M. P., J. D. Kessler and R. J. Wechsler-Reya (2005). "Morphing into cancer: the role of developmental signaling pathways in brain tumor formation." *Journal of neurobiology* **64**(4): 458-475.

Fouladi, M., A. Gajjar, J. M. Boyett, A. W. Walter, S. J. Thompson, T. E. Merchant, J. J. Jenkins, J. W. Langston, A. Liu, L. E. Kun and R. L. Heideman (1999). "Comparison of CSF cytology and spinal magnetic resonance imaging in the detection of leptomeningeal disease in pediatric medulloblastoma or primitive neuroectodermal tumor." *Journal of clinical oncology : official journal of the American Society of Clinical Oncology* **17**(10): 3234-3237.

Friedman, R. C., K. K. Farh, C. B. Burge and D. P. Bartel (2009). "Most mammalian mRNAs are conserved targets of microRNAs." *Genome research* **19**(1): 92-105.

Giangaspero, F., G. Perilongo, M. P. Fondelli, M. Brisigotti, C. Carollo, R. Burnelli, P. C. Burger and M. L. Garre (1999). "Medulloblastoma with extensive nodularity: a variant with favorable prognosis." *Journal of neurosurgery* **91**(6): 971-977.

Gibson, P., Y. Tong, G. Robinson, M. C. Thompson, D. S. Currle, C. Eden, T. A. Kranenburg, T. Hogg, H. Poppleton, J. Martin, D. Finkelstein, S. Pounds, A. Weiss, Z. Patay, M. Scoggins, R. Ogg, Y. Pei, Z. J. Yang, S. Brun, Y. Lee, F. Zindy, J. C. Lindsey, M. M. Taketo, F. A. Boop, R. A. Sanford, A. Gajjar, S. C. Clifford, M. F. Roussel, P. J. McKinnon, D. H. Gutmann, D. W. Ellison, R. Wechsler-Reya and R. J. Gilbertson (2010). "Subtypes of medulloblastoma have distinct developmental origins." *Nature* **468**(7327): 1095-1099.

Gilbertson, R., C. Wickramasinghe, R. Hernan, V. Balaji, D. Hunt, D. Jones-Wallace, J. Crolla, R. Perry, J. Lunec, A. Pearson and D. Ellison (2001). "Clinical and molecular stratification of disease risk in medulloblastoma." *British journal of cancer* **85**(5): 705-712.

Gilbertson, R. J. and D. W. Ellison (2008). "The origins of medulloblastoma subtypes." *Annual review of pathology* **3**: 341-365.

Gokhale, A., R. Kunder, A. Goel, R. Sarin, A. Moiyadi, A. Shenoy, C. Mamidipally, S. Noronha, S. Kannan and N. V. Shirsat (2010). "Distinctive microRNA signature of medulloblastomas associated with the WNT signaling pathway." *Journal of cancer research and therapeutics* **6**(4): 521-529.

Hasler, M. and L. A. Hothorn (2008). "Multiple Contrast Tests in the Presence of Heteroscedasticity." *Biometrical Journal* **50**(5): 793-800.

He, L., J. M. Thomson, M. T. Hemann, E. Hernando-Monge, D. Mu, S. Goodson, S. Powers, C. Cordon-Cardo, S. W. Lowe, G. J. Hannon and S. M. Hammond (2005). "A microRNA polycistron as a potential human oncogene." *Nature* **435**(7043): 828-833.

Hermeking, H. (2007). "p53 enters the microRNA world." *Cancer cell* **12**(5): 414-418.

Hunter, K. W. (2004). "Ezrin, a key component in tumor metastasis." *Trends in molecular medicine* **10**(5): 201-204.

Huynh, C., M. F. Segura, A. Gaziel-Sovran, S. Menendez, F. Darvishian, L. Chiriboga, B. Levin, D. Meruelo, I. Osman, J. Zavadil, E. G. Marcusson and E. Hernando (2011). "Efficient in vivo microRNA targeting of liver metastasis." *Oncogene* **30**(12): 1481-1488.

Jenkin, D., M. A. Shabanah, E. A. Shail, A. Gray, M. Hassounah, Y. Khafaga, A. Kofide, M. Mustafa and H. Schultz (2000). "Prognostic factors for medulloblastoma." *International journal of radiation oncology, biology, physics* **47**(3): 573-584.

Kenney, A. M. and D. H. Rowitch (2000). "Sonic hedgehog promotes G(1) cyclin expression and sustained cell cycle progression in mammalian neuronal precursors." *Molecular and cellular biology* **20**(23): 9055-9067.

Kimura, H., D. Stephen, A. Joyner and T. Curran (2005). "Gli1 is important for medulloblastoma formation in Ptc1+/- mice." *Oncogene* **24**(25): 4026-4036.

Knoepfler, P. S. and A. M. Kenney (2006). "Neural precursor cycling at sonic speed: N-Myc pedals, GSK-3 brakes." *Cell cycle* **5**(1): 47-52.

Kool, M., J. Koster, J. Bunt, N. E. Hasselt, A. Lakeman, P. van Sluis, D. Troost, N. S. Meeteren, H. N. Caron, J. Cloos, A. Mrsic, B. Ylstra, W. Grajkowska, W. Hartmann, T. Pietsch, D. Ellison, S. C. Clifford and R. Versteeg (2008). "Integrated genomics identifies five medulloblastoma subtypes with distinct genetic profiles, pathway signatures and clinicopathological features." *PLoS One* **3**(8): e3088.

Kortmann, R. D., J. Kuhl, B. Timmermann, U. Mittler, C. Urban, V. Budach, E. Richter, N. Willich, M. Flentje, F. Berthold, I. Slavc, J. Wolff, C. Meisner, O. Wiestler, N. Sorensen, M. Warmuth-Metz and M. Bamberg (2000). "Postoperative neoadjuvant chemotherapy before radiotherapy as compared to immediate radiotherapy followed by maintenance chemotherapy in the treatment of medulloblastoma in childhood: results of the German prospective randomized trial HIT '91." *International journal of radiation oncology, biology, physics* **46**(2): 269-279.

Lin, H., T. Dai, H. Xiong, X. Zhao, X. Chen, C. Yu, J. Li, X. Wang and L. Song (2010). "Unregulated miR-96 induces cell proliferation in human breast cancer by downregulating transcriptional factor FOXO3a." *PLoS One* **5**(12): e15797.

Lindsey, J. C., M. E. Lusher, J. A. Anderton, R. J. Gilbertson, D. W. Ellison and S. C. Clifford (2007). "Epigenetic deregulation of multiple S100 gene family members by differential hypomethylation and hypermethylation events in medulloblastoma." *British journal of cancer* **97**(2): 267-274.

Loscher, C. J., K. Hokamp, P. F. Kenna, A. C. Ivens, P. Humphries, A. Palfi and G. J. Farrar (2007). "Altered retinal microRNA expression profile in a mouse model of retinitis pigmentosa." *Genome biology* **8**(11): R248.

Loscher, C. J., K. Hokamp, J. H. Wilson, T. Li, P. Humphries, G. J. Farrar and A. Palfi (2008). "A common microRNA signature in mouse models of retinal degeneration." *Experimental eye research* **87**(6): 529-534.

Louis, D. N., H. Ohgaki, O. D. Wiestler, W. K. Cavenee, P. C. Burger, A. Jouvet, B. W. Scheithauer and P. Kleihues (2007). "The 2007 WHO classification of tumours of the central nervous system." *Acta neuropathologica* **114**(2): 97-109.

Lowery, A. J., N. Miller, R. M. Dwyer and M. J. Kerin (2010). "Dysregulated miR-183 inhibits migration in breast cancer cells." *BMC cancer* **10**: 502.

Lu, J., G. Getz, E. A. Miska, E. Alvarez-Saavedra, J. Lamb, D. Peck, A. Sweet-Cordero, B. L. Ebert, R. H. Mak, A. A. Ferrando, J. R. Downing, T. Jacks, H. R. Horvitz and T. R. Golub (2005). "MicroRNA expression profiles classify human cancers." *Nature* **435**(7043): 834-838.

Lujambio, A., S. Ropero, E. Ballestar, M. F. Fraga, C. Cerrato, F. Setien, S. Casado, A. Suarez-Gauthier, M. Sanchez-Cespedes, A. Git, I. Spiteri, P. P. Das, C. Caldas, E. Miska and M. Esteller (2007). "Genetic unmasking of an epigenetically silenced microRNA in human cancer cells." *Cancer research* **67**(4): 1424-1429.

Marino, S. (2005). "Medulloblastoma: developmental mechanisms out of control." *Trends in molecular medicine* **11**(1): 17-22.

Medina, P. P. and F. J. Slack (2008). "microRNAs and cancer: an overview." *Cell cycle* **7**(16): 2485-2492.

Moskwa P, B. F., Pan Y, Panchakshari R, Gottipati P, Muschel RJ, Beech J, Kulshrestha R, Abdelmohsen K, Weinstock DM, Gorospe M, Harris AL, Helleday T, Chowdhury D. (2011). "miR-182-mediated downregulation of BRCA1 impacts D... [Mol Cell. 2011] - PubMed result." *Mol Cell.* **41**(2): 210-220.

Munzel, U. and L. A. Hothorn (2001). "A Unified Approach to Simultaneous Rank Test Procedures in the Unbalanced One-way Layout." *Biometrical Journal* **43**(5): 553-569.

Nakahara, Y., P. A. Northcott, M. Li, P. N. Kongkham, C. Smith, H. Yan, S. Croul, Y. S. Ra, C. Eberhart, A. Huang, D. Bigner, W. Grajkowska, T. Van Meter, J. T. Rutka and M. D. Taylor (2010). "Genetic and epigenetic inactivation of Kruppel-like factor 4 in medulloblastoma." *Neoplasia* **12**(1): 20-27.

Northcott, P. A., L. A. Fernandez, J. P. Hagan, D. W. Ellison, W. Grajkowska, Y. Gillespie, R. Grundy, T. Van Meter, J. T. Rutka, C. M. Croce, A. M. Kenney and M. D. Taylor (2009). "The miR-17/92 polycistron is up-regulated in sonic hedgehog-driven medulloblastomas and induced by N-myc in sonic hedgehog-treated cerebellar neural precursors." *Cancer Res* **69**(8): 3249-3255.

Northcott, P. A., A. Korshunov, H. Witt, T. Hielscher, C. G. Eberhart, S. Mack, E. Bouffet, S. C. Clifford, C. E. Hawkins, P. French, J. T. Rutka, S. Pfister and M. D. Taylor (2010). "Medulloblastoma Comprises Four Distinct Molecular Variants." *J Clin Oncol*.

O'Donnell, K. A., E. A. Wentzel, K. I. Zeller, C. V. Dang and J. T. Mendell (2005). "c-Myc-regulated microRNAs modulate E2F1 expression." *Nature* **435**(7043): 839-843.

Orom, U. A., F. C. Nielsen and A. H. Lund (2008). "MicroRNA-10a binds the 5'UTR of ribosomal protein mRNAs and enhances their translation." *Molecular cell* **30**(4): 460-471.

Pang, J. C., W. K. Kwok, Z. Chen and H. K. Ng (2009). "Oncogenic role of microRNAs in brain tumors." *Acta neuropathologica* **117**(6): 599-611.

Peters, L. and G. Meister (2007). "Argonaute proteins: mediators of RNA silencing." *Molecular cell* **26**(5): 611-623.

Pfister, S., M. Remke, A. Benner, F. Mendrzyk, G. Toedt, J. Felsberg, A. Wittmann, F. Devens, N. U. Gerber, S. Joos, A. Kulozik, G. Reifenberger, S. Rutkowski, O. D. Wiestler, B. Radlwimmer, W. Scheurlen, P. Lichter and A. Korshunov (2009). "Outcome prediction in pediatric medulloblastoma based on DNA copy-number aberrations of chromosomes 6q and 17q and the MYC and MYCN loci." *J Clin Oncol* **27**(10): 1627-1636.

Pfister, S., C. Schlaeger, F. Mendrzyk, A. Wittmann, A. Benner, A. Kulozik, W. Scheurlen, B. Radlwimmer and P. Lichter (2007). "Array-based profiling of reference-independent methylation status (aPRIMES) identifies frequent promoter methylation and consecutive downregulation of ZIC2 in pediatric medulloblastoma." *Nucleic Acids Research* **35**(7): e51.

Pogoriler, J., K. Millen, M. Utset and W. Du (2006). "Loss of cyclin D1 impairs cerebellar development and suppresses medulloblastoma formation." *Development* **133**(19): 3929-3937.

Polkinghorn, W. R. and N. J. Tarbell (2007). "Medulloblastoma: tumorigenesis, current clinical paradigm, and efforts to improve risk stratification." *Nat Clin Pract Oncol* **4**(5): 295-304.

Pscherer, A., J. Schliwka, K. Wildenberger, A. Mincheva, C. Schwaenen, H. Dohner, S. Stilgenbauer and P. Lichter (2006). Antagonizing inactivated tumor suppressor genes and activated oncogenes by a versatile transgenesis system: application in mantle cell lymphoma. FASEB J. United States. **20:** 1188-1190.

R Development Core Team (2011). R: A language and environment for statistical computing. R Foundation for Statistical Computing, Vienna, Austria.

Remke, M., T. Hielscher and A. Korshunov (in press). "FSTL5 Expression Identifies Non-WNT/SHH Medulloblastomas with a Particularly Poor Prognosis." *J Clin Oncol*.

Remke, M., T. Hielscher, P. A. Northcott, H. Witt, M. Ryzhova, A. Wittmann, A. Benner, A. von Deimling, W. Scheurlen, A. Perry, S. Croul, A. E. Kulozik, P. Lichter, M. D. Taylor, S. M. Pfister and A. Korshunov (2011). "Adult Medulloblastoma Comprises Three Major Molecular Variants." *Journal of Clinical Oncology* **29**(19): 2717-2723.

Rolli, C. G. (2008). Development of a microfluidic chip to study cell migration through micro-size channels. Diplomarbeit, Ruprecht-Karls-Universtät Heidelberg
Max-Planck-Institut für Metallforschng Stuttgart.

Rolli, C. G., T. Seufferlein, R. Kemkemer and J. P. Spatz (2010). "Impact of tumor cell cytoskeleton organization on invasiveness and migration: a microchannel-based approach." *PLoS One* **5**(1): e8726.

Roussel, M. F. and M. E. Hatten (2011). "Cerebellum development and medulloblastoma." *Current topics in developmental biology* **94**: 235-282.

Saito, Y., G. Liang, G. Egger, J. M. Friedman, J. C. Chuang, G. A. Coetzee and P. A. Jones (2006). "Specific activation of microRNA-127 with downregulation of the proto-oncogene BCL6 by chromatin-modifying drugs in human cancer cells." *Cancer cell* **9**(6): 435-443.

Sarver, A. L., A. J. French, P. M. Borralho, V. Thayanithy, A. L. Oberg, K. A. Silverstein, B. W. Morlan, S. M. Riska, L. A. Boardman, J. M. Cunningham, S. Subramanian, L. Wang, T. C. Smyrk, C. M. Rodrigues, S. N. Thibodeau and C. J. Steer (2009). "Human colon cancer profiles show differential microRNA expression depending on mismatch repair status and are characteristic of undifferentiated proliferative states." *BMC cancer* **9**: 401.

Sarver, A. L., L. Li and S. Subramanian (2010). "MicroRNA miR-183 functions as an oncogene by targeting the transcription factor EGR1 and promoting tumor cell migration." *Cancer research* **70**(23): 9570-9580.

Scheurlen, W. G., G. C. Schwabe, S. Joos, J. Mollenhauer, N. Sorensen and J. Kuhl (1998). "Molecular analysis of childhood primitive neuroectodermal tumors defines markers associated with poor outcome." *Journal of clinical oncology : official journal of the American Society of Clinical Oncology* **16**(7): 2478-2485.

Segura, M. F., D. Hanniford, S. Menendez, L. Reavie, X. Zou, S. Alvarez-Diaz, J. Zakrzewski, E. Blochin, A. Rose, D. Bogunovic, D. Polsky, J. Wei, P. Lee, I. Belitskaya-Levy, N. Bhardwaj, I. Osman and E. Hernando (2009). Aberrant miR-182 expression promotes melanoma metastasis by repressing FOXO3 and microphthalmia-associated transcription factor. Proc Natl Acad Sci U S A. United States. **106:** 1814-1819.

Sutter, R., O. Shakhova, H. Bhagat, H. Behesti, C. Sutter, S. Penkar, A. Santuccione, R. Bernays, F. L. Heppner, U. Schuller, M. Grotzer, H. Moch, P. Schraml and S. Marino (2010). "Cerebellar stem cells act as medulloblastoma-initiating cells in a mouse model and a neural stem cell signature characterizes a subset of human medulloblastomas." *Oncogene* **29**(12): 1845-1856.

Suzuki, R. and H. Shimodaira (2006). "Pvclust: an R package for assessing the uncertainty in hierarchical clustering." *Bioinformatics* **22**(12): 1540-1542.

Thompson, M. C., C. Fuller, T. L. Hogg, J. Dalton, D. Finkelstein, C. C. Lau, M. Chintagumpala, A. Adesina, D. M. Ashley, S. J. Kellie, M. D. Taylor, T. Curran, A. Gajjar and R. J. Gilbertson (2006). "Genomics identifies medulloblastoma subgroups that are enriched for specific genetic alterations." *Journal of clinical oncology : official journal of the American Society of Clinical Oncology* **24**(12): 1924-1931.

Uziel, T., F. V. Karginov, S. Xie, J. S. Parker, Y. D. Wang, A. Gajjar, L. He, D. Ellison, R. J. Gilbertson, G. Hannon and M. F. Roussel (2009). "The miR-17~92 cluster collaborates with the Sonic Hedgehog pathway in medulloblastoma." *Proceedings of the National Academy of Sciences of the United States of America* **106**(8): 2812-2817.

Vasudevan, S., Y. Tong and J. A. Steitz (2007). "Switching from repression to activation: microRNAs can up-regulate translation." *Science* **318**(5858): 1931-1934.

Viswanathan, S. R., C. H. Mermel, J. Lu, C. W. Lu, T. R. Golub and G. Q. Daley (2009). "microRNA expression during trophectoderm specification." *PLoS One* **4**(7): e6143.

von Hoff, K., B. Hinkes, N. U. Gerber, F. Deinlein, U. Mittler, C. Urban, M. Benesch, M. Warmuth-Metz, N. Soerensen, I. Zwiener, H. Goette, P. G. Schlegel, T. Pietsch, R. D. Kortmann, J. Kuehl and S. Rutkowski (2009). "Long-term outcome and clinical prognostic factors in children with medulloblastoma treated in the prospective randomised multicentre trial HIT'91." *European journal of cancer* **45**(7): 1209-1217.

Wang, G., W. Mao and S. Zheng (2008). "MicroRNA-183 regulates Ezrin expression in lung cancer cells." *FEBS letters* **582**(25-26): 3663-3668.

Wang, V. Y. and H. Y. Zoghbi (2001). "Genetic regulation of cerebellar development." *Nature reviews. Neuroscience* **2**(7): 484-491.

Weaver, V. M., O. W. Petersen, F. Wang, C. A. Larabell, P. Briand, C. Damsky and M. J. Bissell (1997). "Reversion of the malignant phenotype of human breast cells in three-dimensional culture and in vivo by integrin blocking antibodies." *The Journal of cell biology* **137**(1): 231-245.

Wechsler-Reya, R. J. and M. P. Scott (1999). "Control of neuronal precursor proliferation in the cerebellum by Sonic Hedgehog." *Neuron* **22**(1): 103-114.

Wright, J. H. (1910). "Neurocytoma or Neuroblastoma, a Kind of Tumor Not Generally Recognized." *The Journal of experimental medicine* **12**(4): 556-561.

Wu, M., N. Jolicoeur, Z. Li, L. Zhang, Y. Fortin, D. L'Abbe, Z. Yu and S. H. Shen (2008). "Genetic variations of microRNAs in human cancer and their effects on the expression of miRNAs." *Carcinogenesis* **29**(9): 1710-1716.

Xu, S., P. D. Witmer, S. Lumayag, B. Kovacs and D. Valle (2007). "MicroRNA (miRNA) transcriptome of mouse retina and identification of a sensory organ-specific miRNA cluster." *J Biol Chem* **282**(34): 25053-25066.

Yi, R., Y. Qin, I. G. Macara and B. R. Cullen (2003). "Exportin-5 mediates the nuclear export of pre-microRNAs and short hairpin RNAs." *Genes & development* **17**(24): 3011-3016.

Yu, S., Z. Lu, C. Liu, Y. Meng, Y. Ma, W. Zhao, J. Liu, J. Yu and J. Chen (2010). "miRNA-96 suppresses KRAS and functions as a tumor suppressor gene in pancreatic cancer." *Cancer research* **70**(14): 6015-6025.

Zeng, Y., R. Yi and B. R. Cullen (2003). "MicroRNAs and small interfering RNAs can inhibit mRNA expression by similar mechanisms." *Proceedings of the National Academy of Sciences of the United States of America* **100**(17): 9779-9784.

Zhang, L., T. Liu, Y. Huang and J. Liu (2011). "microRNA-182 inhibits the proliferation and invasion of human lung adenocarcinoma cells through its effect on human cortical actin-associated protein." *International journal of molecular medicine*.

Zhang, L., S. Volinia, T. Bonome, G. A. Calin, J. Greshock, N. Yang, C. G. Liu, A. Giannakakis, P. Alexiou, K. Hasegawa, C. N. Johnstone, M. S. Megraw, S. Adams, H. Lassus, J. Huang, S. Kaur, S. Liang, P. Sethupathy, A. Leminen, V. A. Simossis, R. Sandaltzopoulos, Y. Naomoto, D. Katsaros, P. A. Gimotty, A. DeMichele, Q. Huang, R. Butzow, A. K. Rustgi, B. L. Weber, M. J. Birrer, A. G. Hatzigeorgiou, C. M. Croce and G. Coukos (2008). "Genomic and epigenetic alterations deregulate microRNA expression in human epithelial ovarian cancer." *Proceedings of the National Academy of Sciences of the United States of America* **105**(19): 7004-7009.

6 APPENDIX

6.1 RNA quality analysis with RNA integrity number (RIN)

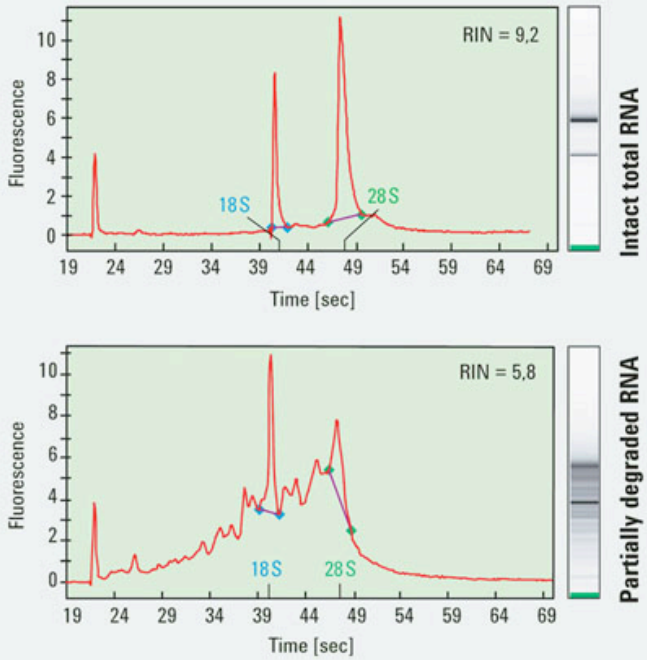

Intact and degraded RNA with corresponding RNA Integrity Number. *The upper electropherogram and gel-like image show the analysis of high quality total RNA resulting in a RIN of 9.2. The lower electropherogram shows the analysis of a partially degraded total RNA sample. Many degradation products appear between the two ribosomal bands and below the 18S band resulting in a RIN of 5.8.*

"The RNA integrity number (RIN) is a software tool designed to help scientists estimate the integrity of total RNA samples. The expert software automatically assigns an integrity number to an eukaryote total RNA sample. Using this tool, sample integrity is no longer determined by the ratio of the ribosomal bands, but by the entire electrophoretic trace of the RNA sample. This includes the presence or absence of degradation products. In this way, interpretation of an electropherogram is facilitated, comparison of samples is enabled and repeatability of experiments is ensured. The assigned RIN is independent of sample concentration, instrument and analyst therefore becoming a de facto standard for RNA integrity." The RNA Integrity Database (RINdb) (http://www.chem.agilent.com/rin/_rinsearch.aspx) showed that the average RIN for frozen brain tissue (both normal and tumor, yet no medulloblastoma) is around 8.1 ~ 9.7. As a result we set the RIN cut-off at 8.0. Information from Agilent official web-site (http://www.home.agilent.com/)